

UiO : **University of Oslo**

Audun Skau Hansen

Local correlation methods for infinite systems

Thesis submitted for the degree of Philosophiae Doctor

Department of Chemistry

The Faculty of Mathematics and Natural Sciences

The Hylleraas Centre for Quantum Molecular Sciences



2021

© **Audun Skau Hansen, 2021**

*Series of dissertations submitted to the
The Faculty of Mathematics and Natural Sciences, University of Oslo
No. 2380*

ISSN 1501-7710

All rights reserved. No part of this publication may be
reproduced or transmitted, in any form or by any means, without permission.

Cover: Hanne Baadsgaard Utigard.

Print production: Representralen, University of Oslo.

To my family

Preface

On the face of it, there may seem to be something self-contradictory about searching for locality in a periodic, infinite system. My years of poking around this problem has taught me that it is not. If you tread carefully, you'll find an extremely rich and enjoyable problem that never cease to provide fresh insight, new puzzles and amazement. If you stray some few whimsical steps off course, however, you may find yourself in a deep hole where the walls cave in as you try to escape. I've had the pleasure of visiting both some dark holes and some illuminating vistas around here, yet it is hard to shake off the feeling of being a tourist. So if you join me on this tour, let me begin with a friendly warning; I do not know the way out of all the holes around here. In fact, I'm quite sure I'm still stuck in some of them. So although the terrain may appear identical in all directions, as one would perhaps expect in an infinite crystal, we shall stick to the path we have cleared, take some delight in the sights along the way, and hopefully arrive safely at our destination; the periodic correlation energy, before we run out of spirit.

First, in Chapter 1, we'll review the bigger picture and provide some historical and theoretical context as well as motivation for the coming discussion. In Chapter 2 we lay the mathematical foundation that underpins most of this work. While this chapter may seem trivial, I actually consider it an essential part of my my research. It greatly simplifies the coming theoretical derivations, and provide a means for efficient calculation of periodic quantities. In Chapter 3 we introduce the central problem of this work; the periodic electron many-body problem, as well as common routes towards solving the problem with a special focus on locality. Finally, in Chapter 4, we'll go the final distance, arriving at a way in which the local MP2 energy can be made computationally feasible for periodic systems. The two last chapters (5 and 6) features a presentation of the main parts of the computational implementation, a summary and motivation of the papers, and some outlooks.

In sum, the first six chapters of this thesis serves as a framing for the three included papers. These papers are presented in a chronological order.

This thesis is submitted in partial fulfillment of the requirements for the degree of *Philosophiae Doctor* at the University of Oslo. The research presented here was conducted at the Hylleraas Centre for Quantum Molecular Sciences, and formerly the Centre for Theoretical and Computational Chemistry, both Centres of Excellence funded by the Research Council of Norway hosted by the University of Oslo.

The research was supervised by Thomas Bondo Pedersen, and co-supervised by Trygve Helgaker and Simen Kvaal.

This work has been supported by the Research Council of Norway (RCN)

through its Centres of Excellence scheme, project number 262695, by the RCN Research Grant No. 240698, and by the Norwegian Supercomputing Program NOTUR Grant No. NN4654K.

Acknowledgements

The Hylleraas Centre for Quantum Molecular Sciences is truly an excellent environment in which to receive a scientific upbringing. Thank you Trygve for making this place a reality. Please know I take a great deal of pride in my place in the Hylleraas group.

Thomas, I have gotten to know you as an outstanding teacher and scientist. You have this sneaky way of planting ideas in my head in such a way that they get stuck, and in time gets mistaken for my own. Thank you for your first-class guidance, inspiration and collaboration, it's been a true pleasure.

There's the perfect person for most imaginable questions at the Hylleraas centre. Simen K., Erik, Simen R. and Andre has been invaluable in this regard. Thank you for inspiration, directions, suggestions and conversations.

Michele, I greatly enjoy our morning routine and discussions. Thank you for getting me properly acquainted with the Ising model, and for inspiring my interest in stochastic methods.

Alex, I wish we had the opportunity to work together on the same problem once, I'm sure it would have been great fun. Thank you for friendship, guidance and conversations.

Elisa, Karl, Gustav and Einar; it's been a pleasure working with all of you. Thank you all for the countless discussions, and for bearing over with my at times unconventional approach to things. This project has benefited greatly from Elisa's experience and determination, Karl's unique ingenuity, Gustav's rigour and mindfulness and Einar's careful attention to detail.

Håkon, our conversations are almost always productive in some sense. You are a great colleague with a sound understanding of science. Fabian, I admire your insight and reasoning, and I truly appreciate the fun we've had. Sigbjørn, your sharp focus and push towards results is inspirational. Thanks to you all!

In the broader CTCC/Hylleraas group I wish to thank David, Ainara, Benedicte, Chandan, Rafael, Rolf, Sangita, Sarah, Julie, Jon, Morten, Manuel, Abril, Joakim, Sverre, Lluís, Jan Ingar, Jonathan and Inge. Thank you all for being such great colleagues!

A special thanks to my former master supervisor Morten, you brought me into all of this in the first place. I had a good laugh, some years after you taught me this profoundly complicated, cool and unfamiliar physics, when I realized you had actually introduced me to chemistry.

Also, I wish to extend a special thanks to Lorenzo, for your masterful guidance into the dark arts of local correlation in periodic systems. It's been immensely helpful.

Dear mom and dad, grandmother and the rest of the family; thank you for your patience.

Finally, dear Kine, Erik, Alfred. I now understand the true sincerity behind the many "thank you"'s directed at the close family frequently included in dissertations. We have in a sense been living in the same house, yet on different planets, the last years. I am immensely thankful that you have supported me throughout this. I love you all!

• **Audun Skau Hansen**

Oslo, March 2021

List of Papers

Paper I

Elisa Rebolini, Gustav Baardsen, Audun Skau Hansen, Karl R. Leikanger, and Thomas Bondo Pedersen “Divide–Expand–Consolidate Second–Order Møller–Plesset Theory with Periodic Boundary Conditions”. In: *Journal of Chemical Theory and Computation*. Vol. 14, no. 5 (2018), pp. 2427–2438. DOI: 10.1021/acs.jctc.8b00021.

Paper II

Audun Skau Hansen, Gustav Baardsen, Elisa Rebolini, Lorenzo Maschio, and Thomas Bondo Pedersen “Representation of the virtual space in extended systems – a correlation energy convergence study”. In: *Molecular Physics* Vol. 118, no. 19-20 (2020), e1733118. DOI: 10.1080/00268976.2020.1733118.

Paper III

Audun Skau Hansen, Einar Aurbakken and Thomas Bondo Pedersen “Smooth potential-energy surfaces in fragmentation-based local correlation methods for periodic systems”. In: *Molecular Physics* (2021) e1733118. DOI: 10.1080/00268976.2021.1896046.

Contents

Preface	iii
List of Papers	vii
Contents	ix
List of Figures	xi
1 Introduction	1
1.1 Overview	1
1.2 Brief historical context	2
2 A mathematical framework for periodic systems	7
2.1 Overview	7
2.2 Infinite Block-Toeplitz matrices	7
2.3 Transpose of IBT-matrices	7
2.4 The IBT matrix-matrix product	8
2.5 Truncated IBT-matrices	9
2.6 The matrix product of truncated IBT-matrices	9
2.7 Discrete Fourier transform of IBT-matrices	10
2.8 The discrete Fourier transform matrices	11
2.9 Periodicity in direct space	12
2.10 Infinite block-circulant matrices	12
2.11 Products with IBC matrices	13
2.12 The convolution theorem	15
2.13 Reciprocal space inversion of IBC-matrices	16
2.14 Unitary IBT and IBC matrices	17
2.15 Triple products	18
3 Periodic and infinite many-electron quantum systems	19
3.1 Overview	19
3.2 The Periodic Hamiltonian	19
3.3 The independent particle model	20
3.4 The periodic wavefunction	21
3.5 Periodic Hartree-Fock theory	22
3.6 Wannier orbitals	23
3.7 Locality in periodic systems	25
3.8 Optimization techniques	30
4 Local correlation methods for periodic systems	35

ix

Contents

4.1	Overview	35
4.2	Periodic correlation	35
4.3	The local subspace	37
4.4	The Divide-Expand-Consolidate scheme	38
4.5	The Extended DEC (XDEC) Scheme	39
4.6	Periodic Fitting	44
5	The XDEC-RI code	49
5.1	Overview	49
5.2	Two versions of XDEC	49
5.3	Comments on The Local Approximation	50
5.4	Modules	52
5.5	Validation	56
6	Summary and outlook	57
6.1	Overview	57
6.2	Research and papers	57
6.3	Prospects	59
	Bibliography	61
	Papers	72
I	Divide–Expand–Consolidate Second–Order Møller–Plesset Theory with Periodic Boundary Conditions	73
II	Representation of the virtual space in extended systems – a correlation energy convergence study	87
III	Smooth potential-energy surfaces in fragmentation-based local correlation methods for periodic systems	101

List of Figures

1.1	Good luck in bringing a crystal to the computational scaling wall of electron correlation methods.	1
2.1	The structure of the blocks in the infinite Toeplitz matrix. An arbitrary block is chosen along the diagonal as a point of reference, and is referred to as the <i>reference block</i> , here indicated by the highlighted index in the center of the image. All information on the infinite matrix is contained in a single column or row, as indicated by the red highlight.	8
2.2	The structure of the truncated BT-matrix, where blocks outside the bandwidth is zero. In this case $\mathcal{B} = [-2, 2]$	10
2.3	It may be clarifying to imagine the circulant operator as cycling through the blocks on a clock-like disc.	13
2.4	The structure of the IBC-matrix. The periodic region is marked in red, indicating that it is infinitely repeated throughout the entire matrix.	14
2.5	The IBC product can be imagined as the sum over aligned blocks in two matrices, here visualized by two rings. Summing together products of the corresponding blocks in the outer and inner rings above would yield the center diagonal block in the IBC product. For the off-diagonal block n in the IBC product, one of the rings would have to be rotated n increments before the blockwise matrix product and summation. Note the opposing sign of the indexes at each increment.	15
3.1	Localization may be envisioned as a the search for a minimum on the surface of a hypersphere.	32
4.1	The product of two Gaussian functions exhibits an exponential decay as they are spatially separated.	37
4.2	Procedure for partitioning the occupied orbitals in the reference cell based on distance, here illustrated for one dimensional ethylene. The Wannier centers are indicated with crosses, "+", and the colored spheres indicate to which fragment they are associated. In this case, $a_{\text{frag}} = 2.0$ Bohr results in two fragments.	40

4.3	Virtual cutoff distance for one dimensional ethylene. With $d_v = 3.0$ Bohr, a number of virtual orbitals are included in the EOS of fragment 1, as defined in Fig. 4.2. The virtual orbitals in the EOS are indicated as blue spheres, while the ones outside are brown. Note that while the illustration only shows the xy-coordinate, the orbitals are in reality not confined to this plane. Consequently, one virtual orbital to the right appears to be within the sphere while its offset in the z-axis places it outside.	41
4.4	Illustration of the fragments (top) and pair fragments (bottom) in the XDEC fragmentation scheme. Virtual and occupied orbitals inside the AOS/EOS are colored red and blue respectively.	42
4.5	A periodic setup for pair fragments, where the color indicates which fragment each AOS belongs to. Their union is the pair AOS.	43
4.6	The periodic pair domain accounting for all amplitudes. The fragment specific domains may or may not overlap in the cells. .	44
4.7	The pair domain as defined by default in the XDEC-RI code. . .	45
5.1	Illustrative overview of our code setup. Consistency across the various codes is maintained by a class called PRISM. Integrals for the XDEC-RI framework is provided by LIBINT. The module TMat handles periodic matrix product, while PRI performs the integral fitting.	50
5.2	Löwdin orthogonalization of a periodic AO basis performed in a Jupyter Notebook using the TMat class. The resulting orbitals are orthogonal to machine precision under Born von Karman boundary conditions.	53
5.3	Construction of periodic projected atomic orbitals (PAOs). [5] .	54
6.1	It still counts, right?	57

Chapter 1

Introduction

1.1 Overview



Figure 1.1: Good luck in bringing a crystal to the computational scaling wall of electron correlation methods.

The computational scaling wall constitutes a fundamental challenge in molecular quantum chemistry, with even more constraining consequences for infinite systems such as crystals. It is likely the main obstacle in our quest for a universally applicable in-silico model of real-world chemistry on the quantum level. Conquering this challenge will unquestionably give us the means to make groundbreaking discoveries in biology, medicine and material science, as well as chemistry, and it has therefore been the subject of extensive research since the middle of the last century. The computational complexity encountered is a direct consequence of the hierarchical way in which we approach the many-body problem, and is thus an intrinsic property of the equations that arise from the second quantization formalism. In the molecular case, linear scaling has been achieved by inferring sparsity in the equations from locality considerations, leading to a family of approaches commonly referred to as local correlation methods. Key to these methods is the fact that the amplitude equations in many cases can be partitioned into weakly intercoupled subspaces, where the coupling

1. Introduction

can be neglected without significant effects on the results.

The extension of local correlation methods into the realm of infinite systems has been limited, in part because the conventional way of dealing with these systems is to apply Born-von Karman boundary conditions and solve the resulting equations in reciprocal space. In this case, the canonical solution to the Hartree-Fock equations are found in the form of completely delocalized Bloch-waves. However, an alternative route is available for insulators. In the localized Wannier-picture, the orbitals have a finite spatial extent, and the systems are thus in many ways much more similar to the molecular case. Even here, however, progress has been slow. One likely explanation for this is that the process of adapting the molecular formulation into its periodic equivalent is cumbersome, with one notable challenge being that of utilizing the translational symmetries in the most efficient way possible.

Several problems takes the spotlight within this context; how do we smoothly and systematically extend our well proven methods for molecules to periodic and infinite systems? How can the spaces be chosen and truncated with sufficient precision and control of the error in the result? Are there bottlenecks in the calculations that can be identified and overcome with suitable approximations? These main venues has been the focus of my research, and the results are presented in this dissertation.

1.2 Brief historical context

Many-body quantum mechanics emerged out of the electrified and creative atmosphere that permeated particle physics in the 1920s, and its key ideas and concepts are often attributed to Paul Dirac and his 1927 second-quantized treatment of fields.[1] Within a short span of time this formalism was extended to fermionic many-body systems, and approximative methods such as truncated configuration interaction (CI), Hückel theory and Hartree-Fock (HF) theory were contrived. Early on, Felix Bloch [2], and Ralph Kronig and William Penney [3] presented their theories in rapid succession, and the theory thus encompassed also infinite crystals. Over the period of some few decades, the ingredients for a complete understanding of the quantum mechanical interactions of electrons were all put to the table, and organized into a coherent theoretical framework.

The Norwegian physicist Egil Hylleraas took part in the very conception of this framework. In 1926, the then aspiring young scientist Hylleraas traveled to Göttingen in order to work on crystallography under the supervision of Max Born.[4] Upon arrival, Hylleraas did however find that Born's focus had shifted, and he soon found himself working on the quantum two-body problem instead.

His method for finding a solution to the ground state of Helium earned him a place in history as one of the pioneers of quantum chemistry. In Hylleraas' own words, his work also sent literally "respectable shock waves" into his immediate surroundings, as his solution procedure required the use of the presumably noisy Mercedes Euclid, an early mechanical calculator. [4] For Hylleraas and his contemporaries, it was clear already in the late 1920s that the equations that

arise from second quantization can not be solved analytically, but rather has to be computed numerically. While the solution procedure typically consists of a series of basic additions and multiplications, the sheer number of such calculations required superseeds by far any reasonable workload for a human. Even in the modern era, looking back at nearly a century of exponential growth in available computational resources while we take our baby steps into the age of quantum computing, the exact solution of the fermionic N-body problem is far beyond our reach for realistic cases.

The limitations concerning wavefunction methods arise mainly from the computational scaling, where methods that describe the correlated wavefunction of electrons typically scales in the range from $\mathcal{O}(n_o^2 n_v^2 n_{AO}^4)$ for the second order Møller-Plesset (MP2) case up to $\mathcal{O}(n_{AO}^{n_{el}})$ in the Full Configuration Interaction (FCI) case, where n_o , n_v and n_{AO} is the number of occupied, virtual and atomic orbitals respectively, and n_{el} is the number of electrons. [1] Scientists, who in the midst of the last century were faced with such poor prospects in application and scant computational resources, realized that additional approximative techniques on top of the hierarchical truncation of excited Slater determinants (SDs) were required in order to push beyond the scaling barriers.

In a paper from 1983[5], Peter Pulay insightfully noted that the canonical solution to the Hartree-Fock equations could potentially impose an unnecessary delocalization of the correlation effects in configuration space. In general, there exists an infinite number of non-canonical solutions, linked to the canonical solution by a unitary rotation within the occupied and virtual spaces respectively [6], which distribute the correlation energy differently throughout configuration space depending on the choice of representation. The problem may thus be seen as the search for a compact representation, where the equations can be solved on weakly coupled subspaces instead of the full space, thus reducing the scaling of the equations towards linearity. A similar effect is especially noteworthy in the periodic case, where the canonical Hartree-Fock solution subject to Born-von Karman (BvK) boundary conditions exhibits an exact decoupling in the correlated treatment due to conservation of crystal momentum.[7]

Pulay pointed out in his 1983 paper that one possible compact representation could emerge from locality considerations, in effect the spatial extent of the orbitals in \mathbb{R}^3 . [5] This idea finds its scientific justification in the fact that physical interactions typically decay with distance, so it is reasonable to expect a distance based decoupling. At the time, it was known that contributions to the correlation energy could be cast in terms of occupied pairs [8, 9, 10], but the delocalized nature of the virtual space still required a computationally expensive (n_{AO}^4) operation. As they lacked the methodology required to localize the virtual space, Pulay proposed instead to construct the virtual space by removing the occupied components from the AO-basis, resulting in a redundant set of local virtual orbitals commonly called Projected Atomic Orbitals (PAOs). [5] Over the next few years, Pulay and Svein Sæbø then published together and separately a series of papers [5, 11, 12, 13], which has formed the basis for what today is referred to as *local correlation methods*. The Divide-Expand-Consolidate method (DEC) [14, 15] is one member of this family, together with cluster-in-molecule

1. Introduction

(CIM) [16, 17, 18] and the pair-natural orbital (PNO) approach [19, 20, 21, 22, 23, 24, 25], to name a few.

In order to achieve spatial locality, several optimizable objective functions have been devised. While Pulay and Sæbø originally employed the PAO basis for the virtual space, Foster and Boys had already in the 1960s introduced the so-called Foster-Boys localization [26, 27], which essentially measures and minimize the sum of variances for a set of orbitals. Edmiston-Ruedenberg localization [28] was introduced in 1963 and targets more directly the correlation energy, while Pipek-Mezey localization [29] was introduced in 1989. The wide range of available measures highlights our ambiguous notion of locality; that the orbitals are in some sense spatially confined.

Optimization methods have become more elaborate the last four decades. The PAOs are intrinsically local, but the various other orbital sets are obtained by optimizing their measure of locality. This can be a computationally costly and complicated affair for higher dimensional orbital spaces. Early on, one would perform optimization by means of Jacobi sweeps [30, 31], where all possible pairs of orbitals was rotated separately and successively until overall convergence was reached. Today, a wide range of techniques are routinely used in these kinds of problems, such as for instance gradient methods, line-searches, Newtonian methods and trust-region methods. [31, 32]

Furthermore, various compression techniques has been devised in order to compactly represent the orbital spaces, such as the PNOs and orbital-specific virtual orbitals (OSVs) [33].

We are currently at a stage where sophisticated methods and faster computers have facilitated the routine usage of local correlation methods for large molecules, and significant progress in the extension of these methods to periodic systems is being made. [18, 34, 35] A timely question is thus: what do we expect to gain with these methods? Why would we be interested in the correlation energy of something like a crystal? Is it a *useful quantity*, as some might ask? [36]

Wavefunction methods provide a physically correct description at the quantum level, given that the Hamiltonian accurately describe the system in question. While crystal structures may be macroscopic objects, they are fundamentally governed by quantum-mechanical interactions. They present us with one of these rare occasions where effects on the quantum level can bubble up to the surface of our tangible, everyday reality. Periodic systems encompasses polymers, helix-structures, surfaces and three dimensional crystals, all sources for rich chemistry pertaining to material science, life science and much of our surrounding reality.

Density functional theory (DFT) is significantly more efficient than wavefunction methods, and is today routinely used to simulate crystals. At the same time DFT lacks a systematic way of improving the exchange-correlation functional towards the exact result [37], a task usually delegated to the more accurate coupled-cluster (CC) theory in the molecular case. CC results in the condensed phase would thus let us ensure the validity of DFT calculations for materials.

It may be hard to predict exactly what kind of beneficial discoveries will be made with accurate and efficient in-silico models of crystal structures beyond

ensuring the quality of DFT results, but it is even harder to argue that there would be none. The ability to discover through simulation, rather than synthesis, opens the door for efficient and strategic exploration of phenomena on the electronic scale in the context of materials. This could be new, targeted medicines, stronger and lighter materials for space exploration, or even solutions to problems we do not yet know we have. In a fast-paced reality where global needs may change quickly and abruptly, it is crucial to stay ahead of the curve. Machine-learning methods may be orders of magnitudes faster than wavefunction methods, but at the same time inherently empirical and in this sense limited to answers inside of the box. First-principle methods, with the predictive power to produce new, decisive data and illuminate the unknown and beyond, provides an unmatched perspective on reality well worth spending our time and resources on.

Chapter 2

A mathematical framework for periodic systems

2.1 Overview

The translational symmetries of infinite periodic systems are intrinsic to a class of matrices called bi-infinite block-Toeplitz (IBT) matrices. [38] When subjected to the cyclic boundary conditions imposed by the discrete Fourier transformation, these matrices transform into infinite block-circulant (IBC) matrices. A link between the direct-space Toeplitz picture and the reciprocal space circulant picture can be established from the convolution theorem. In this chapter we will define and derive various algebraic relations and operations pertaining to these mathematical constructs, in order to more smoothly and compactly derive equations and expressions for periodic systems later on.

2.2 Infinite Block-Toeplitz matrices

Consider a matrix \mathbf{A} with blocks labeled i, j and the following structure:

$$\mathbf{A}^{ij} = \mathbf{A}^{0, j-i} := A^{j-i}, \quad (2.1)$$

for $i, j \in \mathbb{Z}$, implying an infinite number of blocks. From (2.1) it is evident that all blocks along the diagonal are identical:

$$\mathbf{A}^{(i+n), (j+n)} = A^{(j+n)-(i+n)} = A^{j-i} = \mathbf{A}^{ij}. \quad (2.2)$$

Such a construct is called an *bi-infinite block-Toeplitz* (IBT) matrix. [38] A visualization is provided in Fig. 2.1.

2.3 Transpose of IBT-matrices

We define the blocks in a transposed IBT-matrix \mathbf{A}^T to be

$$(\mathbf{A}^T)^{ij} = (A^{i-j})^T, \quad (2.3)$$

so that both the elements within each block and the block-structure itself are affected. An IBT matrix S is therefore symmetric if

$$S^{i-j} = (S^{j-i})^T. \quad (2.4)$$

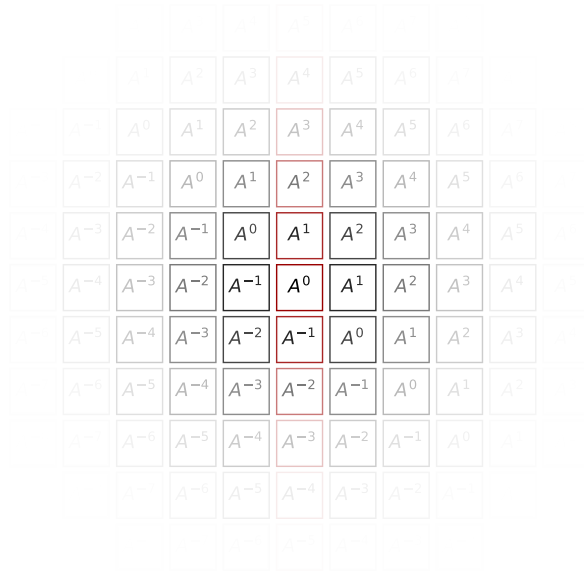


Figure 2.1: The structure of the blocks in the infinite Toeplitz matrix. An arbitrary block is chosen along the diagonal as a point of reference, and is referred to as the *reference block*, here indicated by the highlighted index in the center of the image. All information on the infinite matrix is contained in a single column or row, as indicated by the red highlight.

2.4 The IBT matrix-matrix product

Matrix-matrix multiplication for finite matrices is

$$(\mathbf{AB})_{ij} = \sum_{k=0}^N \mathbf{A}_{ik} \mathbf{B}_{kj}, \quad (2.5)$$

where N is the number of columns in \mathbf{A} and the number of rows in \mathbf{B} (the indices are given in a row-major order). This may be straightforwardly extended to the IBT-matrices by inserting 2.1 into 2.5:

$$(\mathbf{AB})^{ij} = \sum_{k=-\infty}^{\infty} A^{k-i} \cdot B^{j-k}. \quad (2.6)$$

It follows that the product of two IBT-matrices is itself an IBT-matrix, since

$$(\mathbf{AB})^{(i+n),(j+n)} = \sum_{k=-\infty}^{\infty} A^{(k-n)-i} B^{j-(k-n)} = (\mathbf{AB})^{ij}. \quad (2.7)$$

With this taken into account we may write the matrix product of two IBT-matrices as

$$(\mathbf{AB})^{i,j} = (\mathbf{AB})^{0,j-i} \leftrightarrow \sum_{k=-\infty}^{\infty} A^{k-i} \cdot B^{j-k} = \sum_{k=-\infty}^{\infty} A^k \cdot B^{(j-i)-k}. \quad (2.8)$$

Defining $j - i := n$, we finally find that

$$(\mathbf{AB})^n = \sum_{k=-\infty}^{\infty} A^k \cdot B^{n-k}. \quad (2.9)$$

Considered in light of the result in 2.7, it is clear that the set of blocks $(AB)^n$ for $n \in \mathbb{Z}$ contain all the unique blocks of the complete matrix-matrix product.

2.5 Truncated IBT-matrices

Summations this far has been over the entirety of \mathbb{Z} . If we consider instead a matrix \mathbf{A} with only a finite non-zero bandwidth $\mathcal{B}(\mathbf{A}) := [-N, N]$ of blocks along the diagonal such that

$$A^n = 0 \text{ for } |n| > N \quad (2.10)$$

the summation index can be limited to a finite set. We shall refer to this kind of matrix as a truncated IBT-matrix. An illustration is provided in Fig. 2.2.

2.6 The matrix product of truncated IBT-matrices

Considering two truncated IBT-matrices \mathbf{A}, \mathbf{B} with bandwidths

$$\mathcal{B}(\mathbf{A}) = [-N, N], \quad (2.11)$$

and

$$\mathcal{B}(\mathbf{B}) = [-M, M], \quad (2.12)$$

with a finite bandwidth we only need to sum over the non-zero indices in in \mathbf{A} :

$$(\mathbf{AB})^n = \sum_{k=-N}^N A^k \cdot B^{n-k}, \quad (2.13)$$

from which it follows that the bandwidth of the product is

$$\mathcal{B}(\mathbf{AB}) = [-M - N, M + N]. \quad (2.14)$$



Figure 2.2: The structure of the truncated BT-matrix, where blocks outside the bandwidth is zero. In this case $\mathcal{B} = [-2, 2]$.

2.7 Discrete Fourier transform of IBT-matrices

For a truncated IBT matrix \mathbf{A} with bandwidth $\mathcal{B} = [-N, N]$ we now consider the discrete, blockwise Fourier transformation for a given $m \in \mathbb{Z}$

$$\mathcal{F}\{\mathbf{A}\}^m = \sum_{n=-N}^N e^{-i(\frac{2\pi}{M})mn} A^n := \tilde{A}^m, \quad (2.15)$$

where $M = 2N + 1$ is the number of non-zero blocks in A . Due to the periodicity of the complex exponential we have

$$\tilde{A}^{m+M} = \tilde{A}^m, \quad (2.16)$$

thus in eq. (2.15) we need only to consider cases where $m \in \mathcal{B}$. The corresponding backward transform is

$$\mathcal{F}^{-1}\{\tilde{\mathbf{A}}\}^n = \frac{1}{M} \sum_{m=-N}^N e^{-i(\frac{2\pi}{M})mn} \tilde{A}^m = A^n, \quad (2.17)$$

where the normalization factor in front ensures idempotency such that

$$A^n = \frac{1}{M} \sum_{m=-N}^N e^{i(\frac{2\pi}{M})mn} \sum_{n'=-N}^N e^{-i(\frac{2\pi}{M})mn'} A^{n'}. \quad (2.18)$$

which can be recomposed into

$$A^n = \sum_{n'=-N}^N A^{n'} \underbrace{\left(\frac{1}{M} \sum_{m=-N}^N e^{i2\pi \frac{m}{M}(n-n')} \right)}_{\delta_{n,n'}}. \quad (2.19)$$

The transformed matrix behaves no different:

$$\tilde{A}^m = \sum_{m'=-N}^N \tilde{A}^{m'} \underbrace{\left(\frac{1}{M} \sum_{n=-N}^N e^{i2\pi \frac{n}{M}(m'-m)} \right)}_{\delta_{m',m}}. \quad (2.20)$$

These transformations are generally referred to as the discrete Fourier transform (2.15) and the inverse discrete Fourier transform (2.17). [39]

2.8 The discrete Fourier transform matrices

A more compact representation of the discrete Fourier transformations can be given on matrix form

$$\tilde{A}^m = \sum_{n=-N}^N W^{mn} A^n, \quad (2.21)$$

where the elements of W includes the normalization

$$W^{mn} = \frac{1}{\sqrt{M}} \left(e^{-i\frac{2\pi}{M}} \right)^{mn}. \quad (2.22)$$

Similarly, the back transform is

$$A^n = \frac{1}{\sqrt{M}} (W^{-1})^{nm} \tilde{A}^m, \quad (2.23)$$

where

$$(W^{-1})^{nm} = \frac{1}{\sqrt{M}} \left(e^{i\frac{2\pi}{M}} \right)^{mn}. \quad (2.24)$$

2. A mathematical framework for periodic systems

The relationship in eq. 2.19 and 2.20 can thus be reaffirmed by:

$$(W^{-1}W)^{mn} = \frac{1}{M} \sum_k \left(e^{-i\frac{2\pi}{M}} \right)^{mk} \left(e^{i\frac{2\pi}{M}} \right)^{kn} = \delta_{mn}, \quad (2.25)$$

and as such shown to be unitary, since:

$$(W^{-1})^{nm} = (W^{nm})^*. \quad (2.26)$$

2.9 Periodicity in direct space

Note that although the transformation in (2.15) is unitary, it introduces another type of periodicity in the matrix. For example, where we initially had

$$A^{M+n} = \mathbf{0}, \quad (2.27)$$

we will find that after the transformation we have instead

$$A^{M+n} = \sum_{n'=-N}^N A^{n'} \left(\frac{1}{M} \sum_{m=-N}^N e^{i2\pi \frac{m}{M}(M+n-n')} \right) = A^n. \quad (2.28)$$

This demonstrate that the discrete Fourier transform does not conserve the IBT-structure, but instead introduces a new kind of periodicity in the matrix. We shall refer to the resulting structure as an *Infinite Block Circulant* (IBC) matrix.

2.10 Infinite block-circulant matrices

In order to describe the IBC matrices, we define the following (non-standard) *cyclic* operator

$$i \circ N := (i + N) \bmod (2N + 1) - N, \quad (2.29)$$

where mod implies the remainder of integer division. This will produce the following series:

$$\begin{aligned} & \dots, \\ & 0 \circ N = 0, \\ & 1 \circ N = 1, \\ & \dots, \\ & N \circ N = N, \\ & N + 1 \circ N = -N, \\ & \dots \end{aligned} \quad (2.30)$$

Using this notation, we define a IBC matrix to have the structure

$$\mathbf{A}^{ij} = A^{(j-i)\circ N} := A^{n\circ N}. \quad (2.31)$$

For the more visually inclined reader, the circulant operator can be envisioned as rotations on a circular disc, as shown in Fig. 2.3, while the matrix structure is shown in Fig. 2.4

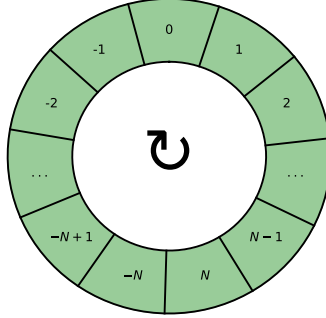


Figure 2.3: It may be clarifying to imagine the circulant operator as cycling through the blocks on a clock-like disc.

2.11 Products with IBC matrices

The product of a truncated IBT matrix \mathbf{A} with $\mathcal{B}(\mathbf{A}) = [-N, N]$ and an $2N + 1$ -periodic IBC matrix \mathbf{B} , is itself an IBC matrix with blocks

$$(AB)_{\text{IBC}}^n = (AB)_{\text{IBC}}^{n \circ N} = \sum_{k=-N}^N A^k \cdot B^{(n-k) \circ N}. \quad (2.32)$$

We shall refer to this kind of product as the IBC-product. For $n = 0$ the block equates to the IBT-product, but for off-diagonal terms we get additional contributions from cyclic blocks in B which in the truncated IBT-case would be zero. For example in the case for $N = 2$, we would have

$$\begin{aligned} (A^{-2}A^{-1}A^0A^1A^2) & \begin{pmatrix} B^0 & B^1 & B^2 & B^{-2} & B^{-1} \\ B^{-1} & B^0 & B^1 & B^2 & B^{-2} \\ B^{-2} & B^{-1} & B^0 & B^1 & B^2 \\ B^2 & B^{-2} & B^{-1} & B^0 & B^1 \\ B^1 & B^2 & B^{-2} & B^{-1} & B^0 \end{pmatrix} \\ & = \begin{pmatrix} (AB)^{-2} \\ (AB)^{-1} \\ (AB)^0 \\ (AB)^1 \\ (AB)^2 \end{pmatrix}_{\text{IBT}} + \begin{pmatrix} A^1B^2 + A^2B^1 \\ A^2B^2 \\ 0 \\ A^{-2}B^{-2} \\ A^{-2}B^{-1} + A^{-1}B^{-2} \end{pmatrix}, \end{aligned} \quad (2.33)$$

where IBT denotes the IBT-product of \mathbf{A} and \mathbf{B} as defined in Eq. 2.13. If both $A^{|n|>1} = 0$ and $B^{|n|>1} = 0$, the latter term is zero and the product thus equates

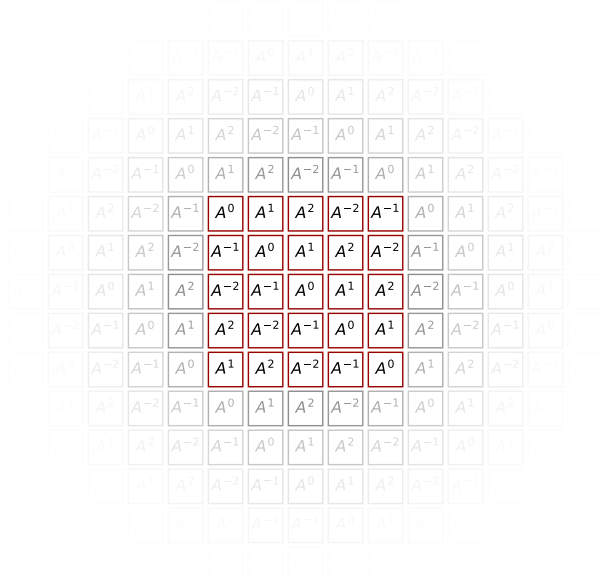


Figure 2.4: The structure of the IBC-matrix. The periodic region is marked in red, indicating that it is infinitely repeated throughout the entire matrix.

to the IBT-product. Again, the visually inclined reader may find it useful to study the provided Fig. 2.5, where the circulant product is envisioned as the sum over sections on rotating discs.

In general, we find that the IBT product can be expressed as

$$(AB)_{\text{IBT}}^n = (AB)_{\text{IBC}}^n - \sum_{k=1}^{k \leq |n|} A^{-\text{sgn}(n)(N-k+1)} B^{n-\text{sgn}(n)(N+k)}, \quad (2.34)$$

where $\text{sgn}(n)$ is the sign of n .

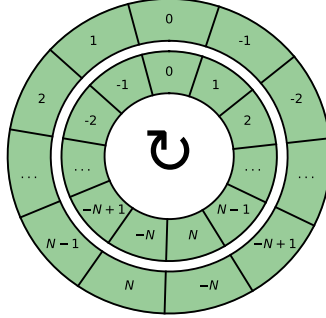


Figure 2.5: The IBC product can be imagined as the sum over aligned blocks in two matrices, here visualized by two rings. Summing together products of the corresponding blocks in the outer and inner rings above would yield the center diagonal block in the IBC product. For the off-diagonal block n in the IBC product, one of the rings would have to be rotated n increments before the blockwise matrix product and summation. Note the opposing sign of the indexes at each increment.

2.12 The convolution theorem

Consider now the inverse Fourier transform of the element-wise multiplication of $\tilde{\mathbf{A}}$ and $\tilde{\mathbf{B}}$ in reciprocal space for a given n :

$$\mathcal{F}^{-1}(\mathcal{F}(\mathbf{A}) * \mathcal{F}(\mathbf{B}))^n = \frac{1}{M} \sum_{m=-N}^N e^{i\frac{2\pi}{M}mn} \tilde{A}^m \tilde{B}^m, \quad (2.35)$$

where blockwise multiplication ($*$) implies that

$$(\mathcal{F}\{\mathbf{A} \cdot \mathbf{B}\})^k = \mathcal{F}\{\mathbf{A}^{-1}\}^k \cdot \mathcal{F}\{\mathbf{B}\}^k. \quad (2.36)$$

We can insert the expansion of \tilde{A}^m and \tilde{B}^m from Eq. 2.15 to find

$$\mathcal{F}^{-1}(\mathcal{F}(\mathbf{A}) * \mathcal{F}(\mathbf{B}))^n = \sum_{n_1=-N}^N \sum_{n_2=-N}^N \underbrace{\left(\frac{1}{M} \sum_{m=-N}^N e^{i\frac{2\pi}{M}m(n-n_1-n_2)} \right)}_{\delta_{n-n_1 \circledast N, n_2}} A^{n_1} B^{n_2}, \quad (2.37)$$

The Kronecker delta is periodic with respect to $n - n_1$ in periods of $2N + 1$, so resolving for this delta results in

$$\mathcal{F}^{-1}(\mathcal{F}(\mathbf{A}) * \mathcal{F}(\mathbf{B}))^n = \sum_{n_1=-N}^N A^{n_1} B^{n-n_1 \circledast N} = (AB)_{IBC}^n. \quad (2.38)$$

2. A mathematical framework for periodic systems

which is the same as Eq. 2.32.

This result is the well known *convolution theorem*, which in our context can be summarized as the fact that the IBC-product can be expressed by a block-wise product of two IBC matrices in reciprocal space. Mathematically, it is stated as follows:

$$\mathcal{F}\{\mathbf{A} \cdot \mathbf{B}\} = \mathcal{F}\{\mathbf{A}\} * \mathcal{F}\{\mathbf{B}\}. \quad (2.39)$$

In our context there is at least two significant consequences of this fact; first, it means that under careful consideration of the result in Eq. 2.32, the IBT product can be exactly computed (by padding outer bands with zeros) or approximated (by assuming the cross-boundary terms to be small) by means of the highly efficient Fast Fourier Transform (FFT) [40] and level 3 BLAS routines. [41] Secondly, it shows that blockwise factorizations of the Fourier transformed matrices carries over to direct space in a well-defined manner which also can be made equivalent by treatment of the cross-boundary terms. This includes diagonalization, Cholesky-factorization, singular value decomposition, inversion and much more. On a more abstract level, it simplifies the linear-algebra notation, since the lattice-summations are implicitly defined in the matrix-product itself, and as such facilitates a smooth theoretical transition between periodic and molecular systems.

2.13 Reciprocal space inversion of IBC-matrices

One practical application of Eq. 2.32 can be made in regards to the inversion of an IBC matrix. Any invertible IBC matrix \mathbf{A} may be inverted by means of a Fourier transformation followed by blockwise inversion at every k-point, which in light of Eq. 2.39 reads

$$\mathcal{F}\{\mathbf{A}^{-1} \cdot \mathbf{A}\} = \mathcal{F}\{\mathbf{I}\} = \mathcal{F}\{\mathbf{A}^{-1}\} * \mathcal{F}\{\mathbf{A}\}. \quad (2.40)$$

Multiplying $(\mathcal{F}\{\mathbf{A}\})^m$ from the right on the above gives

$$\mathcal{F}\{\mathbf{I}\}^m \cdot (\mathcal{F}\{\mathbf{A}\})^m = \mathcal{F}\{\mathbf{A}^{-1}\}^m. \quad (2.41)$$

Furthermore, it is clear that the Fourier transform of the IBC identity matrix is simply identity at every point in k-space

$$(\mathcal{F}\{\mathbf{I}\})^m = \sum_n e^{-i(\frac{2\pi}{M})mn} I^n = I, \quad (2.42)$$

which means that the expression simplifies further, so that

$$(\mathcal{F}\{\mathbf{A}\})^m = \mathcal{F}\{\mathbf{A}^{-1}\}^m. \quad (2.43)$$

Writing out explicitly the Fourier transform of \mathbf{A} , we may thus state the final result by

$$\left(\sum_n e^{-i(\frac{2\pi}{M})mn} A^n \right)^{-1} = \mathcal{F}\{\mathbf{A}^{-1}\}^m, \quad (2.44)$$

which shows that the direct space inverse of a IBC matrix may be found through a (1) Fourier transform, followed by (2) inversion at every k-point, and finally (3) an inverse Fourier transform. The full result may be compactly summarized for a block $(\mathbf{A}^{-1})^n$ in the inverted IBT-matrix \mathbf{A}^{-1}

$$\begin{aligned} (\mathbf{A}^{-1})^n &= \frac{1}{M} \sum_m e^{i(\frac{2\pi}{M})mn} \mathcal{F}\{\mathbf{A}^{-1}\}^m = \\ &\frac{1}{M} \sum_m e^{i(\frac{2\pi}{M})mn} \left(\sum_{n'} e^{-i(\frac{2\pi}{M})mn'} A^{n'} \right)^{-1}. \end{aligned} \quad (2.45)$$

2.14 Unitary IBT and IBC matrices

The result from Eq. 2.32 can also be used in the construction of unitary periodic matrices. For an IBC matrix to be unitary it has to satisfy the condition

$$(\mathbf{U}^\dagger \mathbf{U})_{IBC}^n = \delta_{n,0} \mathbb{I}, \quad (2.46)$$

where \mathbb{I} is the identity matrix. From Eq. 2.35 it is clear that this is equivalent to

$$\frac{1}{M} \sum_{m=-N}^N e^{i\frac{2\pi}{M}mn} \mathcal{F}\{\mathbf{U}^\dagger\}^m \mathcal{F}\{\mathbf{U}\}^m = \delta_{n,0} \mathbb{I}. \quad (2.47)$$

A unitary block U^n can be constructed from any equally sized matrix A^n by means of a matrix exponential [6]:

$$U^n = \exp\left(\frac{1}{2}((A^n)^\dagger - A^n)\right) = \sum_{k=0}^{\infty} \frac{\left(\frac{1}{2}((A^n)^\dagger - A^n)\right)^k}{k!}, \quad (2.48)$$

where $((A^n)^\dagger - A^n)^0 := \mathbb{I}$. If we then replace the transformed blocks in Eq. 2.47 with such unitary blocks, we obtain

$$\frac{1}{M} \sum_{m=-N}^N e^{i\frac{2\pi}{M}mn} (U^\dagger)^m U^m = \delta_{n,0} \mathbb{I}, \quad (2.49)$$

demonstrating the possibility of constructing a unitary IBC matrix in reciprocal space.

A unitary IBT matrix is not as straightforward, as it has to satisfy the condition analogous to Eq. 2.46:

$$(\mathbf{U}^\dagger \mathbf{U})_{IBT}^n = \delta_{n,0} \mathbb{I}. \quad (2.50)$$

A special case can however be noted, namely the IBT matrix \mathbf{U}_0 with blocks

$$U^n = \delta_{n,0} U^0, \quad (2.51)$$

where U^0 is a unitary block.

2.15 Triple products

In many cases, we are interested in inner products of the form

$$(\mathbf{C}^T \mathbf{M} \mathbf{C})^m = \sum_{k \in \mathbb{Z}} (\mathbf{C}^T)^k \sum_{k' \in \mathbb{Z}} M^{k'-k} C^{m-k'} = \sum_{k \in \mathbb{Z}} (\mathbf{C}^T)^k (\mathbf{M} \mathbf{C})^{m-k}, \quad (2.52)$$

where only C is truncated, while M is an infinite but decaying BT-matrix. The summation domain is the infinite \mathbb{Z} , but the product can, however, instead be written

$$(\mathbf{C}^T \mathbf{M} \mathbf{C})^m = \sum_{k \in \mathbb{Z}} \sum_{k' \in \mathbb{Z}} (\mathbf{C}^T)^k M^{k'-k+m} C^{-k'}, \quad (2.53)$$

so that for a given m , we may limit the summations to only non-zero k' and k 's in C . Performing the contractions this way, it is thus possible to ensure that no more than the required blocks in M are computed in advance (or on-the-fly).

Chapter 3

Periodic and infinite many-electron quantum systems

3.1 Overview

The IBT- and IBC-pictures can be used to smoothly extend the familiar and well-proven methods and concepts from general quantum chemistry into the periodic and infinite realm. We review some common techniques for dealing with periodicity in many-body wavefunction methodology, with a focus on local correlation and locality in such systems. In the following discussion, we shall use the standard convention where i, j, k, \dots denotes occupied orbitals, and a, b, c, \dots signifies virtual orbitals. The indices p, q, r, \dots will refer to all orbitals, while μ, ν, γ, \dots represents atomic orbitals.

3.2 The Periodic Hamiltonian

Lattice structures emerge naturally from the electronic many-body problems as a special condition where the bonding between two or more atoms gives rise to new sites where the same type of bonding may occur. We commonly call these systems crystals, and define their periodic dimensionality to be the number of dimensions along which periodicity occurs. While the interactions responsible for keeping this structure together occur at the quantum level, the crystal as a whole can be a macroscopic object; visible to the naked eye and accessible to the touch. For this reason, the atoms in the bulk of the crystal far outnumber the ones at its surface, and the conditions inside the bulk thus closely resembles those of an infinite and perfectly regular lattice where surface effects are non-existent.

This infinite and perfect N_d -dimensional crystal model can be realised as a set of atoms repeatedly placed relative to a set of lattice points $\mathbf{R}_m = \mathbf{R}\mathbf{m}$, where $\mathbf{m} \in \mathbb{Z}^{N_d}$ are called *lattice coordinates* and the columns of the N_d by N_d matrix \mathbf{R} are called the *lattice vectors*. Within the Born-Oppenheimer approximation, we can define a many-electron spin-free and non-relativistic Hamiltonian operator [6] for this system as

$$\begin{aligned}
 \hat{H} = & -\frac{1}{2} \sum_{\mathbf{n} \in \mathbb{Z}^{N_d}} \sum_i \nabla_{\mathbf{n}i}^2 - \sum_{\mathbf{n} \in \mathbb{Z}^{N_d}} \sum_{\mathbf{m} \in \mathbb{Z}^{N_d}} \sum_A \sum_i \frac{Z_A}{|\mathbf{r}_i - \mathbf{R}_{\mathbf{n}} - \mathbf{r}_A + \mathbf{R}_{\mathbf{m}}|} \\
 & + \sum_{\mathbf{n} \in \mathbb{Z}^{N_d}} \left(\sum_i \sum_{j>i} \frac{1}{|\mathbf{r}_i - \mathbf{r}_j|} + \frac{1}{2} \sum_{\mathbf{m} \in \mathbb{Z}^{N_d} \setminus \mathbf{n}} \sum_{ij} \frac{1}{|\mathbf{r}_i - \mathbf{R}_{\mathbf{n}} - \mathbf{r}_j + \mathbf{R}_{\mathbf{m}}|} \right) \quad (3.1) \\
 & + \sum_{\mathbf{n} \in \mathbb{Z}^{N_d}} \left(\sum_A \sum_{B>A} \frac{Z_A Z_B}{|\mathbf{r}_A - \mathbf{r}_B|} + \frac{1}{2} \sum_{\mathbf{m} \in \mathbb{Z}^{N_d} \setminus \mathbf{n}} \sum_{AB} \frac{Z_A Z_B}{|\mathbf{r}_A - \mathbf{R}_{\mathbf{n}} - \mathbf{r}_B + \mathbf{R}_{\mathbf{m}}|} \right),
 \end{aligned}$$

where the indices $\mathbf{n}i, \mathbf{m}j$ refers to electrons i in cell \mathbf{n} and j in cell \mathbf{m} , A, B refers to nuclei, and the terms are respectively the kinetic energy, the electron-nucleus interaction, the electron-electron interaction at $\mathbf{m} = \mathbf{0}$, the electron-electron interaction for the remaining crystal, the nucleus-nucleus interaction at $\mathbf{m} = \mathbf{0}$ and nucleus-nucleus interaction for the remaining crystal. Note that the expression is equivalent to the molecular case when \mathbf{n} and \mathbf{m} are confined to simply $\mathbf{0}$, and decouples to an infinite set of molecular cases when the elements in the columns of \mathbf{R} goes to infinity. The realistic Hamiltonian may in fact also be recovered by letting \mathbf{n} and \mathbf{m} be in the actual set of lattice points in the macroscopic crystal. We will however never actually do the latter, since it curiously turns out that *macroscopically large* is much more difficult to deal with than *infinitely large*.

3.3 The independent particle model

As for all quantum mechanical systems, the exact solutions of the time-independent Schrödinger equation can in theory be found by diagonalizing \hat{H} in a complete basis. Such a calculation would however be too computationally costly for most practical purposes, so quantum chemistry is instead typically concerned with approximate wavefunctions for the ground state within a subspace of the Hilbert space spanned by all possible eigenfunctions $|\Psi\rangle$ of \hat{H} .

Like its molecular counterpart, the periodic Hamiltonian in Eq. 3.1 is a Hermitian operator and bounded below. We may therefore apply the variational method [6] where a ground state solution is found by minimizing the energy of a parameterized trial function $\Phi(\mathbf{r}_0, \mathbf{r}_1, \dots, \mathbf{r}_N)$, where \mathbf{r}_i is the coordinate of electron i , so that

$$E(\Phi) = \frac{\langle \Phi | \hat{H} | \Phi \rangle}{\langle \Phi | \Phi \rangle} \geq E_0, \quad (3.2)$$

and E_0 is the true ground-state energy of the system.

Although the only technical requirement of this trial function is that it is well defined in terms of Eq. 3.2, we would like it to account for important properties of the exact wavefunction such as describing the correct number of electrons, antisymmetry, size-extensivity and orthogonality. [6] Furthermore, it should satisfy the system-specific boundary conditions.

Another feature of the Hamiltonian operator is that it can be partitioned into terms involving only single particles and terms involving (in our case) two particles. In the absence of two-particle terms, the Schrödinger equation would be separable, and an exact solution could be found within the tensor product of all the independent-particle Hilbert spaces. We call such a component the Hartree product:

$$\Phi_{\text{Hartree}} := \prod_p^N \varphi_p(\mathbf{r}_p) \quad (3.3)$$

In order to make the Hartree product antisymmetric, we can explicitly include terms of products in the trial function where the coordinates of the single particles are permuted with the appropriate sign in such a way that the full series satisfy the antisymmetry requirement. Such a construct is called a Slater determinant, and the minimization of the energy of this parameterized determinant under the condition that the single particle states remain orthogonal is commonly referred to as the Hartree-Fock method.

The independent particle model is of central importance in quantum chemistry, since it provides the most common practical starting ground for approximating the wavefunction for molecular and periodic systems, while it simultaneously forms the conceptual basis for orbitals.

3.4 The periodic wavefunction

There are many similarities between the periodic Hamiltonian in Eq. 3.1 and the IBT structure presented in Chapter 2. The interactions as seen relative to a single cell are the same for every coordinate of the lattice, meaning that the single particle part of the potential must be invariant with respect to lattice translations. Hence, electrons associated with any cell should correspond to identical densities relative to the cell in which they belong. In mathematical terms, the single particle part of the Hamiltonian commute with lattice translations:

$$[\hat{\mathbf{H}}, \hat{\mathbf{T}}_{\mathbf{m}}] = 0, \quad (3.4)$$

where $\hat{\mathbf{T}}_{\mathbf{m}}\varphi(\mathbf{r}) = \varphi(\mathbf{r} - \mathbf{R}_{\mathbf{m}})$. Based on the work of Gaston Floquet [42], Felix Bloch [2] and subsequently by Ralph Kronig and William Penney[3] pointed out that this implies that they share a common set of eigenstates, conventionally named the *Bloch functions* [43] (BF). Consequently, the eigenstates of a one body $\hat{\mathbf{H}}$ can be chosen as the product of a plane wave and a function with the same periodicity as the lattice. [44, 45] This fact, commonly referred to as Bloch's theorem, lets us construct our basis from the eigenstates of the translation operator:

$$\hat{T}_{-\mathbf{m}}\psi(\mathbf{r}) = e^{i\mathbf{k}\cdot\mathbf{R}_{\mathbf{m}}}\psi(\mathbf{r}) \quad (3.5)$$

where the vectors \mathbf{k} are called *wave vectors* [44] and defines points in a *reciprocal* lattice $\{\mathbf{k}_{\mathbf{n}}\}$ where for any lattice point $\mathbf{R}_{\mathbf{m}}$ there is a $\mathbf{k}_{\mathbf{n}}$ so that

$$e^{i\mathbf{k}_{\mathbf{n}}\cdot\mathbf{R}_{\mathbf{m}}} = 1. \quad (3.6)$$

3. Periodic and infinite many-electron quantum systems

This condition is satisfied whenever $\mathbf{k}_n \cdot \mathbf{R}_m = M2\pi$ for any $M \in \mathbb{Z}$, and the set $\{\mathbf{k}_n\}$ for $M = 1$ is sufficient to span the reciprocal lattice. A Bloch function can within this context be expressed [44]:

$$\psi_{\mathbf{k}} = e^{i\mathbf{k} \cdot \mathbf{r}} u_{\mathbf{k}}(\mathbf{r}), \quad (3.7)$$

where the function $u_{\mathbf{k}}(\mathbf{r} + \mathbf{R}_m) = u_{\mathbf{k}}(\mathbf{r})$ for $\mathbf{m} \in \mathbb{Z}^{N_d}$. It follows that for a finite set of \mathbf{k} 's, any linear combination of functions of the type in Eq. 3.7 will satisfy the following condition:

$$\psi(\mathbf{r} + \mathbf{R}_M \cdot \mathbf{m}) = \psi(\mathbf{r}), \quad (3.8)$$

for $\mathbf{m} \in \mathbb{Z}^3$ where the columns of the 3 by 3 matrix \mathbf{R}_M contains multiples of the lattice vectors, defining the so-called Born-von Karman supercell. [44] This property of the periodic wavefunction emerge from truncations in the set $\{\mathbf{k}\}$, and is commonly referred to as the Born-von Karman boundary condition. [44, 45, 46] It is essentially the same as the one we saw emerge from the discrete Fourier transform as a structure in the IBC matrices in Chapter 2.

3.5 Periodic Hartree-Fock theory

In a cell-wise finite (but lattice-wise infinite) basis $\{\chi_{\mu}^{\mathbf{m}}\}$ the Hartree-Fock Hamiltonian is referred to as the Fock matrix, and takes an IBT form with elements

$$\mathbf{F}_{\mu\nu}^{\mathbf{m}} = \mathbf{T}_{\mu\nu}^{\mathbf{m}} + \mathbf{Z}_{\mu\nu}^{\mathbf{m}} + \mathbf{J}_{\mu\nu}^{\mathbf{m}} + \mathbf{K}_{\mu\nu}^{\mathbf{m}}. \quad (3.9)$$

The constituent terms in the above are the kinetic integrals

$$\mathbf{T}_{\mu\nu}^{\mathbf{m}} = -\frac{1}{2} \langle \chi_{\mu}^{\mathbf{0}} | \nabla^2 | \chi_{\nu}^{\mathbf{m}} \rangle, \quad (3.10)$$

the nuclear integrals

$$\mathbf{Z}_{\mu\nu}^{\mathbf{m}} = \sum_{\mathbf{n} \in \mathbb{Z}^{N_d}} \sum_A^{N_A} \langle \chi_{\mu}^{\mathbf{0}} | \frac{1}{|\mathbf{r} - \mathbf{r}_A - \mathbf{R}_n|} | \chi_{\nu}^{\mathbf{m}} \rangle, \quad (3.11)$$

where the index A runs over each atom in the cell. We furthermore have the bi-electronic coulomb term

$$\mathbf{J}_{\mu\nu}^{\mathbf{m}} = \sum_{\mathbf{n}, \mathbf{n}' \in \mathbb{Z}^{N_d}} \sum_{\gamma\delta}^{N_{\text{AO, cell}}} \mathbf{P}_{\gamma\delta}^{\mathbf{n}' - \mathbf{n}} (\chi_{\mu}^{\mathbf{0}} \chi_{\nu}^{\mathbf{m}} | \chi_{\gamma}^{\mathbf{n}} \chi_{\delta}^{\mathbf{n}'}), \quad (3.12)$$

and the exchange term

$$\mathbf{K}_{\mu\nu}^{\mathbf{m}} = -\frac{1}{2} \sum_{\mathbf{n}, \mathbf{n}' \in \mathbb{Z}^{N_d}} \sum_{\gamma\delta}^{N_{\text{AO, cell}}} \mathbf{P}_{\gamma\delta}^{\mathbf{n}' - \mathbf{n}} (\chi_{\mu}^{\mathbf{0}} \chi_{\gamma}^{\mathbf{n}} | \chi_{\nu}^{\mathbf{m}} \chi_{\delta}^{\mathbf{n}'}), \quad (3.13)$$

where

$$(\chi_{\mu}^0 \chi_{\nu}^{\mathbf{m}} | \chi_{\gamma}^{\mathbf{n}} \chi_{\delta}^{\mathbf{n}'}) := \iint \frac{\chi_{\mu}^*(\mathbf{r}) \chi_{\nu}(\mathbf{r} - \mathbf{R}_{\mathbf{m}}) \chi_{\gamma}^*(\mathbf{r}' - \mathbf{R}_{\mathbf{n}}) \chi_{\delta}(\mathbf{r}' - \mathbf{R}_{\mathbf{n}'})}{|\mathbf{r} - \mathbf{r}'|} d\mathbf{r}' d\mathbf{r}. \quad (3.14)$$

and \mathbf{P} is the density matrix constructed from the coefficient matrices \mathbf{C}_{occ} containing the expansion coefficients for the occupied orbitals

$$\mathbf{P}_{\mu\nu}^{\mathbf{m}} = (\mathbf{C}_{\text{occ}} \mathbf{C}_{\text{occ}}^T)_{\mu\nu}^{\mathbf{m}}, \quad (3.15)$$

where the IBT matrix product (Eq. 2.2) is implied.

The Hartree-Fock equations decouple with respect to wave vectors in reciprocal space [47], so in order to diagonalize the Fock matrix, it can be Fourier transformed:

$$\tilde{\mathbf{F}}^{\mathbf{n}} = \sum_{\mathbf{m} \in \mathbb{Z}^{Nd}} e^{-i\mathbf{k}_{\mathbf{n}} \cdot \mathbf{R}_{\mathbf{m}}} \mathbf{F}^{\mathbf{m}}, \quad (3.16)$$

whereby the following generalized eigenvalue problem is solved separately for every \mathbf{n} :

$$\tilde{\mathbf{F}}^{\mathbf{n}} \tilde{\mathbf{C}}^{\mathbf{n}} = \tilde{\mathbf{S}}^{\mathbf{n}} \tilde{\mathbf{C}}^{\mathbf{n}} \epsilon(\mathbf{n}) \quad (3.17)$$

This decoupling of the equations in reciprocal space greatly alleviates the computational cost of the optimization, since it reduces the problem of diagonalizing an infinite matrix to an infinite number of diagonalizations of finite matrices (of dimension N_{AO} by N_{AO}).

As with the molecular equations, the periodic Hartree-Fock equations are solved iteratively to reach self-consistency. The Fock matrix has to be constructed at every iteration, which requires an inverse transform of the density matrix using interpolation techniques with respect to the mesh in reciprocal space. [43]

This procedure yields the canonical set of Bloch orbitals that diagonalizes each block in the Fourier transformed Fock matrix, such that we have

$$\tilde{\mathbf{F}}_{ij}^{\mathbf{n}} = \epsilon_i^{\mathbf{n}} \delta_{ij}, \quad (3.18)$$

where the set of eigenvalues $\epsilon_i^{\mathbf{n}}$ describes the energy band structure of the periodic system.

3.6 Wannier orbitals

The Bloch functions as presented in Eq. 3.7 may appear unfamiliar from a quantum chemistry perspective, since we expect them to describe the electronic wavefunction in the neighbourhood of atoms. They are intrinsically non-local, non-normalizable in \mathbb{R}^3 and not much like the more common-place Gaussian distributions [6] used in molecular calculations. The crystalline orbitals, as linear combinations of Bloch functions, have matrix elements defined with respect to Born-von Karman boundary conditions [46] which can be inconvenient in many quantum chemistry applications. [48] Locality is also essential in order to achieve linear scaling in post Hartree-Fock methods. [5, 8, 10, 11, 12, 13, 49]

3. Periodic and infinite many-electron quantum systems

This conceptual gap between the local and infinite picture has in many ways separated the world of quantum chemistry from the world of material science, despite they are focused on the same interactions between the same actors, on similar stages. ¹

Efforts to bridge this gap was first undertaken by Gregory Wannier in 1937 [50], by showing that for insulators, it is possible to construct local orbitals as linear combinations of Bloch-functions by means of an inverse Fourier transform. A few years later, Per-Olov Löwdin took the opposite approach and constructed Bloch-functions using a linear combination of non-orthogonal local functions. [46] The local representation of the periodic orbitals available for insulators is referred to as Wannier functions [48, 51, 52].

In a Gaussian basis $\{\chi_\mu^{\mathbf{m}}\}$, where μ is the atomic orbital index and the functions are positioned relative to \mathbf{R}_m , the atomic Bloch functions are [48]

$$\tilde{\chi}_\mu^{\mathbf{n}}(\mathbf{r}) := \sum_{\mathbf{m} \in \mathbb{Z}^{N_d}} e^{-i\mathbf{k}_n \mathbf{R}_m} \chi_\mu^{\mathbf{m}}(\mathbf{r}), \quad (3.19)$$

so that an orbital p can be expressed as a linear combination:

$$\tilde{\varphi}_p^{\mathbf{k}_n}(\mathbf{r}) = \sum_{\mu}^{N_{AO}} \tilde{C}_{\mu p}^{\mathbf{n}} \tilde{\chi}_\mu^{\mathbf{n}}(\mathbf{r}), \quad (3.20)$$

where the matrix $\tilde{\mathbf{C}}$ contains the expansion coefficients that can be varied in order to minimize the energy. The post Hartree-Fock determination of Wannier orbitals may then in general be expressed

$$\varphi_p^{\mathbf{n}}(\mathbf{r}) = \sum_{\mathbf{n}'} \sum_{\mu} \left(\frac{1}{\sqrt{M}} \sum_{\mathbf{m}} e^{i\frac{2\pi}{M} \mathbf{m}(\mathbf{n}' - \mathbf{n})} \tilde{U}^{\mathbf{m}} \tilde{C}^{\mathbf{m}} \right)_{\mu p} \chi_\mu^{\mathbf{n}'}(\mathbf{r}) = \sum_{\mathbf{n}'} \sum_{\mu} C_{\mu p}^{\mathbf{n}' - \mathbf{n}} \chi_\mu^{\mathbf{n}'}(\mathbf{r}), \quad (3.21)$$

where M is the number of cells in the Born-von Karman supercell and the blocks in $\tilde{\mathbf{U}}$ are unitary matrices that only rotates within the occupied and virtual space separately. [52] The non-uniqueness of the Wannier orbitals signified by $\tilde{\mathbf{U}}$ is analogous to the non-canonical molecular orbitals, in the sense that as long as the Brillouin condition [6] is satisfied:

$$F_{ia}^{\mathbf{n}} = (\mathbf{C}^T \mathbf{F}_{AO} \mathbf{C})_{ia}^{\mathbf{n}} = 0, \quad (3.22)$$

the representation is an equally valid solution to the Hartree-Fock equations as the canonical one. Note that the matrix product in the above is the IBC-product as defined in Eq. 2.32.

In addition to potentially² having the supercell-cyclicity of the Bloch-function, the Wannier orbitals are translationally orthonormal:

$$\int_{\Omega} \varphi_p^{\mathbf{m}}(\mathbf{r})^* \varphi_q^{\mathbf{m}'}(\mathbf{r}) d\mathbf{r} = (\mathbf{C}^T \mathbf{S} \mathbf{C})_{pq}^{\mathbf{m}' - \mathbf{m}} = \delta_{\mathbf{m}\mathbf{m}'} \delta_{pq}, \quad (3.23)$$

¹The stages are subject to different boundary conditions.

²Depending on whether or not Born-von Karman boundary conditions or interpolation techniques are applied.

where Ω is the volume of the Born-von Karman supercell, S is the IBT overlap matrix with elements $S_{\mu\nu}^{\mathbf{m}} = (\mathbf{0}\mu|\mathbf{m}\nu)$ and

$$\varphi_p^{\mathbf{m}}(\mathbf{r}) := \hat{T}_{\mathbf{m}}\varphi_p^{\mathbf{0}}(\mathbf{r}) = \varphi_p^{\mathbf{0}}(\mathbf{r} - \mathbf{R}_{\mathbf{m}}). \quad (3.24)$$

The Wannier orbitals can also be determined a priori either by a cluster embedding [53] or by inclusion of a penalty operator in the Fock-matrix. [54] Under the assumption that no other effect limits the variational flexibility of such a representation, we may consider these kind of Wannier orbitals to be equivalent to the ones representing the infinite crystal, i.e. a fully IBT representation. If we instead construct the Wannier orbitals as in Eq. 3.21, they are subject to the same boundary condition as the Bloch-orbitals. The extent to which these two interpretations agree can be measured by Eq. 3.23; if the IBT-product is applied in the inner product and the expression holds true, the cyclic Wannier orbitals are close to equivalent to the infinite case.

With the theory discussed this far, it is clear that there are several paths that will bring us to the correlation energy of an insulator. Specifically, considering exclusively the choice of basis and representation, we have four in total; reciprocal space representations using either a plane wave [55, 56, 57] or local [58, 59, 60, 61, 62] basis, and the Wannier representation using again either plane waves³ or a local [63, 64, 65, 66, 67, 68, 69, 70] basis. We shall follow the path provided by the Wannier representation using Gaussian basis functions.

3.7 Locality in periodic systems

Our interest in locality in periodic systems in the current context is that it is a prerequisite for the application of local correlation methods, which, in turn, may open the door to linear scaling. The explicit connection will be dealt with in more detail later, but for now it is sufficient to note that first, we require the orbitals to at least exhibit some distance decay in order to apply such methods in the first place. Secondly, a higher degree of locality of the orbital spaces typically means better performance in the local method. For this reason, we shall investigate closer how locality can be defined, measured and achieved for periodic systems.

A Wannier orbital is basically a linear combination of Bloch orbitals. The molecular concept of locality is usually loosely interpreted as a measure of how confined a quantity such as an orbital is in \mathbb{R}^3 space. [71] Hence, a Wannier orbital subject to Born-von Karman boundary conditions can never truly be local in the same way we know it for molecular systems unless the Born-von Karman supercell is infinitely large. If we instead consider locality as a measure of the degree of spatial confinement within a supercell, we may extend many well-proven measures from molecular quantum chemistry to the periodic realm by using the formalism derived in Chapter 2.

³The author could not find any attempts at pursuing this path in the context of wavefunction methods, but Wannier functions in a plane wave basis in general certainly have their place in material science. [52]

3. Periodic and infinite many-electron quantum systems

In order to measure locality of an orbital, we typically analyze its spatial shape and location in terms of Cartesian moments [71] or basis projections [29]. With both the Wannier functions and atomic Bloch functions defined in fundamentally the same Gaussian basis sets, the integrals required to perform such analysis are the same as in the molecular case. However, a slight complication comes to light when we realize that the Cartesian moment matrices are neither IBT or IBC, but rather are explicitly dependent on the lattice, as can be demonstrated with the first order Cartesian moment:

$$\langle \mathbf{0}\mu | \hat{r} | \mathbf{0}\mu \rangle = \langle \mathbf{M}\mu | \hat{r} | \mathbf{M}\mu \rangle - \mathbf{R}_\mathbf{M}. \quad (3.25)$$

In order to generalize the intuitive relation above, and moreover incorporate this structure into the extension of locality measures to the periodic case, we shall consider the translation operator \hat{T} in more detail. We have

$$\hat{T}_\mathbf{L} \chi_\alpha(\mathbf{x}) := \chi_\alpha(\mathbf{x} - \mathbf{L}) := |\mathbf{L}\alpha\rangle. \quad (3.26)$$

Its conjugate operator is

$$\left(\hat{T}_\mathbf{L}\right)^\dagger = \hat{T}_{-\mathbf{L}} \rightarrow \hat{T}_\mathbf{L} \left(\hat{T}_\mathbf{L}\right)^\dagger = \left(\hat{T}_\mathbf{L}\right)^\dagger \hat{T}_\mathbf{L} = \mathbb{1}. \quad (3.27)$$

The position operator, given by

$$\hat{r} = \hat{r}_x \hat{i} + \hat{r}_y \hat{j} + \hat{r}_z \hat{k}, \quad (3.28)$$

does not commute with lattice translations, as can be seen by considering the following relation:

$$\hat{r} \hat{T}_\mathbf{L} = (\mathbf{r} - \mathbf{L}) \hat{T}_\mathbf{L}, \quad (3.29)$$

hence, we find the commutation relation:

$$\left[\hat{T}_\mathbf{L}, \hat{r}\right] = \hat{T}_\mathbf{L} \hat{r} - \hat{r} \hat{T}_\mathbf{L} = \mathbf{L} \hat{T}_\mathbf{L}. \quad (3.30)$$

The perhaps most commonly known measure of locality is the *Foster-Boys* function [26, 27], which in the molecular case measures the variance for an orbital p by:

$$f_{\text{fb}} = \sum_p (\langle p | \hat{r}^2 | p \rangle - \langle p | \hat{r} | p \rangle^2) := \sum_p \sigma_p^2. \quad (3.31)$$

The general way in which the above can be extended to Wannier orbitals may be illuminated by considering only the first term. If we substitute the orbital p with a Wannier orbital from Eq. 3.21 (with U chosen to be \mathbb{I}), we find

$$\langle \mathbf{0}p | \hat{r}^2 | \mathbf{0}p \rangle = \int_{\mathbb{R}^3} \left(\sum_{\mathbf{n}} \sum_{\mu} C_{\mu p}^{\mathbf{n}} \chi_{\mu}^{\mathbf{n}}(\mathbf{r}) \hat{r}^2 \sum_{\mathbf{m}} \sum_{\nu} C_{\nu p}^{\mathbf{m}} \chi_{\nu}^{\mathbf{m}}(\mathbf{r}) \right) d\mathbf{r}. \quad (3.32)$$

With a slight restructuring of the expression, explicit use of the translation operator (Eq. 3.26) and using the notation $\chi_{\mu}^{\mathbf{n}} := |\mathbf{n}\mu\rangle$, we may cast the above as

$$\langle \mathbf{0}p | \hat{r}^2 | \mathbf{0}p \rangle = \sum_{\mathbf{n}, \mathbf{m}} \sum_{\mu\nu} C_{\mu p}^{\mathbf{n}} \langle \mathbf{0}\mu | \hat{T}_{-\mathbf{n}} \hat{r} \hat{r} | \mathbf{m}\nu \rangle C_{\nu p}^{\mathbf{m}}. \quad (3.33)$$

We furthermore apply the commutation relation in Eq. 3.30, so that

$$\hat{T}_{-\mathbf{n}}\hat{r}\hat{r} = (\hat{r} - \mathbf{R}_{\mathbf{n}})^2\hat{T}_{-\mathbf{n}}, \quad (3.34)$$

in order to find that

$$\langle \mathbf{0}p|\hat{r}^2|\mathbf{0}p\rangle = \sum_{\mathbf{n},\mathbf{m}} \sum_{\mu\nu} C_{\mu p}^{\mathbf{n}} \langle \mathbf{0}\mu|(\hat{r} - \mathbf{R}_{\mathbf{n}})^2|\mathbf{m} - \mathbf{n}\nu\rangle C_{\nu p}^{\mathbf{m}}. \quad (3.35)$$

Taking into account that $\hat{r}^2 = \sum_{i=x,y,z} \hat{r}_i^2$, the above can now be refactored into three terms

$$\begin{aligned} \langle \mathbf{0}p|\hat{r}^2|\mathbf{0}p\rangle = & \sum_{i=x,y,z} \sum_{\mathbf{n},\mathbf{m}} \sum_{\mu\nu} \left(C_{\mu p}^{\mathbf{n}} \langle \mathbf{0}\mu|\hat{r}_i^2|\mathbf{m} - \mathbf{n}\nu\rangle C_{\nu p}^{\mathbf{m}} - \right. \\ & 2\mathbf{R}_{\mathbf{n},i} C_{\mu p}^{\mathbf{n}} \langle \mathbf{0}\mu|\hat{r}_i|\mathbf{m} - \mathbf{n}\nu\rangle C_{\nu p}^{\mathbf{m}} + \\ & \left. \mathbf{R}_{\mathbf{n},i}^2 C_{\mu p}^{\mathbf{n}} \langle \mathbf{0}\mu|\mathbf{m} - \mathbf{n}\nu\rangle C_{\nu p}^{\mathbf{m}} \right), \end{aligned} \quad (3.36)$$

where we can recognize the IBT structure of the matrix elements being contracted from the triple products discussed in section 2.15. The full inner product may therefore be recast in terms of IBT or IBC products⁴, so that

$$\langle \mathbf{0}p|\hat{r}^2|\mathbf{0}p\rangle = \sum_{i=x,y,z} (\mathbf{C}^T \mathbf{M}_i^2 \mathbf{C} - 2\mathbf{R}_i \odot \mathbf{C}^T \mathbf{M}_i \mathbf{C} + \mathbf{R}_i^2 \odot \mathbf{C}^T \mathbf{S} \mathbf{C})_{pp}^{\mathbf{0}} := (\mathbf{R}_{MO}^2)_{pp}^{\mathbf{0}}, \quad (3.37)$$

where

$$(\mathbf{R}_i \odot \mathbf{A})^{\mathbf{m}} := R_{\mathbf{m},i} \mathbf{A}^{\mathbf{m}}. \quad (3.38)$$

and \mathbf{M}_i are the cartesian moments provided as IBT-matrices in AO-basis.

By the same logic for the second term in Eq. 3.31, we will find that the periodic Foster-Boys function can be expressed by

$$\begin{aligned} f_{fb}(\mathbf{C}) = & \sum_{i=x,y,z} \sum_p \left((\mathbf{C}^T \mathbf{M}_i^2 \mathbf{C} + 2\mathbf{R}_i \odot \mathbf{C}^T \mathbf{M}_i \mathbf{C} + \mathbf{R}_i^2 \odot \mathbf{C}^T \mathbf{S} \mathbf{C}) - \right. \\ & \left. (\mathbf{C}^T \mathbf{M}_i \mathbf{C} + \mathbf{R}_i \odot \mathbf{C}^T \mathbf{S} \mathbf{C})^2 \right)_{pp}^{\mathbf{0}}. \end{aligned} \quad (3.39)$$

The orbital variance, as present in the Foster-Boys function, is part of a family of measures of distributive properties which generally may be expressed as *powers of moments* [72]. In the general case, we can define a class of measurements on orbital sets as *m*th powers of the *X*th moment (PXM-*m*):

$$f_{\text{PXM-}m} = \sum_p \left(\langle p|(\hat{r} - \langle p|\hat{r}|p\rangle)^X|p\rangle \right)^m. \quad (3.40)$$

⁴In this case it actually does not make any difference whether the IBT or IBC product is applied, since we are only interested in the reference cell matrix elements which are exactly the same in both cases.

3. Periodic and infinite many-electron quantum systems

In this context, Foster-Boys corresponds to PSM-1 (first power of the second moment). A motivation for exploring higher powers is that in the context of optimization, the Foster-Boys function may unintentionally indicate overall locality at the cost of a single (or a few) orbitals. This could then in turn compromise the local correlation calculation with excessively large orbital spaces. The PSM-2 function was therefore devised by Jansik et al. [73] in order to penalize outliers, so that it is more likely to give proper overall locality in terms of orbital variance.

Higher order moments measures other distributive properties. The fourth moment (PFM-m) is of special interest, since it in relation to the second moment provides a measure of the magnitude of the tails in the set. [72] The complicated tails of the Wannier functions is a result of the strong demands with respect to translational orthogonality in periodic systems. The PFM-2 function is

$$f_{\text{PFM-2}} = \sum_p \left(\langle p | (\hat{r} - \langle p | \hat{r} | p \rangle)^4 | p \rangle \right)^2 := \sum_p (\sigma_{4,pp})^2. \quad (3.41)$$

Deriving the periodic PFM-2 function follows the same logic we used for the Foster-Boys function, but due to many terms and higher order moments it is most accurately done by computer generation. We shall therefore not derive the PFM-2 expression here, but rather state the result compactly:

$$\begin{aligned} \sigma_4(\mathbf{C}) = & \sum_{i=x,y,z} \left(\mathbf{M}_i^4 - 4\mathbf{M}_i^3\mathbf{M}_i + 6\mathbf{M}_i^2(\mathbf{M}_i)^2 - 3(\mathbf{M}_i)^4 \right) + \\ & 2 \left(\mathbf{M}_{x^2}\mathbf{M}_{y^2} + \mathbf{M}_{x^2}\mathbf{M}_{z^2} + \mathbf{M}_{y^2}\mathbf{M}_{z^2} \right) + \\ & 2 \left(\mathbf{M}_{x^2}(\mathbf{M}_y)^2 + \mathbf{M}_{x^2}(\mathbf{M}_z)^2 + \mathbf{M}_{y^2}(\mathbf{M}_x)^2 + \right. \\ & \left. \mathbf{M}_{y^2}(\mathbf{M}_z)^2 + \mathbf{M}_{z^2}(\mathbf{M}_x)^2 + \mathbf{M}_{z^2}(\mathbf{M}_y)^2 \right) - \\ & 4 \left(\mathbf{M}_{x^2y}\mathbf{M}_y + \mathbf{M}_{x^2z}\mathbf{M}_z + \mathbf{M}_{xy^2}\mathbf{M}_x + \right. \\ & \left. \mathbf{M}_{xz^2}\mathbf{M}_x + \mathbf{M}_{y^2z}\mathbf{M}_z + \mathbf{M}_{yz^2}\mathbf{M}_y \right) - \\ & 6 \left((\mathbf{M}_x)^2(\mathbf{M}_y)^2 + (\mathbf{M}_x)^2(\mathbf{M}_z)^2 + (\mathbf{M}_y)^2(\mathbf{M}_z)^2 \right) + \\ & 8 \left(\mathbf{M}_{xz}\mathbf{M}_x\mathbf{M}_z + \mathbf{M}_{xy}\mathbf{M}_x\mathbf{M}_y + \mathbf{M}_{yz}\mathbf{M}_y\mathbf{M}_z \right). \end{aligned} \quad (3.42)$$

The products between the Cartesian moment matrices are here defined to be elementwise, to be distinguished with parenthesis, so for instance

$$(\mathbf{M}_i)^2(\mathbf{M}_j)^2 = \mathbf{M}_i * \mathbf{M}_i * \mathbf{M}_j * \mathbf{M}_j, \quad (3.43)$$

and where for brevity we have defined

$$\begin{aligned}
 \mathbf{M}_{i^4} = & \mathbf{C}^T \mathbf{M}_{i^4,ao} \mathbf{C} - \\
 & 4\mathbf{R}_i \odot \mathbf{C}^T \mathbf{M}_{i^3,ao} \mathbf{C} + \\
 & 6\mathbf{R}_i^2 \odot \mathbf{C}^T \mathbf{M}_{i^2,ao} \mathbf{C} - \\
 & 4\mathbf{R}_i^3 \odot \mathbf{C}^T \mathbf{M}_{i,ao} \mathbf{C} + \\
 & \mathbf{R}_i^4 \odot \mathbf{C}^T \mathbf{S}_{ao} \mathbf{C},
 \end{aligned} \tag{3.44}$$

$$\begin{aligned}
 \mathbf{M}_{i^3} = & \mathbf{C}^T \mathbf{M}_{i^3,ao} \mathbf{C} - \\
 & 3\mathbf{R}_i \odot \mathbf{C}^T \mathbf{M}_{i^2,ao} \mathbf{C} + \\
 & 3\mathbf{R}_i^2 \odot \mathbf{C}^T \mathbf{M}_{i,ao} \mathbf{C} - \\
 & \mathbf{R}_i^3 \odot \mathbf{C}^T \mathbf{S}_{ao} \mathbf{C},
 \end{aligned} \tag{3.45}$$

$$\begin{aligned}
 \mathbf{M}_{i^2} = & \mathbf{C}^T \mathbf{M}_{i^2,ao} \mathbf{C} - \\
 & 2\mathbf{R}_i \odot \mathbf{C}^T \mathbf{M}_{i,ao} \mathbf{C} + \\
 & \mathbf{R}_i^2 \odot \mathbf{C}^T \mathbf{S}_{ao} \mathbf{C},
 \end{aligned} \tag{3.46}$$

$$\begin{aligned}
 \mathbf{M}_{ij} = & \mathbf{C}^T \mathbf{M}_{ij,ao} \mathbf{C} - \\
 & \mathbf{R}_i \odot \mathbf{C}^T \mathbf{M}_{i,ao} \mathbf{C} - \\
 & \mathbf{R}_j \odot \mathbf{C}^T \mathbf{M}_{j,ao} \mathbf{C} + \\
 & \mathbf{R}_i \mathbf{R}_j \odot \mathbf{C}^T \mathbf{S}_{ao} \mathbf{C},
 \end{aligned} \tag{3.47}$$

$$\begin{aligned}
 \mathbf{M}_{i^2j} = & \mathbf{C}^T \mathbf{M}_{i^2j,ao} \mathbf{C} - \\
 & 2\mathbf{R}_j \odot \mathbf{C}^T \mathbf{M}_{ji,ao} \mathbf{C} + \\
 & \mathbf{R}_j^2 \odot \mathbf{C}^T \mathbf{M}_{i,ao} \mathbf{C} - \\
 & \mathbf{R}_i \odot \mathbf{C}^T \mathbf{M}_{j^2,ao} \mathbf{C} + \\
 & 2\mathbf{R}_i \mathbf{R}_j \odot \mathbf{C}^T \mathbf{M}_{j,ao} \mathbf{C} - \\
 & \mathbf{R}_j^2 \mathbf{R}_i \odot \mathbf{C}^T \mathbf{S}_{ao} \mathbf{C},
 \end{aligned} \tag{3.48}$$

and

$$\begin{aligned}
 \mathbf{M}_{i^2j^2} = & \mathbf{C}^T \mathbf{M}_{i^2j^2,ao} \mathbf{C} - \\
 & 2\mathbf{R}_i \odot \mathbf{C}^T \mathbf{M}_{ij^2} + \\
 & \mathbf{R}_i^2 \odot \mathbf{C}^T \mathbf{M}_{j^2,ao} \mathbf{C} - \\
 & 2\mathbf{R}_j \odot \mathbf{C}^T \mathbf{M}_{i^2j,ao} \mathbf{C} + \\
 & 4\mathbf{R}_i \mathbf{R}_j \odot \mathbf{C}^T \mathbf{M}_{ij,ao} \mathbf{C} - \\
 & 2\mathbf{R}_i^2 \mathbf{R}_j \odot \mathbf{C}^T \mathbf{M}_{j,ao} \mathbf{C} + \\
 & \mathbf{R}_j^2 \odot \mathbf{C}^T \mathbf{M}_{i^2,ao} \mathbf{C} - \\
 & 2\mathbf{R}_j^2 \mathbf{R}_i \odot \mathbf{C}^T \mathbf{M}_i \mathbf{C} + \\
 & \mathbf{R}_i^2 \mathbf{R}_j^2 \odot \mathbf{C}^T \mathbf{S}_{ao} \mathbf{C}.
 \end{aligned} \tag{3.49}$$

Locality is in general not unambiguously defined and alternatives outside the PXM-m form exists. Notably, Pipek-Mezey localization [29] measures locality based on maximizing the function

$$D_{pp} = \sum_A \left(\sum_{\mu \in A} \langle p | \hat{P}_\mu | p \rangle \right)^2, \tag{3.50}$$

where \hat{P}_μ projects the orbital p onto an AO-function μ associated with an atom A . The Pipek-Mezey function is at its maximum when the orbitals distributes across fewest possible atoms. By limiting the summation to A is in the reference cell, the Pipek-Mezey function can easily be extended to periodic systems.

Another, more energetically focused, way of defining locality is the *Edmiston-Ruedenberg* function. [28] Here, the objective function is the so called self-repulsion energy:

$$ER = \sum_p \langle pp | \frac{1}{\hat{r}_{12}} | pp \rangle, \tag{3.51}$$

which is a sum over the diagonal terms in the electron repulsion integrals. For periodic systems, this quantity requires a computationally expensive $\mathcal{O}(N_{\text{BvK}}^4 N_{\text{AO}}^4)$ transformation, thus presenting a challenge for extending this localization criterion to infinite systems.

3.8 Optimization techniques

We have seen that locality, in quantum chemical terms, typically is a single scalar indicative of the degree of spatial confinement for a set of one or more orbitals. The method in which this scalar is optimized is commonly called localization, and is generally based on *linear optimization* techniques. [32] The common objective for these methods is in our context to determine a unitary matrix \mathbf{U} such that a localization measure $f(\mathbf{C} \cdot \mathbf{U})$, where \mathbf{C} are the Wannier coefficients, is at a

maximum or minimum:

$$\min_{U \in \text{SU}(n)} [f(\mathbf{C} \cdot \mathbf{U})]. \quad (3.52)$$

In the molecular case, $\text{SU}(n)$ is the Lie group of $n \times n$ unitary matrices with $\det(U) = 1$ (or $\text{SO}(n)$ when complex matrix elements are excluded). In the periodic case these matrices correspond to the IBT and IBC structures discussed in section 2.14, and as present in the definition of the Wannier functions in Eq. (3.21).

For some time historically, optimization of the Foster-Boys, Pipek-Mezey or Edmiston-Ruedenberg objective functions was performed by means of Jacobi sweeps. [30, 31] This is a method where the orbitals are rotated pairwise in a sequential manner with special orthogonal group 2 ($\text{SO}(2)$)-matrices, and a rotation is accepted if it improves the overall locality measure. The approach is both costly, since it requires the successive rotation of $\frac{1}{2}N(N-1)$ pairs (where N is the number of orbitals), and prone to poor convergence, especially for the virtual orbitals. [31] Both these problems regarding localization of the virtual space can be solved by introducing linear optimization techniques such as approximative Hessians and trust-region methods. [31]

In the context of linear optimization, the function f is referred to as the *objective function*, its domain is called *state space* and a possible choice of \mathbf{U} is called a *state*. [74] While the scalar value $f(\mathbf{C} \cdot \mathbf{U})$ is conventionally termed the *energy*, we shall instead refer to this quantity as the *locality* to avoid ambiguity.

In order to formulate these methods for periodic systems, we can generalize the sequential $\text{SO}(2)$ Jacobi sweeps to a full parameterized $\text{SO}(N)$ rotation in reciprocal space:

$$\tilde{U}(\{\theta\})^{\mathbf{m}} = \prod_{p < q}^N (|p\rangle \cos(\theta_{pq}^{\mathbf{m}}) \langle p| - |q\rangle \sin(\theta_{pq}^{\mathbf{m}}) \langle p| + |p\rangle \sin(\theta_{pq}^{\mathbf{m}}) \langle q| + |q\rangle \cos(\theta_{pq}^{\mathbf{m}}) \langle q|), \quad (3.53)$$

where the parameterization $\theta_{pq}^{\mathbf{m}}$ corresponds to rotational angles between orbitals p and q at reciprocal coordinate vector \mathbf{m} , with respect to Eq. (3.21).

Two important limitations on these rotations should be imposed: first, we require that $\theta_{ia} = 0$ so that the transformation conserves the Brillouin condition. Secondly, we can ensure real-valued Wannier coefficients by requiring that [48]

$$(\tilde{U}^{\mathbf{m}})^{\dagger} = \tilde{U}^{-\mathbf{m}}. \quad (3.54)$$

In principle, with a parameterization of \mathbf{U} it is possible to compute Jacobians and Hessians of the objective function $f(\mathbf{C} \cdot \mathbf{U}(\{\theta\}))$ with respect to $\{\theta\}$, so that Newton's method and quasi-Newton methods can be applied. In practice however, these differentials are generally cumbersome to compute for periodic measures such as the PFM-2 function, and while simple cases can be handled for example by means of automatic differentiation [32] or numerical approximations to the derivatives, we should be open to alternative approaches.

The optimization routine basically constitute a search for an extremum of the objective function in the state space spanned by all possible \mathbf{U} s, in effect all

3. Periodic and infinite many-electron quantum systems

possible rotations on a hypersphere of dimension N , as illustrated in Fig. 3.1. A more common parameterization of this space can be expressed with the

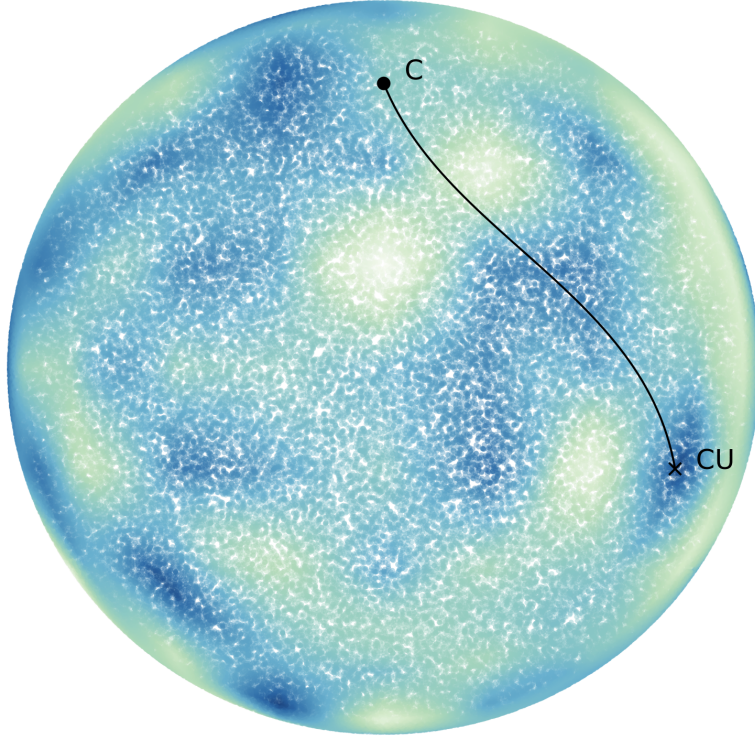


Figure 3.1: Localization may be envisioned as the search for a minimum on the surface of a hypersphere.

anti-Hermitian κ -matrix [6]:

$$U(\kappa) = \exp\left(-\sum_{pq} \kappa_{pq} \hat{a}_p^\dagger \hat{a}_q\right) = \exp\left(-\sum_{pq} \kappa_{pq} \hat{a}_p \hat{a}_q^\dagger\right), \quad (3.55)$$

where \hat{a} and \hat{a}^\dagger are the creation- and annihilation operators, respectively. [6] Furthermore, the matrices spanning such a state space can be randomly generated by first constructing an anti-Hermitian matrix

$$(X^{\mathbf{m}})^\dagger = -X^{\mathbf{m}}, \quad (3.56)$$

and thereafter using the exponential representation to produce [6]:

$$\tilde{U}^{\mathbf{m}} = \exp(X^{\mathbf{m}}). \quad (3.57)$$

The generation of \mathbf{U} in this manner is both efficient and conceptually simple. In cases where it is computationally cheap to sample points in state space, it is reasonable to consider stochastic methods as alternatives or preprocessing to quasi Newton methods.

For this purpose, we have demonstrated that both the PSM-m and PFM-m objective functions can be optimized for periodic systems using an approach called simulated annealing. [74, 75] This optimization is performed by sampling \mathbf{CUU}' in the *vicinity* of \mathbf{CU} , whereby the move is accepted or rejected based on the change in locality $\Delta f(\mathbf{U}, \mathbf{U}') = f(\mathbf{CUU}') - f(\mathbf{CU})$ it entails. The pseudocode for the annealing algorithm is presented in Algorithm 1.

Algorithm 1 Outline of the Annealing algorithm

```

1: Load initial orbitals  $C$ .
2: Define objective function  $f$ .
3: Set initial temperature  $T$ .
4: Set initial state  $U = \mathbb{I}$ .
5: Set acceptance probability  $P_0 \in (0, 1)$ .
6: Compute energy  $E = f(C)$ .
7: for a maximum number of iterations do
8:     Generate a random unitary rotation of the state  $\tilde{U}$ .
9:     if  $f(CU\tilde{U}) < f(CU)$  then
10:        Accept and update  $U = U\tilde{U}$ .
11:     else
12:        if  $\exp\left(-\frac{f(CU\tilde{U})-f(CU)}{t}\right) > P_0$  then
13:           Accept and update  $U = U\tilde{U}$ 
14:        else
15:           Pass
16:        end if
17:     end if
18:     Update temperature
19:     if converged then
20:        Break
21:     end if
22: end for
    
```

In our periodic implementation of the annealing algorithm, our initial set of orbitals are already optimized according to the PSM-1 objective function, as they are obtained from the Wannierization routine available in the CRYSTAL code [47, 48].

The step size of the incremental rotations can be controlled as follows: A random matrix A is generated with uniformly distributed elements $A_{ij} \in (-\Delta u, \Delta u)$, whereby we define

$$\tilde{U} = \exp\left(\frac{1}{2}(A^T - A)\right) = \sum_{n=0}^{\infty} \frac{\left(\frac{1}{2}(A^T - A)\right)^n}{n!}, \quad (3.58)$$

3. Periodic and infinite many-electron quantum systems

where $(A^T - A)^0 := \mathbb{I}$. The choice of Δu is thus proportional to the step size and can serve as a input parameter.

In contrast to certain other stochastic approaches, such as for instance the Metropolis algorithm [76], the acceptance probability in simulated annealing is decreased throughout the optimization by introducing a controllable temperature. The algorithm has a probability of accepting unfavourable changes, which in more blunt terms may be called "uphill steps". One important effect is that the algorithm should in principle be able to locate the global extremum, as opposed to the Newtonian (linear) methods. This is an attractive feature, which may be even more appreciated by revisiting the PFM-2 function, in Eq. 3.42, knowing that the annealing algorithm does not require any differentiation of the objective function.

Chapter 4

Local correlation methods for periodic systems

4.1 Overview

In a local basis, the periodic second order Møller-Plesset (MP2) equations can be solved in an approximative way by inferring sparsity in the electron repulsion integrals (ERIs) and subsequently in the amplitudes based on sparsity considerations. In order to circumvent scaling issues due to the AO to MO transformation of the ERIs, the resolution of identity (RI) approximation [77, 78, 79, 80, 81, 82, 83, 84, 85, 86, 87] can be applied. A global periodic fitting of the ERIs yields a framework well suited for handling flexible orbital spaces, as required by the divide-expand-consolidate (DEC) family of local correlation methods.

4.2 Periodic correlation

The term *correlation energy* was coined by Per-Olov Löwdin at around 1955 [88] in order to describe the inter-electronic interactions that are missing from the independent particle model. The Hartree-Fock approximation includes some correlation, since the single determinant solution ensures that the probability of finding two same-spin electrons in the same position is zero. What is missing from this wavefunction is, however, the effect of the instantaneous repulsive coulomb interaction for pairs of electrons of opposite spins. [1] In order to account for electronic correlation following a Hartree-Fock optimization, a range of methods has been developed on different levels of approximation. Second-order Møller-Plesset (MP2) perturbation theory is on the very first level of approximation, and can be considered the first stepping stone within the hierarchy of CC methods.

The ground state energy of a many-body system can be computed as the sum of the Hartree-Fock energy and the correlation energy

$$E_0 = E_{\text{HF}} + E_c. \quad (4.1)$$

In the CC formalism the correlation energy for a closed-shell molecule can be expressed as[6]

$$E_c = \sum_{ij} \sum_{ab} (t_{ij}^{ab} + t_i^a t_j^b) (2(ia|jb) - (ib|ja)), \quad (4.2)$$

where i, j refer to occupied orbitals, a, b refer to virtual orbitals, t are the

4. Local correlation methods for periodic systems

amplitude tensors and the ERIs for real valued orbitals are

$$(ia|jb) := \int \int_{\mathbb{R}^3} \frac{\varphi_i(\mathbf{r})\varphi_a(\mathbf{r})\varphi_j(\mathbf{r}')\varphi_b(\mathbf{r}')}{|\mathbf{r} - \mathbf{r}'|} d\mathbf{r}' d\mathbf{r}. \quad (4.3)$$

In the canonical MP2 case, we find that $t_i^a = 0$ and

$$t_{ij}^{ab} = \frac{(ia|jb)}{F_{ii} + F_{jj} - F_{aa} - F_{bb}}, \quad (4.4)$$

where F is the Fock matrix in MO basis. Several steps has to be taken in order to extend the above to the non-canonical (and possibly non-orthogonal), periodic case. First, we account for periodicity by including summations over lattice-indices. As discussed in Chapter 3, it is sufficient to consider the energy associated with a single cell of the crystal, so the cell-wise energy can be expressed:

$$\Delta E_{\text{MP2}} = \sum_{\mathbf{J}} \sum_{\mathbf{AB}} \sum_{ij} \sum_{ab} t_{\mathbf{0iJj}}^{\mathbf{AaBb}} (2(\mathbf{0iAa}|\mathbf{JjBb}) - (\mathbf{0iBb}|\mathbf{JjAa})). \quad (4.5)$$

The lattice summations in the above runs over the infinite lattice. Secondly, in the non-canonical basis the Fock-matrix is no longer diagonal, and the amplitudes has to be determined from a set of equations that can be derived from the Hylleraas function [12]:

$$0 = (\mathbf{IiAa}|\mathbf{JjBb}) + \sum_{\mathbf{Cc}} t_{\mathbf{IiJj}}^{\mathbf{CcBb}} F_{ac}^{\mathbf{C-A}} + \sum_{\mathbf{Cc}} t_{\mathbf{IiJj}}^{\mathbf{AaCc}} F_{bc}^{\mathbf{C-B}} - \sum_{\mathbf{Kk}} t_{\mathbf{KkJj}}^{\mathbf{AaBb}} F_{ki}^{\mathbf{I-K}} - \sum_{\mathbf{Kk}} t_{\mathbf{IiKk}}^{\mathbf{AaBb}} F_{kj}^{\mathbf{J-K}}. \quad (4.6)$$

Again, the uppercase, bold summation indices run over the entire \mathbb{Z}^{N_d} lattice. Finally, we consider the MP2 equations for a non-orthogonal virtual space[12]. In the periodic case, these equations are:

$$0 = (\mathbf{IiAa}|\mathbf{JjBb}) + \sum_{\mathbf{CcDd}} s_{ac}^{\mathbf{C-A}} t_{\mathbf{IiJj}}^{\mathbf{CcDd}} F_{db}^{\mathbf{B-D}} + \sum_{\mathbf{CcDd}} F_{ac}^{\mathbf{C-A}} t_{\mathbf{IiJj}}^{\mathbf{CcDd}} s_{db}^{\mathbf{B-D}} - \sum_{\mathbf{Kk}} \bar{t}_{\mathbf{KkJj}}^{\mathbf{CcDd}} F_{ik}^{\mathbf{K-I}} - \sum_{\mathbf{Kk}} \bar{t}_{\mathbf{IiKk}}^{\mathbf{CcDd}} F_{kj}^{\mathbf{J-K}}, \quad (4.7)$$

where

$$\bar{t}_{\mathbf{IiJj}}^{\mathbf{AaBb}} = \sum_{\mathbf{CcDc}} S_{ac}^{\mathbf{C-A}} t_{\mathbf{IiJj}}^{\mathbf{CcDd}} S_{db}^{\mathbf{B-D}}. \quad (4.8)$$

The translational symmetries are still present in these equations, notably both the ERIs and the amplitudes satisfy:

$$t_{\mathbf{IiJj}}^{\mathbf{AaBb}} = t_{\mathbf{0iJ-Ij}}^{\mathbf{A-IaB-Ib}}. \quad (4.9)$$

Hence, the complete set of amplitudes can be derived from the subset where the first occupied index is kept fixed to the reference cell. This can be utilized to

reduce the number of amplitudes explicitly referenced by a solver, but at the same time introduces a slight complication when contracting over the cell-index that is chosen to be fixed.

If we for a moment disregard the problem of infinite summations, we find that the MP2 equations (Eqs. (4.6) and (4.7)) may be iteratively solved with fixed-point iterations by extracting the diagonal terms from the sums over the Fock-matrix, as commonly done for CC-equations. [1] At the first iteration, the amplitudes are then simply

$$t_{\mathbf{0}i\mathbf{J}j}^{\mathbf{A}a\mathbf{B}b} = \frac{(\mathbf{0}i\mathbf{A}a|\mathbf{J}j\mathbf{B}b)}{F_{ii}^{\mathbf{0}} + F_{jj}^{\mathbf{0}} - F_{aa}^{\mathbf{0}} - F_{bb}^{\mathbf{0}}}. \quad (4.10)$$

4.3 The local subspace

For localized Wannier orbitals, the ERIs tend exponentially to zero with the *inter-orbital* distances $R_{\mathbf{0}i\mathbf{A}a}$ and $R_{\mathbf{J}j\mathbf{B}a}$, and proportional to $R_{\mathbf{0}i\mathbf{J}j}^{-3}$ with the *inter-pair* distance $R_{\mathbf{0}i\mathbf{J}j}$ [72, 89, 90], where

$$R_{\mathbf{P}p\mathbf{Q}q} = \sqrt{(\langle \varphi_{\mathbf{P}p} | \hat{\mathbf{r}} | \varphi_{\mathbf{P}p} \rangle - \langle \varphi_{\mathbf{Q}q} | \hat{\mathbf{r}} | \varphi_{\mathbf{Q}q} \rangle)^2}. \quad (4.11)$$

The first decay property can be attributed to the fact that for exponentially decaying Wannier orbitals, their product orbitals $\Phi(\mathbf{r})_{\mathbf{0}p\mathbf{R}q} = \varphi_{\mathbf{0}p}(\mathbf{r})\varphi_{\mathbf{R}q}(\mathbf{r})$ tend to zero as the constituents are spatially separated, as illustrated in Fig. 4.1. The decay in the inter-pair separation $R_{\mathbf{0}i\mathbf{J}j}$ may be derived from a

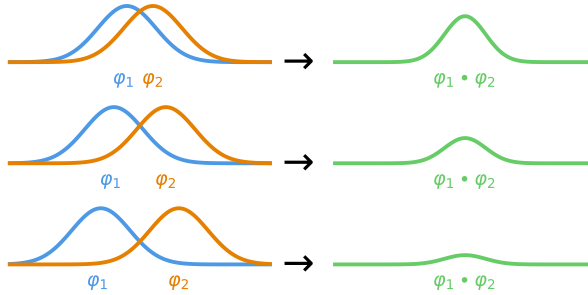


Figure 4.1: The product of two Gaussian functions exhibits an exponential decay as they are spatially separated.

multipole expansion of the ERIs, under the condition that the orbital spaces are orthogonal. [72]

Distance decay can be used to infer sparsity in the ERIs by introducing distance cutoffs d_o and d_v in such a way that

$$(\mathbf{0}i\mathbf{A}a|\mathbf{J}j\mathbf{B}b) = 0 \quad \text{for} \quad (R_{\mathbf{0}i\mathbf{J}j} \leq d_o) \vee (R_{\mathbf{0}i\mathbf{A}a} \leq d_v) \vee (R_{\mathbf{J}j\mathbf{B}b} \leq d_v). \quad (4.12)$$

It can be seen from Eq. (4.6) and the initial amplitudes (4.10) that this sparsity in the ERIs is inherited by the amplitudes. In a local basis, the Fock matrix also exhibits distance-based decay, so the only way for the amplitudes to cancel out the first term in the MP2-equations is by having its most significant elements defined in correspondence to the ERI-tensor.

As such, the local basis brings forth a condition where it becomes possible to solve the MP2 equations approximately on weakly intercoupled *local subspaces*, as opposed to the full (infinite) space. Local correlation methods [5, 8, 10, 11, 12, 13, 49] are concerned with how to best partition, truncate and represent these local subspaces. In light of this, these methods may in general be seen as approximations where the total correlation energy is cast as a sum over the contribution from each subspace Ω_k :

$$E_c \approx \sum_k \Delta E_c(\Omega_k). \quad (4.13)$$

Linear scaling can thus be achieved with a suitable choice for subspace partitioning, a process we shall refer to as *fragmentation*.

We shall use the following concise and general notation in our discussion of local correlation methods; a local subspace is defined as

$$\Omega_k := \mathcal{V}_k \cup \mathcal{O}_k, \quad (4.14)$$

where \mathcal{V}_k and \mathcal{O}_k are virtual and occupied orbitals in the vicinity of k . Exactly how location is ascribed to the orbitals may vary, and by omitting the subindex, \mathcal{V} and \mathcal{O} shall refer to the full virtual and occupied spaces.

4.4 The Divide-Expand-Consolidate scheme

The Divide-Expand-Consolidate (DEC) scheme was originally devised [14] as a local correlation method for dealing with large molecules on the level of CC theory. [72] The scheme is focused on error control, by means of converging the energies of the local subspaces to a given *fragment optimization threshold* (FOT). [14] It is additionally well suited for massive parallelization, if you accept the additional cost of recomputing the integrals. [91]

In the case of monotonically decreasing magnitudes with respect to distance in the ERIs, we may expect that the energy contribution from a given subspace is more or less convergent towards the exact value as we include larger portions of the ERIs and amplitudes in the vicinity of the given subspace. The main idea of DEC is to first converge the amplitude equations in subspaces for designated *atomic sites*, or *atomic fragments*, with respect to the size of the subspace, and then correlate pairs of these subspaces called *pair fragments*. It is assumed that the error in the energy attributed to the pair fragments is proportional to the error in the fragment energies [14, 91], thus an error-control of the total correlation energy can be imposed.

An *atomic fragment* P is defined as a set of occupied orbitals \mathcal{O}_P and a set of virtual orbitals \mathcal{V}_P [14] in the vicinity of a given atom. Fragments can be

partitioned in various ways [91]. While the original DEC-formulation assigns orbitals to atoms based on Mulliken or Löwdin charges. [14, 15, 92, 93], we may alternatively simply assign them to *fragments* based on their orbital centers. Beginning with the first occupied orbitals, we assign all orbitals within a given distance to this fragment and then proceed until all orbitals belong to a fragment.

Independently of exactly how the fragments are chosen, we refer to these subspaces as the *amplitude orbital space* (AOS) of fragment P :

$$\Omega_{P,AOS} := \mathcal{V}_P \cup \mathcal{O}_P. \quad (4.15)$$

Within the AOS we define yet another subspace called the *energy orbital space* (EOS), where both occupied indices are confined to a unique set of occupied orbitals that do not appear in any other EOS on other atomic fragments:

$$\Omega_{P,EOS} := \mathcal{V}_P \cup \mathcal{O}'_P \text{ where } \mathcal{O}'_P \subset \mathcal{O}_P. \quad (4.16)$$

If no truncation of the virtual space is made, we can recast the correlation energy for a closed-shell molecule as[94]

$$E_{\text{corr}} = \sum_P E_P + \sum_{P>Q} \Delta E_{PQ}, \quad (4.17)$$

where the quantity

$$E_P = \sum_{ij \in \mathcal{O}'_P} \sum_{ab} t_{ij}^{ab} (2(ia|jb) - (ib|ja)) \quad (4.18)$$

is called the *fragment energy* for fragment P and

$$\begin{aligned} \Delta E_{PQ} = & \sum_{i \in \mathcal{O}'_P, j \in \mathcal{O}'_Q} \sum_{ab} t_{ij}^{ab} (2(ia|jb) - (ib|ja)) \\ & + \sum_{j \in \mathcal{O}'_P, i \in \mathcal{O}'_Q} \sum_{ab} t_{ij}^{ab} (2(ia|jb) - (ib|ja)) \end{aligned} \quad (4.19)$$

is the *pair fragment energy* for pair PQ . The corresponding amplitudes for the fragments and pair fragments can be obtained by solving the MP2 equations on respectively $\Omega_{P,AOS}$ and $\Omega_{P,AOS} \cup \Omega_{Q,AOS}$ (for untruncated virtual spaces).

The DEC method can now be summarized as follows: first, the occupied space is divided into fragments. We then incrementally expand each fragment's AOS and solve the equations on the resulting subspace, until the change in energy in its EOS is below the FOT. Finally, the energies from each fragment are summed up, and the pair fragments are then computed successively up to a given cutoff distance.

4.5 The Extended DEC (XDEC) Scheme

Several features of the DEC scheme are appealing from a periodic perspective. Converged orbital subspaces is a reasonable way of dealing with infinite spaces,

4. Local correlation methods for periodic systems

and the prospect of parallelisation is essential with respect to performance. The DEC scheme can be extended to the periodic case by optimizing the fragments in the reference cell as if they were fragments in a molecule whereby translational symmetry can be used for pair fragments [15], but in order to fully exploit the translational symmetry we shall in this section derive the approach used in paper three of this dissertation.

The occupied space in the reference cell is partitioned into fragments as follows: first, the Wannier centers are computed according to the procedure outlined in section 3.7:

$$\mathbf{r}_{0p} = \langle \mathbf{0}p | \hat{\mathbf{r}} | \mathbf{0}p \rangle. \quad (4.20)$$

Since translational symmetry dictates the positions throughout the lattice, we can now compute the inter-orbital distances as

$$d_{pq}^{\mathbf{L}} = \|\mathbf{r}_{0p} - \mathbf{r}_{\mathbf{L}q}\|. \quad (4.21)$$

Beginning with the first occupied orbital i , we then construct a fragment P by including all occupied orbitals j within a distance a_{frag} , called the fragment cutoff

$$\mathcal{O}'_{0P} = \{\varphi_{0j}\}, \quad \forall d_{ij}^{\mathbf{0}} \leq a_{\text{frag}}. \quad (4.22)$$

We then repeat the procedure for the next unassigned occupied orbital in the reference cell, and continue so forth until the whole occupied space of the reference cell is partitioned into non-overlapping fragments. The procedure is illustrated for a one dimensional chain of ethylene in Fig. 4.2. The position of each fragment can be defined to be the position of the first occupied orbital i , so that $d_{Pq}^{\mathbf{L}} = d_{iq}^{\mathbf{L}}$.

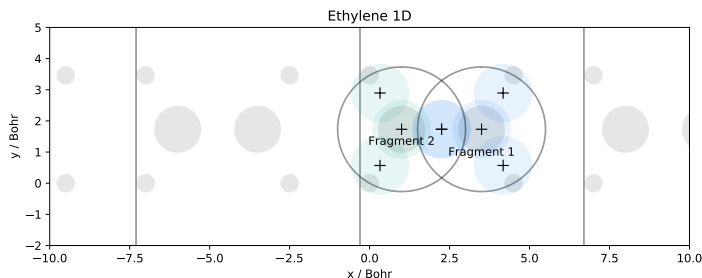


Figure 4.2: Procedure for partitioning the occupied orbitals in the reference cell based on distance, here illustrated for one dimensional ethylene. The Wannier centers are indicated with crosses, "+", and the colored spheres indicate to which fragment they are associated. In this case, $a_{\text{frag}} = 2.0$ Bohr results in two fragments.

Next, we assign to each fragment two distance cutoffs d_o and d_v defining its occupied and virtual spaces, respectively

$$\mathcal{O}_{0P} = \{\varphi_{\mathbf{L}j}\}, \quad \forall d_{ij}^{\mathbf{L}} \leq d_o, \quad (4.23)$$

and

$$\mathcal{V}_{\mathbf{0}P} = \{\varphi_{\mathbf{L}a}\}, \quad \forall d_{ia}^{\mathbf{L}} \leq d_v, \quad (4.24)$$

so that the initial AOS and EOS for fragment P are

$$\Omega_{P,AOS} := \mathcal{V}_{\mathbf{0}P} \cup \mathcal{O}_{\mathbf{0}P} \quad (4.25)$$

and

$$\Omega_{P,EOS} := \mathcal{V}_{\mathbf{0}P} \cup \mathcal{O}'_{\mathbf{0}P}. \quad (4.26)$$

The construction of the virtual space for one dimensional ethylene is illustrated in Fig. 4.3.

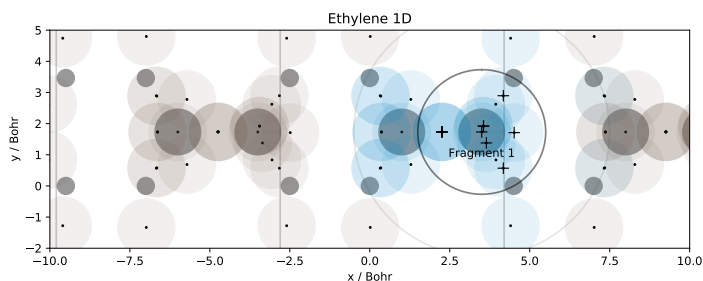


Figure 4.3: Virtual cutoff distance for one dimensional ethylene. With $d_v = 3.0$ Bohr, a number of virtual orbitals are included in the EOS of fragment 1, as defined in Fig. 4.2. The virtual orbitals in the EOS are indicated as blue spheres, while the ones outside are brown. Note that while the illustration only shows the xy -coordinate, the orbitals are in reality not confined to this plane. Consequently, one virtual orbital to the right appears to be within the sphere while its offset in the z -axis places it outside.

We now optimize each fragment separately. This procedure consists of successively increasing d_v and d_o , solving the MP2 amplitude equations on the resulting subspace, and computing the energy, as outlined in Algorithm 2. At the end of this expansive step, we have produced a set of fragments with associated subspaces and energies as illustrated in Fig. 4.4, and the scene is now set for the pair fragment calculation.

The pair fragments are uniquely determined by the optimized fragments, and their energy contributions are assumed to decay with distance. The pair fragment P_0Q_L has the AOS

$$\Omega_{iLj,AOS} = \mathcal{V}_{\mathbf{0}P} \cup \mathcal{V}_{\mathbf{L}Q} \cup \mathcal{O}_{\mathbf{0}P} \cup \mathcal{O}_{\mathbf{L}Q} \quad (4.27)$$

and EOS

$$\Omega_{P_0Q_L,EOS} = \mathcal{V}_{\mathbf{0}P} \cup \mathcal{V}_{\mathbf{L}Q} \cup \mathcal{O}'_{\mathbf{0}P} \cup \mathcal{O}'_{\mathbf{L}Q}. \quad (4.28)$$

4. Local correlation methods for periodic systems

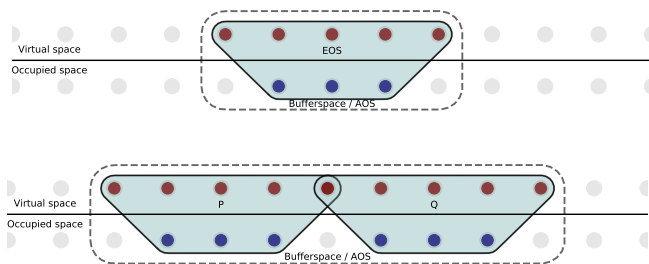


Figure 4.4: Illustration of the fragments (top) and pair fragments (bottom) in the XDEC fragmentation scheme. Virtual and occupied orbitals inside the AOS/EOS are colored red and blue respectively.

Algorithm 2 Outline of the Divide-Expand-Consolidate scheme

- 1: Subdivide occupied space into initial atomic fragments P based on distance measures.
 - 2: Define initial EOS and AOS for each atomic fragment P
 - 3: **for** Each atomic fragment **do**
 - 4: Solve amplitude equations on the AOS
 - 5: Compute the initial atomic fragment energy $E_{P,0}$.
 - 6: **while** $|E_{P,\text{new}} - E_{P,\text{old}}| \geq \text{FOT}$ **do**
 - 7: Converge energy within FOT with respect to d_o .
 - 8: Converge energy within FOT with respect to d_v .
 - 9: **end while**
 - 10: Store final domains and energy.
 - 11: **end for**
 - 12: Compute pair fragment energies.
 - 13: Sum together all energies to yield the final approximate correlation.
-

Clearly, all pair fragments should have one index fixed in the reference cell when computing their energy:

$$\begin{aligned} \Delta E_{P_0 Q_L} = & \sum_{i \in \mathcal{O}'_{P_0}, j \in \mathcal{O}'_{Q_L}} \sum_{ab \in \mathcal{V}_{P_0} \cup \mathcal{V}_{Q_L}} t_{ij}^{ab} (2 (ia|jb) - (ib|ja)) + \\ & \sum_{j \in \mathcal{O}'_{P_0}, i \in \mathcal{O}'_{Q_L}} \sum_{ab \in \mathcal{V}_{P_0} \cup \mathcal{V}_{Q_L}} t_{ij}^{ab} (2 (ia|jb) - (ib|ja)). \end{aligned} \quad (4.29)$$

Upon closer inspection with respect to periodicity, we will however find that the local subspaces for pair fragments with one fragment outside the reference cell contain translationally redundant amplitudes, as apparent in Eq. 4.10. For this reason, the spaces that constitute the molecular pair fragments are slightly more tricky to reconcile with the periodic symmetry than the fragment domains.

These subspaces are subject to translational symmetries, so that for instance

$$\hat{T}_M \mathcal{O}_{LQ} = \mathcal{O}_{L+MQ} \quad (4.30)$$

For a pair fragment $P_0 Q_L$ where $L \neq 0$, the pair AOS is the union of the two constituent fragments AOS'. This space is illustrated in Fig. 4.5. Inside this

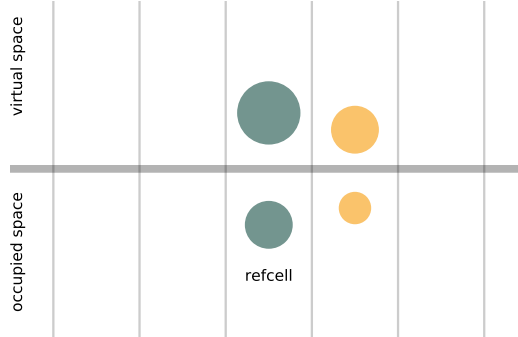


Figure 4.5: A periodic setup for pair fragments, where the color indicates which fragment each AOS belongs to. Their union is the pair AOS.

space we account for

1. Occupied indices placed both on P_0 .
2. Occupied indices placed both on Q_L
3. Occupied indices placed on both P_0 and Q_L .

Recall that in the periodic case, we have fixed the first occupied index of the MP2 equations in the reference cell, since all remaining amplitudes can be derived from translation. This means that of the three situations above, only the first is explicitly captured by the periodic amplitudes. For (3), the pair AOS only explicitly account for amplitudes with the first occupied index on P_0 and the second on Q_L , not the other way around. To account for case (2) with both occupied indices on Q_L , we have to modify the spaces accordingly. This can be done by constructing a composite AOS:

$$\Omega'_{iLj,AOS} = \Omega_{iLj,AOS} \cup \hat{T}_{-L} \Omega_{iLj,AOS}, \quad (4.31)$$

where

$$\hat{T}_{-L} \Omega_{iLj,AOS} = \mathcal{V}_{-LP} \cup \mathcal{V}_{0Q} \cup \mathcal{O}_{-LP} \cup \mathcal{O}_{0Q}. \quad (4.32)$$

The resulting space is illustrated in Fig. 4.6.

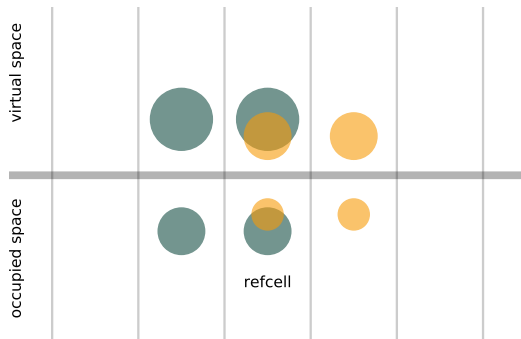


Figure 4.6: The periodic pair domain accounting for all amplitudes. The fragment specific domains may or may not overlap in the cells.

In contrast to molecular DEC, this composite pair subspace naturally results in potentially larger bufferspaces for the amplitudes originally assumed to be in the cell outside the reference cell, in addition to a generally larger virtual space for all the amplitudes. Still, it reduces the dimensionality of the MP2 equations, so from a periodic perspective it makes sense.

Further consideration may now be made with regards to the remaining pair fragments. The AOS of P_0Q_L will by construction have some overlap with Q_0P_L , and from Fig. 4.6 it is easy to see that the virtual and occupied space pertaining to the reference cell will be identical in these cases. Since we generally would like to avoid doing the same calculation more than once, we can construct the subspace

$$\Omega'_{iLj,AOS} = \Omega_{iLj,AOS} \cup \hat{T}_{-L}\Omega_{iLj,AOS} \cup \hat{T}_L\Omega_{iLj,AOS}, \quad (4.33)$$

as shown in Fig. 4.7. Solving the MP2-equations on this AOS will determine all amplitudes required to compute the energies $\Delta E_{P_0Q_L}$, $\Delta E_{P_0Q_{-L}}$, $\Delta E_{Q_0P_L}$ and $\Delta E_{Q_0P_{-L}}$ simultaneously. While we know that $\Delta E_{P_0Q_L} = \Delta E_{Q_0P_{-L}}$ from translational invariance, the other combination would otherwise have to be computed separately. In the current XDEC implementation, these spaces can be determined on input, while the default is Eq. 4.33. The periodic pair energy may now finally be evaluated according to Eq. 4.19.

4.6 Periodic Fitting

While the local approximation solves the problem of infinite orbital spaces, the N_{AO}^4 scaling limitation discussed by Pulay [5] (see Chapter 3) remains. This is due to the evaluation of the ERIs, which when fully expanded in the AO basis

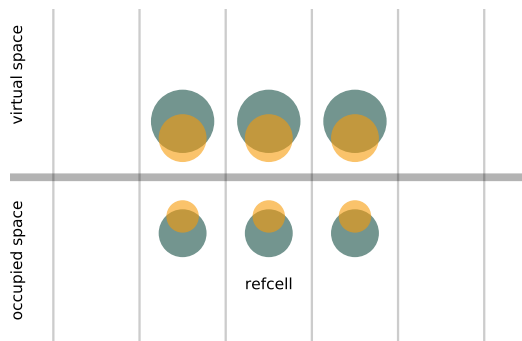


Figure 4.7: The pair domain as defined by default in the XDEC-RI code.

reads

$$(\mathbf{O}i\mathbf{A}a|\mathbf{J}j\mathbf{B}b) = \sum_{\mathbf{K}\mu} \sum_{\mathbf{L}\nu} \sum_{\mathbf{M}\gamma} \sum_{\mathbf{N}\delta} C_{\mu,i}^{\mathbf{K}} C_{\nu,a}^{\mathbf{L}} (\mathbf{K}\mu\mathbf{L}\nu|\mathbf{M}\gamma\mathbf{N}\delta) C_{\gamma,j}^{\mathbf{M}} C_{\delta,b}^{\mathbf{N}}. \quad (4.34)$$

This transformation is especially challenging in three dimensional periodic systems, where the number of atomic orbitals can become relatively large depending on the system in question, and the expansion domain of the Wannier functions.

For molecules, the RI approximation [77, 78, 79, 80, 81, 82, 83, 84, 85, 86, 87] is routinely used to speed up calculation of the ERIs, and a few extensions to the periodic case have been proposed and implemented. [95, 96, 97, 98] It is sometimes referred to as *density fitting*. The basic idea is to represent the product orbitals in the ERIs as linear combinations in a separate basis, called the auxiliary basis $\{\chi_K\}$

$$|pq\rangle \approx \sum_K |K\rangle d_{K,pq} := |\tilde{p}q\rangle, \quad (4.35)$$

leading to the approximated ERIs

$$(pq|rs) \approx \sum_{KL} d_{K,pq}(K|L)d_{L,rs}, \quad (4.36)$$

where

$$(K|L) = \iint \frac{\chi_K(\mathbf{r})\chi_L(\mathbf{r}')}{|\mathbf{r} - \mathbf{r}'|} d\mathbf{r}'d\mathbf{r}. \quad (4.37)$$

With regards to periodic systems, it makes sense to distinguish between local and global fitting schemes. Where the global scheme in principle utilizes the infinite auxiliary basis set for the fitting, a local fitting scheme instead employs

4. Local correlation methods for periodic systems

a suitable subset of the global auxiliary basis, which may even be specific for each product of orbitals. [95] The transition between these formulations may, however, be seen as smooth, and from a computational perspective it will at any rate become necessary to truncate the infinite auxiliary basis in one way or another.

When a local fitting is performed, it becomes important to properly assess exactly which auxiliary functions to retain, which requires some knowledge of the orbital spaces involved. The XDEC approach instead works with flexible orbital spaces, and for this reason we have devised our RI approximation as a global fitting.

Let us first assume that the coefficients \mathbf{d} have been determined. Analogous to Eq. (4.35), the periodic product orbitals are then represented by

$$|\mathbf{0}p\mathbf{Q}q\rangle \approx \sum_{\mathbf{NK}} |\mathbf{NK}\rangle d_{\mathbf{K},\mathbf{0}p\mathbf{Q}q}^{\mathbf{N}} := |\widetilde{\mathbf{0}p\mathbf{Q}q}\rangle = \Phi_{\mathbf{0}p\mathbf{Q}q}, \quad (4.38)$$

so that the periodic ERIs can be approximated

$$(\mathbf{0}p\mathbf{Q}q|\mathbf{R}r\mathbf{S}s) \approx (\widetilde{\mathbf{0}p\mathbf{Q}q}|\widetilde{\mathbf{R}r\mathbf{S}s}), \quad (4.39)$$

The product orbitals are translationally invariant, so from a periodic perspective it makes sense to define a relative indexing of the $\mathbf{Q}s$ and $\mathbf{S}s$, such that

$$(\mathbf{0}p\Delta\mathbf{Q}q|\mathbf{R}r\Delta\mathbf{S}s) := \int \int \frac{\Phi_{\mathbf{0}p\Delta\mathbf{Q}q}(\mathbf{r})\Phi_{\mathbf{0}r\Delta\mathbf{S}s}(\mathbf{r}' - \mathbf{R}_{\mathbf{R}})}{|\mathbf{r} - \mathbf{r}'|} d\mathbf{r}d\mathbf{r}', \quad (4.40)$$

where $\mathbf{S} = \Delta\mathbf{S} + \mathbf{R}$ and of course $\Delta\mathbf{Q} = \mathbf{Q}$. This allows us to cast the coefficients as a set of IBT matrices $\{\mathbf{d}_{\Delta\mathbf{Q}}\}$ where the contraction required to obtain the ERIs may be performed as an IBT or IBC product:

$$(\mathbf{0}p\mathbf{Q}q|\mathbf{R}r\mathbf{S}s) \approx (\widetilde{\mathbf{0}p\mathbf{Q}q}|\widetilde{\mathbf{R}r(\mathbf{S})s}) = (\mathbf{d}_{\Delta\mathbf{Q}}^T \mathbf{V} \mathbf{d}_{\Delta\mathbf{S}})_{pqrs}^{\mathbf{R}}, \quad (4.41)$$

where \mathbf{V} is the Coulomb IBT matrix with elements

$$V_{\mathbf{K}J}^{\mathbf{M}} := (\mathbf{0}\mathbf{K}|\mathbf{M}J). \quad (4.42)$$

Provided that \mathbf{d} has a finite bandwidth¹, we can use the triple IBT-products defined in section 2.15 to compute this product without worrying about the decay properties of \mathbf{V} . The challenge then becomes to accurately determine \mathbf{d} globally.

In the molecular case, we know the coefficients \mathbf{d} to be the solution to a set of linear equations

$$\mathbf{V}\mathbf{d} = \mathbf{O}, \quad (4.43)$$

where the Colomb matrix \mathbf{V} have elements $\mathbf{V}_{JK} = (J|K)$ and the three-index Coulomb matrix \mathbf{O} containing the elements

$$\mathbf{O}_{J,pq} = \sum_{\mu\nu} (J|\mu\nu) C_{\mu p} C_{\mu q}. \quad (4.44)$$

¹See Chapter 2 for details.

The coefficients may thus be obtained on paper by the inversion of \mathbf{V} . In practice, however, these equations are typically solved either using a linear solver, pseudoinversion or Cholesky-factorization. [99] The latter case can be expressed

$$(\tilde{p}q|\tilde{r}s) = (\mathbf{d}^T \mathbf{V} \mathbf{d})_{rs}^{pq} = (\mathbf{d}^T \mathbf{L} \mathbf{L}^T \mathbf{d})_{rs}^{pq}, \quad (4.45)$$

where

$$\mathbf{V} \mathbf{d} = \mathbf{L} \mathbf{L}^T \mathbf{d} = \mathbf{O}. \quad (4.46)$$

By defining $\mathbf{L}^T \mathbf{d} := \mathbf{y}$, which can be determined by means of back-substitution in the above, we now have simply

$$(\tilde{p}q|\tilde{r}s) = (\mathbf{d}^T \mathbf{L} \mathbf{L}^T \mathbf{d})_{rs}^{pq} = (\mathbf{y}^T \mathbf{y})_{rs}^{pq}. \quad (4.47)$$

The periodic extension of the coefficients \mathbf{d} can be derived analogous to the molecular case by means of the IBT-matrix formulation. The Coulomb IBT matrix \mathbf{V} now has elements as in Eq.(4.42), and the periodic three-index Coulomb matrix now contains the elements:

$$(\mathbf{L}J|\mathbf{0}p\mathbf{Q}q) = \sum_{\mathbf{M}\mu} \sum_{\mathbf{N}\nu} (\mathbf{L}J|\mathbf{M}\mu(\mathbf{M} + \mathbf{N})\nu) C_{\mu p}^{-\mathbf{M}} C_{\nu q}^{-(\mathbf{M}+\mathbf{N})+\mathbf{Q}}, \quad (4.48)$$

where C are the Wannier coefficients (Eq. 3.21) and the summations in \mathbf{N} and \mathbf{M} are over the entire lattice. Note that the lattice summation for ν have been offset in such a way that if we restrict \mathbf{N} to $\mathbf{0}$ we have simply

$$\sum_{\mathbf{M}\mu} \sum_{\nu} (\mathbf{L}J|\mathbf{M}\mu\mathbf{M}\nu) C_{\mu p}^{-\mathbf{M}} C_{\nu q}^{-\mathbf{M}+\mathbf{Q}}. \quad (4.49)$$

Hence, if the summation over \mathbf{N} is ordered in terms of increasing distance $\|\mathbf{R}_{\mathbf{N}}\|$, we may expect an exponential decay in the three-index AO integrals due to the incremental separation in $\|\mathbf{R}_{\mathbf{0}\mu,\mathbf{N}\nu}\|$. Moreover, in this form the three index AO integrals can be considered an IBT matrix with elements

$$(\mathbf{O}_{AO})_{J,\mu\nu}^{\mathbf{M}} = (\mathbf{0}J|\mathbf{M}\mu\mathbf{M}\nu). \quad (4.50)$$

The equation we have to solve in order to obtain the periodic fitting coefficients then becomes

$$\sum_{\mathbf{M}J} (\mathbf{N}K|\mathbf{M}J) d_{J,\mathbf{0}p\mathbf{L}q}^{\mathbf{M}} = (\mathbf{N}K|\mathbf{0}p\mathbf{L}q), \quad (4.51)$$

which is the same as Eq. (4.43). The IBT matrix \mathbf{V} may now in theory be inverted by the procedure described in sec. 2.13, but in doing so we will run into a number of serious numerical problems. First, for most realistic systems the distance decay is too slow for any reasonable truncation[95], resulting in a huge memory demand and poor computational performance. Furthermore, we will find that premature truncation and insufficiently dense sampling in reciprocal space may cause close to zero or even negative eigenvalues in $\mathcal{F}(\mathbf{V})^{\mathbf{m}}$. From a computational standpoint, this approach is therefore not especially well-suited for the XDEC scheme.

4. Local correlation methods for periodic systems

The process of fitting a function in a new basis is commonly done throughout science. The distinct aspects of the RI-approximation as outlined above are that we perform the fitting of products of functions using the Coulomb metric. The more general situation is the basis change of a single function using overlap metric. By metric, we refer to the operator used in defining the inner product space of the orbitals, as for instance in Eq. (4.42). In fact, any positive definite metric may be chosen. [82] While it has been shown, perhaps unsurprisingly, that the Coulomb metric indeed offers the best fitting metric for the ERIs [100], it is at the same time a fact that the overlap metric has a much steeper distance decay. It has therefore been speculated [96, 97, 98] that an intermediate metric, the so called attenuated coulomb operator [97, 101], could offer a reasonable compromise in periodic systems. This operator is found by expressing the Coulomb operator in terms of the error function[101]:

$$\frac{1}{r} = \lim_{\omega \rightarrow 0} \frac{\operatorname{erfc}(\omega r)}{r}, \quad (4.52)$$

This operator tends asymptotically to the overlap metric as the attenuation parameter ω approaches infinity. This makes it possible to choose the metric in an intermediate range, where a reasonable trade-off between distance decay in the resulting matrices and accuracy in the results is reached. We shall distinguish the matrix quantities where the attenuated metric is employed with a tilde, so that

$$\tilde{\mathbf{V}}_{JK}^{\mathbf{L}} = (\mathbf{0} \mathbf{J} \tilde{\mathbf{L}} \mathbf{K}). \quad (4.53)$$

We may now derive the global periodic attenuated RI-scheme simply by first solving

$$\tilde{\mathbf{V}} \mathbf{d} = \tilde{\mathbf{O}}, \quad (4.54)$$

and subsequently evaluating Eq. (4.41) as before.

The typical auxiliary basis sets used for density fitting in quantum chemistry are *incomplete*, meaning that depending on how well they span the same space as all possible products of the original Gaussian basis, they will introduce errors in the ERIs. Considering an error in the fit ε , such that

$$|\mathbf{0} p \mathbf{Q} q\rangle = |\widetilde{\mathbf{0} p \mathbf{Q} q}\rangle + \varepsilon_{\mathbf{0} p \mathbf{Q} q}, \quad (4.55)$$

we'll find that it is possible to constrain the error in the ERIs to second order by approximating them as

$$\begin{aligned} (\mathbf{0} p \mathbf{Q} q | \mathbf{R} r \mathbf{S} s) &= (\mathbf{0} p \mathbf{Q} q | \widetilde{\mathbf{R} r \mathbf{S} s}) + (\widetilde{\mathbf{0} p \mathbf{Q} q} | \mathbf{R} r \mathbf{S} s) - (\widetilde{\mathbf{0} p \mathbf{Q} q} | \widetilde{\mathbf{R} r \mathbf{S} s}) = \\ &= (\mathbf{0} p \mathbf{Q} q | \mathbf{R} r \mathbf{S} s) - (\varepsilon_{\mathbf{0} p \mathbf{Q} q} | \varepsilon_{\mathbf{R} r \mathbf{S} s}). \end{aligned} \quad (4.56)$$

This correction, originally introduced by Dunlap [102], is commonly referred to as *robust* fitting. Whenever a Coulomb-metric is used, the additional integrals required to obtain the ERIs in Eq. (4.56) are actually already computed in construction of the intermediate matrix elements in Eq. (4.48), and the correction is computationally inexpensive. If we instead employ the attenuated metric, these integrals will have to be computed separately.

Chapter 5

The XDEC-RI code

5.1 Overview

The theoretical framework presented in this dissertation has been used to develop a working code for dealing with periodic correlation calculations. This chapter gives an overview of its implementation, and details some of the practical aspects such as screening and numerical thresholds.

In a hyperbolic way, this whole dissertation is about transforming a set of lattice vectors, atomic positions and charges into a single number; the periodic electronic correlation energy. However, in the bigger picture, we simultaneously gain access to a wide range of ab-initio quantum chemistry methods that in principle can provide properties and potential energy surfaces for these systems without having to perform the analysis in the lab.

There are currently only a few periodic local correlation codes available for public use, with perhaps CRYSCOR, the MP2-extension for CRYSTAL, being the most prominent. [35, 47, 96, 103, 104, 105, 106] A comparison between CRYSCOR and the XDEC-RI code has been made in paper three of this dissertation, and we have used CRYSCOR extensively in the testing and verification of all iterations of the XDEC-RI code.

The Wannier functions used in this work are obtained from Crystal. [47] They are initially localized according to a Foster-Boys criterion [48], but can be localized further using PSM-m or PFM-m type objective functions. All integrals are obtained from LIBINT [107], except the fourth-order Cartesian moments which are computed with LSDALTON. [108, 109] The XDEC-RI code is mostly written in Python, with some few extensions in C++. Consistent cross-code interfacing is achieved with a Python-class called PRISM. A class called TMat (Toeplitz matrix) facilitates efficient and conceptually simple handling of periodic matrices and algebra, as presented in Chapter 2. The periodic resolution of identity approximation is implemented as a module called PRI (Periodic RI), and is imported in the main program called XDEC-RI. Part of the code can utilize the MPI4PY module [110], and can be run on high performance computing clusters, although the workload is not yet well balanced. An illustrative overview of the code is provided in Fig. 5.1

5.2 Two versions of XDEC

There are two different XDEC implementations being discussed in this dissertation and included papers, to be referred to as XDEC (Extended Divide-Expand-Consolidate) and XDEC-RI (XDEC-Resolution of Identity). The XDEC code is presented in the first paper [15] included in this dissertation, and

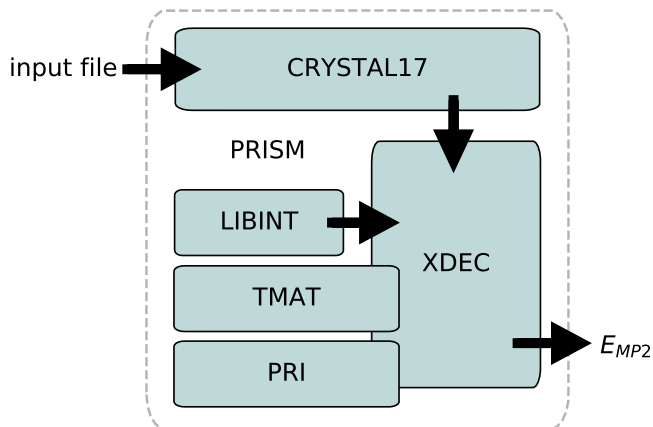


Figure 5.1: Illustrative overview of our code setup. Consistency across the various codes is maintained by a class called PRISM. Integrals for the XDEC-RI framework is provided by LIBINT. The module TMAT handles periodic matrix product, while PRI performs the integral fitting.

was our initial implementation. In its final state, the XDEC code featured a Cholesky-based RI approximation, but design choices made it fundamentally irreconcilable with certain periodic features in the integrals and amplitudes. It furthermore relied on recurrently re-fitting every incrementally changed local subspace, accounting for more than 90 percent of the computational effort, and a re-diagonalization of the Fock matrix in the local subspace. Building on the same pipeline for obtaining the Wannier functions, the XDEC-RI code was therefore developed independently from the original implementation. This chapter deals mainly with the XDEC-RI code.

5.3 Comments on The Local Approximation

While the general theory regarding the distance based decoupling of the amplitude equations may provide a complete picture of how a local approximation can be made, there are choices made on the implementational level that will affect the energy in various ways. We therefore briefly provide more details pertaining to the local approximation.

Provided the partitioning of the occupied space and the two distance cutoff parameters d_v and d_o , a unique subspace is defined according to the procedure discussed in Chapter 4, in which the amplitudes may be initialized. Upon

initialization and the subsequent calculation of energy, we require the ERIs for all combinations of orbitals in the local subspace, in effect:

$$\Delta E_{\text{MP2}} = \sum_{\mathbf{J}} \sum_{\mathbf{AB}} \sum_{ij} \sum_{ab} t_{\mathbf{0}i\mathbf{J}j}^{\mathbf{A}a\mathbf{B}b} (2 (\mathbf{0}i\mathbf{A}a|\mathbf{J}j\mathbf{B}b) - (\mathbf{0}i\mathbf{B}b|\mathbf{J}j\mathbf{A}a)). \quad (5.1)$$

For a given set of indexes in the amplitude, we require in the above both the direct- and exchange type ERIs. As discussed in Chapter 3, the global fitting allows for efficient calculation of the ERIs by means of the IBC product for all \mathbf{J} s:

$$(\mathbf{0}i\Delta\mathbf{A}a|\mathbf{J}j(\mathbf{J} + \Delta\mathbf{B})b) \approx (\mathbf{d}_{\Delta\mathbf{A}}^T \mathbf{V} \mathbf{d}_{\Delta\mathbf{B}})_{iajb}^{\mathbf{J}}. \quad (5.2)$$

The exchange type integrals are however not as easily recovered, since they typically require another set of fitting coefficients:

$$(\mathbf{0}i(\mathbf{J} + \Delta\mathbf{B})b|\mathbf{J}j\Delta\mathbf{A}a) \approx (\mathbf{d}_{\Delta\mathbf{B}+\mathbf{J}}^T \mathbf{V} \mathbf{d}_{\Delta\mathbf{A}-\mathbf{J}})_{iajb}^{\mathbf{J}}. \quad (5.3)$$

Due to the exponential decay with distance between the product orbitals, it is reasonable to assume that optimization of the local subspace will converge rapidly with the increase in d_v . The much slower decay of the ERIs with respect to the distance $R_{\mathbf{0}i\mathbf{J}j}$ will however result in subspaces where the exchange type integrals in Eq. 5.1 are vanishingly small, and yet formally included in our equations.

Based on this, there are several layers of approximation within the subspace in the XDEC-RI code. With respect to this issue, the implementation is structured as follows:

We begin by computing all the fitting coefficients $\mathbf{d}_{\Delta\mathbf{A}}$ where $R_{\mathbf{0}i\Delta\mathbf{A}} \leq d_v$. Next, we initialize all amplitudes according to Eq.4.10, in the local subspace defined by \mathcal{O} and \mathcal{V} in Chapter 4. Depending on the subspace definition, we likely now have easy access to more integrals than we actually require, since for every product orbital $\Phi_{\mathbf{0}i\Delta\mathbf{A}a}$ we have from translational symmetry simultaneously obtained all $\Phi_{\mathbf{J}i\mathbf{J}+\Delta\mathbf{A}a}$. For a more balanced treatment of the amplitude equation, we thus have the option of including this "excess" virtual space, which is done internally in the code by providing the solver with `relative_indexing=True`. From our experience with the code we have found this effect to be only minor, and the code therefore by default runs without these kinds of contributions.

The amplitude equations are then converged according to the input specifications, and upon convergence the energy is computed. At this point, if `relative_indexing` has been activated, we will likely have contributions to the energy from exchange-type ERIs where the fitting coefficients have not been computed and are assumed to be zero. If these are explicitly required, they can be computed on demand in the energy calculation by setting `compute_missing_exchange=True`.

5.4 Modules

5.4.1 PRISM (Interface)

An instance of PRISM is initialized using an input-file, either for LSDALTON or CRYSTAL. System data such as lattice parameters, atomic positions and charges, basis set and so on may thereafter be accessed directly with various methods of the class. Input-files for LIBINT or LSDALTON with consistent setup can be generated as strings. PRISM will also generate efficiently evaluable lambda-functions or analytical sympy-functions [111] for the basis set if requested. The most important feature of this class is to maintain consistency between the integrators involved, since different conventions for basis set ordering and lattice structure are used in CRYSTAL, LSDALTON and LIBINT.

5.4.2 TMat (Toeplitz algebra)

Most of the algebraic manipulations are performed with the TMat class, where the IBT or IBC structure is implicitly assumed in all operations. The periodic matrices are loaded in a sparse structure where only non-zero blocks are allocated. The methods in the class can be roughly sorted into three groups. First, there are methods for retrieving and setting blocks, book-keeping and utilities such as screening and changing the bandwidth of the matrix. Second, there are overloaded operators corresponding to commonly used arithmetics such as addition, subtraction, multiplication and division. The matrix-matrix products are defined in two methods, where the default DOT is an IBT-IBT product, while the CIRCULANTDOT is the IBT-IBC product. Third, there is a number of methods which facilitates the Fast Fourier Transform and its inverse on the matrices. The NUMPY module, backed by level 3 BLAS is extensively used where possible.

The TMat class is conceptually useful since many methods from quantum chemistry can be easily extended to the periodic case with the lattice summations implicitly imposed on the formulation. Examples are provided in figures 5.2 and 5.3, where Löwdin-orthogonalization is performed on the AO basis to provide a orthonormalized set of MOs, and a set of projected atomic orbitals (PAOs) [5] are generated. Furthermore, the class is computationally efficient, since the most demanding operations are all performed with highly optimized Fast Fourier Transforms (FFT) in combination with level 3 BLAS routines. [41]

The TMat class can also "unfold" the periodic symmetry in order to work on conventional matrices. This process requires the user to provide the row-coordinates and column-coordinates to unfold relative to the reference cell, whereby a large, finite block-Toeplitz matrix is returned. This procedure makes it possible to compare many IBT and IBC operation to large, finite matrices, where the results should all asymptotically tend to the same in the limit when the resolution in reciprocal space becomes infinitely dense.

```

In [2]: # Example of Löwdin-orthogonalization in reciprocal space
import prism as pr
import toeplitz as tp
import PRI

# Load a system
p = pr.prism("/Users/audunhansen/papers/XDEC-RI-MP2/results/ethylene_id_
crystcor/Crystal/ethylene_old.d12")

# Compute the IBT overlap matrix (using Libint)
S = PRI.compute_overlap_matrix(p, tp.lattice_coords([15,0,0])) # 1D per
iodicity, bandwidth = (-15,15)

C = tp.get_identity_tmat( p.get_n_ao() ) # Construct the IBT identity ma
trix

S_12 = S.kspace_svd_lowdin() # Compute  $S^{-.5}$  using a SVD in reciprocal
space

C = C.circulantdtdot(S_12) # Form initial IBC coefficients

S_mo = C.tT().circulantdtdot(S.circulantdtdot(C)) #Compute overlap IBC matri
x

cell_distance, absolute_max_element = S_mo.absmax_decay(p) # Get absolute
maximum element per cell

# Visualize results
plt.plot(cell_distance, absolute_max_element, "o", label = "Absolute max
imum element in cell")
plt.yscale("log")
plt.xlabel("Cell distance  $\|\mathbf{R}_i\|$ ")
plt.ylabel("Abs. magnitude  $S_{i0,L}$ ")
plt.legend()
plt.show()

```

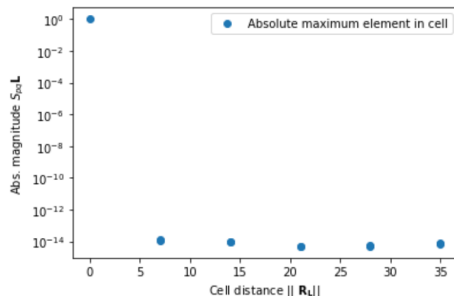


Figure 5.2: Löwdin orthogonalization of a periodic AO basis performed in a Jupyter Notebook using the TMat class. The resulting orbitals are orthogonal to machine precision under Born von Karman boundary conditions.

5.4.3 Orbital refinery (optimization)

Post processing of the Wannier orbitals prior to the correlation calculation can be performed in a module named Orbital refinery. Various stochastic localization procedures is available, mainly the PSM-m and PFM-m objective functions. In addition, this module features a periodic Pipek-Mezey localization, and furthermore an experimental differential overlap integral (DOI) [23] optimizer. It is also possible to minimize the spread of the positions within a set of orbitals,

```

In [2]: import prism as pr
import toeplitz as tp
import PRI

p = pr.prism("/Users/audunhansen/papers/XDEC-RI-MP2/results/adsorption/lih_id_verif/Crystal/lih_id.d12")

c = tp.tmat()
c.load("/Users/audunhansen/papers/XDEC-RI-MP2/results/adsorption/lih_id_verif/psml.npy")

c_occ, c_virt = PRI.occ_virt_split(c,p) # split virtual and occupied space

s = PRI.compute_overlap_matrix(p, tp.lattice_coords([15,0,0])) #compute overlaps

d = c_occ.circulantdots(c_occ.tT()) # compute density matrix

i = tp.get_identity_tmat(p.get_n_ao()) # get identity matrix

# C_pao = I - DS
c_pao = i - d.circulantdots(s)

```

Figure 5.3: Construction of periodic projected atomic orbitals (PAOs). [5]

or move them all to the same center.

The annealing algorithm, as presented in Algorithm 1, is a separate module exclusively called from the orbital refinery.

5.4.4 PRI (Periodic Fitting)

The fitting module consists mainly of two classes; `integral_builder_static` and `coefficient_fitter_static`, and in addition a range of functions for preparing integrals, processing basis sets, screening and domain size estimation. The integral builder is the class responsible for providing the ERIs for the main MP2 correlation calculation. Initialization of `integral_builder_static` is done by providing the following input parameters; First, we require two sets of orbitals, typically the occupied and virtual set for the reference cell. Second, it requires a set of screening parameters in order to determine the bandwidth. Finally, we have to provide the RI-fitting basis and the attenuation parameter.

For the sake of reproducibility, we shall elaborate a little further on the integral screening. If we write out the full AO-expansion for the matrix \mathbf{O} , as presented in Eq. 4.48, we find that it can be reorganised into

$$(\mathbf{L}\tilde{J}\tilde{\mathbf{O}}i\mathbf{A}a) = \sum_{M\mu N\nu} (\mathbf{L}\tilde{J}\tilde{\mathbf{M}}\mu(\mathbf{M} + \mathbf{N})\nu)c_{\mu i}^{-\mathbf{M}}c_{\nu a}^{-(\mathbf{M}+\mathbf{N})+\mathbf{A}} := \sum_{N\nu} \bar{O}_{JiN\nu}^{-\mathbf{L}}c_{\nu a}^{-\mathbf{N}+\mathbf{A}}, \quad (5.4)$$

where an intermediate contraction tensor for only the occupied space has been defined:

$$\bar{O}_{JiN\nu}^{-\mathbf{L}} := \sum_{M\mu} (\mathbf{L}\tilde{J}\tilde{\mathbf{M}}\mu\mathbf{N}\nu)c_{\mu i}^{-\mathbf{M}}. \quad (5.5)$$

This is useful, since we may now in the MP2 case compute \mathbf{O} only once, and subsequently include more virtual orbitals as we expand the spaces. The calculation of $\bar{\mathbf{O}}$ is however not without complication since it can potentially be infinite, so in the PRI-module, these integrals are converged by successively computing spherical shells extending outwards from the reference cell until the contributions fall below certain screening thresholds; ξ_0 and ξ_1 , by default both set to 10^{-10} . The procedure is provided as pseudocode in Algorithms 3 and 4. Note that the latest version of this screening is slightly changed from the one in paper three, since we now truncate relative to the maximum element in the reference cell.

Algorithm 3 AO screening procedure implemented in the XDEC-RI-LMP2 code

- 1: Compile a list Ω containing chunks of coordinate vectors $\{\mathbf{M}\}_{\mathbf{R}}$ grouped together into concentric spherical shells in order of increasing radial distance $\|\mathbf{R}_{\mathbf{M}}\|$ to the reference cell.
 - 2: **for** $\{\mathbf{M}\}_{\mathbf{R}}$ in Ω **do**
 - 3: Compute all $(\mathbf{O}J|\mathbf{0}\mu\mathbf{M}\nu)$'s for the shell
 - 4: **if** all $|(\mathbf{O}J|\mathbf{0}\mathbf{M}\nu)|_{\max} \leq \xi_0 (\mathbf{O}J|\mathbf{0}\mu\mathbf{0}\nu)|_{\max}$ **then**
 - 5: Break
 - 6: **end if**
 - 7: Append all \mathbf{M} s to the screened domain Ξ
 - 8: **end for**
 - 9: Set an initial reasonably large cutoff R_{cut}
 - 10: **for** \mathbf{M} in Ξ **do**
 - 11: Compute all cells $(\mathbf{N}J|\mathbf{0}\mu\mathbf{M}\nu)$ within $R_N \leq R_{\text{cut}}$
 - 12: **if** any $(\mathbf{K}_{\text{boundary}}J|\mathbf{0}\mu\mathbf{M}\nu) \geq \xi_0$, where $0.95R_{\text{cut}} < R_{\mathbf{K}_{\text{boundary}}} \leq R_{\text{cut}}$ **then**
 - 13: Halt execution, warn/advise user to increase domains.
 - 14: **else**
 - 15: Append all blocks where $(\mathbf{N}J|\mathbf{0}\mu\mathbf{M}\nu) \geq \xi_0$ to screening domain $\Xi_{\mathbf{M}}$
 - 16: Let $R_{\text{cut}} = 1.1R_{\mathbf{N}_{\text{outer}}}$ where $R_{\mathbf{N}_{\text{outer}}}$ corresponds to the outermost cell in the appended blocks.
 - 17: **end if**
 - 18: **end for**
-

5.4.5 XDEC (MP2 solver)

The code which is called from the command line is the XDEC-RI code, responsible for solving the equations and producing the MP2 correlation energy. The main pipeline consists of reading in all required input, such as system data, coefficients, matrices and input parameters, and thereafter carrying out the calculation according to the users specification. The default optimization procedure is a XDEC-calculation with FOT set to 10^{-3} and attenuation $\omega = 0.3$.

Algorithm 4 MO fitting screening procedure implemented in the XDEC-RI-LMP2 code

- 1: Set $R_{tolerance} = 10^{-12}$
 - 2: Construct a list Ω of cell-indices \mathbf{L} in order of increasing distance $\|\mathbf{R}_{\mathbf{L}}\|$ to the reference cell.
 - 3: **for** \mathbf{L} in Ω **do**
 - 4: Compute all $\bar{O}_{J\mathbf{N}\nu i}^{\mathbf{L}}$
 - 5: **if** $R_{\mathbf{L}} - R_{\mathbf{L}_{prev}} \geq R_{tolerance}$ and $|\bar{O}_{J\mathbf{N}\nu i}^{\mathbf{L}}| \leq \xi_1 \bar{O}_{J\mathbf{N}\nu i}^0|_{max}$ **then**
 - 6: Break
 - 7: **end if**
 - 8: Store columns ($\mathbf{N}\nu$) and column indices of $\bar{O}_{Ji,\mathbf{N}\nu}^{\mathbf{L}}$ with max absolute value above ξ_1 for subsequent contraction of virtual coefficients.
 - 9: **end for**
-

Initial subspace cutoffs d_o and d_v should be chosen by the user, and by default the minimum number of orbitals included in each expansive step is set to 6. It is possible to assign position to orbitals in various ways. By default, the XDEC code computes orbital centers and assigns position from these. Optionally, it is possible to assign to nearest atom. A localized virtual orbital may be assigned to the center of the PAO with which it has maximum overlap.

5.5 Validation

Our first implementation, the XDEC code, was validated by comparing total MP2 energies for a range of test systems, designed not as realistic systems in nature, but rather as computationally inexpensive, yet with features that could reveal errors and weaknesses in the code. These test systems was a chain and a single-layer surface of Neon, and chains of ethylene, both compared to CRYSCOR, as presented in paper 1. The final implementation was also validated against CRYSCOR, only this time we additionally compared pair-specific contributions as presented in paper three of this dissertation. We also compared across the XDEC and XDEC-RI codes. We find in general good agreement across the codes, as presented in paper three of this dissertation.

As a result of the findings in paper two, we did not perform any further localization of the Wannier orbitals in paper three. The localization routine was however validated by ensuring that it reproduced exactly the localization measures for PSM-1 produced by CRYSTAL.

Chapter 6

Summary and outlook

6.1 Overview

This dissertation illuminates one out of many possible paths towards linearly scaling correlation methods for periodic systems. While the procedure demonstratively works, as shown by the validating results in paper three of this dissertation, new questions has been raised along the way which warrant further exploration. In this chapter we shall briefly summarize my work on this project in light of the three papers submitted with the dissertation, with an additional emphasis on new venues which have been revealed along the way.



Figure 6.1: It still counts, right?

6.2 Research and papers

My first year working on this project was spent on obtaining the reference state. We originally intended to obtain it ourselves in an a-priori Wannier [112] procedure in LSDALTON [108, 109], but were ultimately unable to reproduce results from the literature. [53, 113] Consequently, we decided to instead base our XDEC code on the Wannier functions available from CRYSTAL. [47] The interfacing of CRYSTAL, LSDALTON and LIBINT [107] was mostly focused on obtaining the data in a readable form and converting between the various

conventions used in these codes. We simultaneously started development and testing of the XDEC code. We first aimed at performing orbital optimization beyond the Boys localization in CRYSTAL [48] by means of an intermediate PSM-2 localization in LSDALTON, but due to instabilities and in order to more fully exploit the translational symmetry, I ended up developing and implementing the annealing approach presented in Chapter 3 instead. This procedure is extremely useful in both prototyping and implementation, since it does not rely on any derivatives and thus easily accepts any kind of objective function one might come up with.

We established a collaboration with Lorenzo Maschio from the Theoretical Chemistry Group at the University of Turin, who is one of the main developers behind CRYSCOR. This was extremely useful with regards to validation, interfacing the codes, and discussing all aspects of our implementations. The current version of CRYSCOR is fully integrated into CRYSTAL and employs a range of different approaches to periodic density fitting, which has been the outcome of several years of systematic experimentation by the Turin group and their collaborators. [95] We found a lot of answers and inspiration in their scholarship.

Our work resulted in the first paper of this dissertation, titled "**Divide–Expand–Consolidate Second-Order Møller–Plesset Theory with Periodic Boundary Conditions**". We demonstrated in this paper that the DEC-approach can be extended to the periodic case with a few modifications. We showed that the XDEC scheme provides error control by means of the FOT, and can easily facilitate methods beyond MP2. We furthermore proposed a method for determining a pair-distance cutoff using cubic spline interpolation on a subset of the pair-fragment energies. **My contributions** to this paper was in the general development of the code, setting up the systems, interfacing the various frameworks involved, development of the localization and the cluster extrapolations.

While our original XDEC implementation provided reliable results, it had serious performance issues with respect to the ERIs. The $\mathcal{O}(N_{\text{AO}}^4)$ -scaling issue was originally addressed by reducing the size of the Wannier expansion domains by means of fitting the Wannier orbitals in a subspace of the AO basis, but this procedure still yielded extensively large expansion domains. We therefore concluded that further acceleration such as RI was required. In addition, we had seen indications that there were features of the PAOs making them more suitable for local correlation methods than localized virtual orbitals (LVOs). More specifically, we had seen indications that in actual energy-calculations, the PAOs managed to recover more energy within the local subspace than the LVOs. We therefore began implementing them in our own code under the assumption that this effect was caused by the PAOs being more local than the LVOs. The locality measures, however, would indicate otherwise.

This counter-intuitive finding resulted in the second paper of this dissertation, titled "**Representation of the virtual space in extended systems – a correlation energy convergence study**". In this paper, we performed a systematic comparison of energy convergence of PAOs to LVOs, where we

presented and discussed these results in light of locality considerations. We furthermore reaffirmed the common practice of using PAOs in LMP2 calculations. **My contribution** to this work was to develop the method and implementation of the various localization schemes, an implementation of the DOI-calculation for periodic systems, as well as being the lead author and producing the figures.

Simultaneously with our work on the PAOs, we continued work on implementing the RI-approximation in our original code. While this significantly improved the performance of our code, we realised that the code was fundamentally treating many of the quantities involved in a non-periodic manner, and the adaptation of more translational symmetry proved cumbersome. For example, the RI-approximation makes no assumption as to the translational symmetry of the orbital spaces, and the ERIs are discarded after each expansive step in the fragment optimization. The AO integrals did not incorporate the translational symmetry, and the amplitude equations were explicitly solved for redundant amplitudes where both occupied indices was outside the reference cell. For this reason, we decided to derive all the required expressions using the IBT-formulation, and thus integrating the translational symmetry in all calculations where possible. The change was fundamental, and basically required us to write a completely separate code. This resulted in the current XDEC-RI code, which is the end-point of this dissertation and the code used in producing the results in our third paper.

In this third paper, titled "**Smooth potential-energy surfaces in fragmentation-based local correlation methods for periodic systems**", we investigated how local methods may cause discontinuous potential energy surfaces (PES) for periodic systems. We identified the same mechanisms known to cause these kinds of problems for molecules in the periodic case, and furthermore explored how the principle of converging the local subspace can solve this problem. We performed a theoretical comparison of the DEC-fragmentation scheme to other locality based decoupling schemes, and demonstrated that the same kind of convergence can be performed for other fragmentation schemes. We also presented the attenuated fitting procedure and gave a brief overview of the IBT-formalism presented in Chapter 2 of this dissertation. **My contribution** to this paper was to be the lead author, develop the code and theory required to perform the calculations and produce most of the figures and analysis.

6.3 Prospects

In summary, the three mentioned papers covers the most essential parts of my work at CTCC, and later the Hylleraas Centre for Quantum Molecular Sciences. In my opinion, the attenuated fitting scheme and the XDEC-RI-approach has some very attractive features that should be developed further. With regards to this, I would like to conclude by mentioning some future prospects.

We have experienced some difficulties with linear dependencies in the auxiliary basis that agrees with what has been previously reported for periodic systems. [47, 114, 115, 116, 117, 118] Currently, we have largely disregarded this problem by

6. Summary and outlook

pruning the auxiliary basis sets, but exactly how these dependencies emerge in periodic systems seems to not be especially well understood in the literature. First, in the case of MP2-fitting basis sets, it may not be a perfectly reasonable assumption that the atomic MP2-optimized basis sets are particularly suitable for periodic systems. As opposed to the molecular case, repeated lattice structures of AO-functions possess the ability to "span themselves", in the sense that a single AO function may be perfectly spanned by all its periodic repetitions excluding itself. Removing it, however, simultaneously removes all its repetitions and may thus significantly impact the span of the auxiliary basis. This could possibly be accounted for with a suitable preconditioning, or one could consider optimizing the basis in order to minimize the condition number [118, 119] of the auxiliary attenuated coulomb matrix. Preliminary, unpublished results, shows promise in this regard. Alternatively, one could possibly construct the basis sets using rules that avoid linear dependencies, but it is somewhat unclear what such rules would be aside from explicitly including lattice dependence in the basis. [117] If the problem of linear dependence can be solved, and a more balanced parallelization of the fitting scheme can be implemented, the XDEC-RI code will likely be able to perform MP2 calculations on a much wider range of three dimensional systems.

There is also the prospect of pushing beyond MP2. The framework and methodology presented in this dissertation can, at least on paper, be straightforwardly extended to CCSD and beyond. Technically, it is a matter of adding some extra terms in the iterative MP2 solver, and providing the fitting module with the additional orbital sets, such as occupied-occupied products and virtual-virtual products. After the initial intermediate fitting (Eq. 4.48), the calculation of the ERIs (Eq. 4.41) for a given $\Delta\mathbf{A}$ and $\Delta\mathbf{B}$ is normally about one order of magnitude faster than calculating the fitting coefficients (Eq. 4.43). Still, the intermediate fitting at the onset of the calculation scales linearly with the number of orbitals involved, so extending this to include also the virtual space should not be too difficult. We should however be prepared for significant changes in computational demands with respect to both performance and memory usage. A major contribution to the latter will come from the "ladder"-term, where the contraction involves ERIs with virtual orbitals in all indices. Several interesting developments from the molecular domain could potentially be extended to the periodic case in order to reduce these memory demands, such as systematic reduction of the auxiliary basis [120] or avoiding storage of the ERIs all together. [121, 122] We will likely find that each approach originally devised for molecules have both drawbacks and advantages when applied to periodic systems, as we have seen throughout this entire dissertation. Basis set reduction may benefit greatly from the presumably high degree of redundancy in the periodic auxiliary basis. An IBC-based contraction of the ERIs avoiding intermediate storage could likely utilize a lot of the "excess" integrals produced on-demand in the contraction.

In sum, the XDEC-RI code should in principle be flexible enough to easily accommodate most methods originally devised for molecules, and should serve as a foundation to build upon for future studies.

Bibliography

- [1] Shavitt, I. and Bartlett, R. J. *Many-body methods in chemistry and physics: MBPT and coupled-cluster theory*. Cambridge university press, 2009.
- [2] Bloch, F. “Über die Quantenmechanik der Elektronen in Kristallgittern”. In: *Zeitschrift für Physik*. vol. 52, no. 7 (1929), pp. 555–600.
- [3] Kronig, R. D. L., Penney, W. G., and Fowler, R. H. “Quantum mechanics of electrons in crystal lattices”. In: *Proceedings of the Royal Society of London. Series A, Containing Papers of a Mathematical and Physical Character*. vol. 130, no. 814 (1931), pp. 499–513.
- [4] Hylleraas, E. A. “Reminiscences from early quantum mechanics of two-electron atoms”. In: *Reviews of Modern Physics*. vol. 35, no. 3 (1963), p. 421.
- [5] Pulay, P. “Localizability of dynamic electron correlation”. In: *Chemical Physics Letters*. vol. 100, no. 2 (1983), pp. 151–154.
- [6] Helgaker, T., Jørgensen, P., and Olsen, J. *Molecular Electronic-Structure Theory*. Chichester: John Wiley and Sons, Ltd, 2000.
- [7] Hirata, S. et al. “Coupled-cluster singles and doubles for extended systems”. In: *The Journal of Chemical Physics*. vol. 120, no. 6 (2004), pp. 2581–2592.
- [8] Sinanoğlu, O. “Many-Electron Theory of Atoms, Molecules and Their Interactions”. In: *Advances in Chemical Physics*. John Wiley & Sons, Ltd, 1964, pp. 315–412.
- [9] Nesbet, R. “Electronic pair correlation in atoms and molecules”. In: *International Journal of Quantum Chemistry*. vol. 5, no. S4 (1970), pp. 117–125.
- [10] Cullen, J. M. and Zerner, M. C. “The linked singles and doubles model: An approximate theory of electron correlation based on the coupled-cluster ansatz”. In: *The Journal of Chemical Physics*. vol. 77, no. 8 (1982), pp. 4088–4109.
- [11] Sæbø, S. and Pulay, P. “Local configuration interaction: An efficient approach for larger molecules”. In: *Chemical Physics Letters*. vol. 113, no. 1 (1985), pp. 13–18.
- [12] Pulay, P. and Sæbø, S. “Orbital-invariant formulation and second-order gradient evaluation in Møller-Plesset perturbation theory”. In: *Theoretica Chimica Acta*. vol. 69, no. 5-6 (1986), pp. 357–368.

- [13] Pulay, P. and Saebø, S. “Fourth-Order Møller-Plesset Perturbation Theory in the Local Correlation Treatment. I”. In: *The Journal of Chemical Physics*. vol. 914 (1987), pp. 914–922.
- [14] Ziólkowski, M. et al. “Linear scaling coupled cluster method with correlation energy based error control”. In: *The Journal of Chemical Physics*. vol. 133, no. 1 (2010), p. 014107.
- [15] Rebolini, E. et al. “Divide–Expand–Consolidate Second-Order Møller–Plesset Theory with Periodic Boundary Conditions”. In: *Journal of Chemical Theory and Computation*. vol. 14, no. 5 (2018). PMID: 29554431, pp. 2427–2438.
- [16] Li, S., Ma, J., and Jiang, Y. “Linear scaling local correlation approach for solving the coupled cluster equations of large systems”. In: *Journal of Computational Chemistry*. vol. 23, no. 2 (2002), pp. 237–244.
- [17] Li, S. et al. “An efficient implementation of the “cluster-in-molecule” approach for local electron correlation calculations”. In: *The Journal of Chemical Physics*. vol. 125, no. 7 (2006), p. 074109.
- [18] Wang, Y. et al. “Cluster-in-molecule local correlation approach for periodic systems”. In: *Journal of Chemical Theory and Computation*. vol. 15, no. 5 (2019), pp. 2933–2943.
- [19] Meyer, W. “PNO–CI studies of electron correlation effects. I. Configuration expansion by means of nonorthogonal orbitals, and application to the ground state and ionized states of methane”. In: *The Journal of Chemical Physics*. vol. 58, no. 3 (1973), pp. 1017–1035.
- [20] Neese, F., Wennmohs, F., and Hansen, A. “Efficient and accurate local approximations to coupled-electron pair approaches: An attempt to revive the pair natural orbital method”. In: *The Journal of Chemical Physics*. vol. 130, no. 11 (2009), p. 114108.
- [21] Neese, F., Hansen, A., and Liakos, D. G. “Efficient and accurate approximations to the local coupled cluster singles doubles method using a truncated pair natural orbital basis”. In: *The Journal of Chemical Physics*. vol. 131, no. 6 (2009), p. 064103.
- [22] Riplinger, C. and Neese, F. “An efficient and near linear scaling pair natural orbital based local coupled cluster method”. In: *The Journal of Chemical Physics*. vol. 138, no. 3 (2013), p. 034106.
- [23] Pinski, P. et al. “Sparse maps—A systematic infrastructure for reduced-scaling electronic structure methods. I. An efficient and simple linear scaling local MP2 method that uses an intermediate basis of pair natural orbitals”. In: *The Journal of Chemical Physics*. vol. 143 (2015), p. 034108.
- [24] Riplinger, C. et al. “Sparse maps—A systematic infrastructure for reduced-scaling electronic structure methods. II. Linear scaling domain based pair natural orbital coupled cluster theory”. In: *The Journal of Chemical Physics*. vol. 144 (2016), p. 024109.

- [25] Werner, H.-J. et al. “Scalable electron correlation methods I.: PNO-LMP2 with linear scaling in the molecular size and near-inverse-linear scaling in the number of processors”. In: *Journal of Chemical Theory and Computation*. vol. 11, no. 2 (2015), pp. 484–507.
- [26] Foster, J. M. and Boys, S. F. “Canonical Configurational Interaction Procedure”. In: *Reviews of Modern Physics*. vol. 32, no. 2 (1960), pp. 300–302.
- [27] Boys, S. F. “Construction of Some Molecular Orbitals to Be Approximately Invariant for Changes from One Molecule to Another”. In: *Reviews of Modern Physics*. vol. 32, no. 2 (1960), pp. 296–299.
- [28] Edmiston, C. and Ruedenberg, K. “Localized Atomic and Molecular Orbitals”. In: *Reviews of Modern Physics*. vol. 35 (3 1963), pp. 457–464.
- [29] Pipek, J. and Mezey, P. G. “A fast intrinsic localization procedure applicable for ab initio and semiempirical linear combination of atomic orbital wave functions”. In: *The Journal of Chemical Physics*. vol. 90, no. 9 (1989), pp. 4916–4926.
- [30] Edmiston, C. and Ruedenberg, K. “Localized atomic and molecular orbitals”. In: *Reviews of Modern Physics*. vol. 35, no. 3 (1963), p. 457.
- [31] Høyvik, I.-M., Jansik, B., and Jørgensen, P. “Trust Region Minimization of Orbital Localization Functions”. In: *Journal of Chemical Theory and Computation*. vol. 8, no. 9 (2012). PMID: 26605725, pp. 3137–3146.
- [32] Bonnans, J. F. et al. *Numerical Optimization: Theoretical and Practical Aspects (Universitext)*. Berlin, Heidelberg: Springer-Verlag, 2006.
- [33] Yang, J. et al. “Tensor factorizations of local second-order Møller–Plesset theory”. In: *The Journal of Chemical Physics*. vol. 134, no. 4 (2011), p. 044123.
- [34] Maschio, L. “Local MP2 with density fitting for periodic systems: A parallel implementation”. In: *Journal of Chemical Theory and Computation*. vol. 7, no. 9 (2011), pp. 2818–2830.
- [35] Usvyat, D., Maschio, L., and Schütz, M. “Periodic local MP2 method employing orbital specific virtuals”. In: *The Journal of Chemical Physics*. vol. 143, no. 10 (2015), p. 102805.
- [36] Herbert, J. M. “Fantasy versus reality in fragment-based quantum chemistry”. In: *The Journal of Chemical Physics*. vol. 151, no. 17 (2019), p. 170901.
- [37] Cohen, A. J., Mori-Sánchez, P., and Yang, W. “Challenges for density functional theory”. In: *Chemical Reviews*. vol. 112, no. 1 (2012), pp. 289–320.
- [38] Mee, C. V. van der, Seatzu, S., and Rodriguez, G. “Spectral factorization of bi-infinite multi-index block Toeplitz matrices”. In: *Linear Algebra and its Applications*. vol. 343 (2002), pp. 355–380.

- [39] Boas, M. *Mathematical Methods in the Physical Sciences*. Wiley, 2006.
- [40] Nussbaumer, H. J. “The fast Fourier transform”. In: *Fast Fourier Transform and Convolution Algorithms*. Springer, 1981, pp. 80–111.
- [41] Lawson, C. L. et al. “Basic linear algebra subprograms for Fortran usage”. In: *ACM Transactions on Mathematical Software (TOMS)*. vol. 5, no. 3 (1979), pp. 308–323.
- [42] Floquet, G. “Sur les équations différentielles linéaires à coefficients périodiques”. In: *Annales scientifiques de l'École normale supérieure*. Vol. 12. 1883, pp. 47–88.
- [43] Dovesi, R. et al. “Ab Initio Quantum Simulation in Solid State Chemistry”. In: *Reviews in Computational Chemistry*. John Wiley & Sons, Ltd, 2005. Chap. 1, pp. 1–125.
- [44] Ashcroft, N. W. and Mermin, N. D. *Solid State Physics*. Holt-Saunders, 1976.
- [45] Sólyom, J. *Fundamentals of the Physics of Solids: Volume 1: Structure and Dynamics*. Vol. 1. Springer Science & Business Media, 2007.
- [46] Löwdin, P. “On the Non-Orthogonality Problem Connected with the Use of Atomic Wave Functions in the Theory of Molecules and Crystals”. In: *The Journal of Chemical Physics*. vol. 18, no. 3 (1950), pp. 365–375.
- [47] Dovesi, R. et al. “Quantum-mechanical condensed matter simulations with CRYSTAL”. In: *Wiley Interdisciplinary Reviews: Computational Molecular Science* vol. 8, no. 4 (2018), e1360.
- [48] C. M. Zicovich-Wilson, R. Dovesi, and V. R. Saunders. “A general method to obtain well localized Wannier functions for composite energy bands in linear combination of atomic orbital periodic calculations”. In: *The Journal of Chemical Physics*. vol. 115, no. 21 (2001), pp. 9708–9719.
- [49] Nesbet, R. K. “Electronic Correlation in Atoms and Molecules”. In: *Advances in Chemical Physics*. John Wiley & Sons, Ltd, 1965, pp. 321–363.
- [50] Wannier, G. H. “The structure of electronic excitation levels in insulating crystals”. In: *Physical Review*. vol. 52, no. 3 (1937), p. 191.
- [51] Marzari, N. and Vanderbilt, D. “Maximally localized generalized Wannier functions for composite energy bands”. In: *Physical review B*. vol. 56, no. 20 (1997), p. 12847.
- [52] Marzari, N. et al. “Maximally localized Wannier functions: Theory and applications”. In: *Reviews of Modern Physics*. vol. 84 (4 2012), pp. 1419–1475.
- [53] Shukla, A. et al. “Wave-function-based correlated ab initio calculations on crystalline solids”. In: *Physical Review B*. vol. 60, no. 8 (1999), p. 5211.
- [54] Shukla, A., Dolg, M., and Stoll, H. “A Wannier-function-based ab initio Hartree–Fock study of polyethylene”. In: *Chemical Physics Letters*. vol. 294, no. 1-3 (1998), pp. 126–134.

- [55] Kühne, T. D. et al. “CP2K: An electronic structure and molecular dynamics software package-Quickstep: Efficient and accurate electronic structure calculations”. In: *The Journal of Chemical Physics*. vol. 152, no. 19 (2020), p. 194103.
- [56] Booth, G. H. et al. “Towards an exact description of electronic wavefunctions in real solids”. In: *Nature*. vol. 493, no. 7432 (2013), pp. 365–370.
- [57] Grüneis, A. et al. “Making the random phase approximation to electronic correlation accurate”. In: *The Journal of Chemical Physics*. vol. 131, no. 15 (2009), p. 154115.
- [58] Sun, J.-Q. and Bartlett, R. J. “Second-order many-body perturbation-theory calculations in extended systems”. In: *The Journal of Chemical Physics*. vol. 104, no. 21 (1996), pp. 8553–8565.
- [59] Hirata, S. and Iwata, S. “Analytical energy gradients in second-order Møller–Plesset perturbation theory for extended systems”. In: *The Journal of Chemical Physics*. vol. 109, no. 11 (1998), pp. 4147–4155.
- [60] Hirata, S. and Bartlett, R. J. “Many-body Green’s-function calculations on the electronic excited states of extended systems”. In: *The Journal of Chemical Physics*. vol. 112, no. 17 (2000), pp. 7339–7344.
- [61] Ayala, P. Y., Kudin, K. N., and Scuseria, G. E. “Atomic orbital Laplace-transformed second-order Møller–Plesset theory for periodic systems”. In: *The Journal of Chemical Physics*. vol. 115, no. 21 (2001), pp. 9698–9707.
- [62] McClain, J. et al. “Gaussian-based coupled-cluster theory for the ground-state and band structure of solids”. In: *Journal of Chemical Theory and Computation*. vol. 13, no. 3 (2017), pp. 1209–1218.
- [63] Suhai, S. “Bond alternation in infinite polyene: Peierls distortion reduced by electron correlation”. In: *Chemical Physics Letters*. vol. 96, no. 6 (1983), pp. 619–625.
- [64] Suhai, S. “Quasiparticle energy-band structures in semiconducting polymers: correlation effects on the band gap in polyacetylene”. In: *Physical Review B* vol. 27, no. 6 (1983), p. 3506.
- [65] Liegener, C.-M. “A binitio calculations of correlation effects in trans-polyacetylene”. In: *The Journal of Chemical Physics*. vol. 88, no. 11 (1988), pp. 6999–7004.
- [66] Ye, Y.-J., Förner, W., and Ladik, J. “Numerical application of the coupled cluster theory with localized orbitals to polymers. I. Total correlation energy per unit cell”. In: *Chemical Physics*. vol. 178, no. 1-3 (1993), pp. 1–23.
- [67] Suhai, S. “Cooperative effects in hydrogen bonding: Fourth-order many-body perturbation theory studies of water oligomers and of an infinite water chain as a model for ice”. In: *The Journal of Chemical Physics*. vol. 101, no. 11 (1994), pp. 9766–9782.

- [68] Suhai, S. “Electron correlation in extended systems: Fourth-order many-body perturbation theory and density-functional methods applied to an infinite chain of hydrogen atoms”. In: *Physical Review B*. vol. 50, no. 20 (1994), p. 14791.
- [69] Suhai, S. “Electron correlation and dimerization in trans-polyacetylene: Many-body perturbation theory versus density-functional methods”. In: *Physical Review B*. vol. 51, no. 23 (1995), p. 16553.
- [70] Sun, J.-Q. and Bartlett, R. J. “Convergence behavior of many-body perturbation theory with lattice summations in polymers”. In: *Physical Review Letters*. vol. 80, no. 2 (1998), p. 349.
- [71] Høyvik, I.-M. and Jørgensen, P. “Characterization and generation of local occupied and virtual Hartree–Fock orbitals”. In: *Chemical Reviews*. vol. 116, no. 5 (2016), pp. 3306–3327.
- [72] Høyvik, I.-M. et al. “The divide-expand-consolidate family of coupled cluster methods”. In: *The Journal of Chemical Physics*. vol. 136, no. 1, 014105 (2012), p. 014105.
- [73] Jansik, B. et al. “Local orbitals by minimizing powers of the orbital variance”. In: *The Journal of Chemical Physics*. vol. 134, no. 19 (2011), p. 194104.
- [74] Salamon, P., Sibani, P., and Frost, R. *Facts, Conjectures, and Improvements for Simulated Annealing*. Society for Industrial and Applied Mathematics, 2002.
- [75] Hansen, A. S. et al. “Representation of the virtual space in extended systems—a correlation energy convergence study”. In: *Molecular Physics*. (2020), pp. 1–11.
- [76] Metropolis, N. et al. “Equation of State Calculations by Fast Computing Machines”. In: *The Journal of Chemical Physics*. vol. 21, no. 6 (1953), pp. 1087–1092.
- [77] Whitten, J. L. “Coulombic potential energy integrals and approximations”. In: *The Journal of Chemical Physics*. vol. 58, no. 10 (1973), pp. 4496–4501.
- [78] Baerends, E., Ellis, D., and Ros, P. “Self-consistent molecular Hartree–Fock–Slater calculations I. The computational procedure”. In: *Chemical Physics*. vol. 2, no. 1 (1973), pp. 41–51.
- [79] Dunlap, B. I., Connolly, J., and Sabin, J. “On some approximations in applications of $X \alpha$ theory”. In: *The Journal of Chemical Physics*. vol. 71, no. 8 (1979), pp. 3396–3402.
- [80] Dunlap, B. “Fitting the Coulomb potential variationally in $X \alpha$ molecular calculations”. In: *The Journal of Chemical Physics*. vol. 78, no. 6 (1983), pp. 3140–3142.

- [81] Feyereisen, M., Fitzgerald, G., and Komornicki, A. "Use of approximate integrals in ab initio theory. An application in MP2 energy calculations". In: *Chemical Physics Letters*. vol. 208, no. 5-6 (1993), pp. 359–363.
- [82] Vahtras, O., Almlöf, J., and Feyereisen, M. "Integral approximations for LCAO-SCF calculations". In: *Chemical Physics Letters*. vol. 213, no. 5-6 (1993), pp. 514–518.
- [83] Eichkorn, K. et al. "Auxiliary basis sets to approximate Coulomb potentials". In: *Chemical Physics Letters*. vol. 240, no. 4 (1995), pp. 283–290.
- [84] Eichkorn, K. et al. "Auxiliary basis sets for main row atoms and transition metals and their use to approximate Coulomb potentials". In: *Theoretical Chemistry Accounts*. vol. 97, no. 1-4 (1997), pp. 119–124.
- [85] Weigend, F. et al. "RI-MP2: optimized auxiliary basis sets and demonstration of efficiency". In: *Chemical Physics Letters*. vol. 294, no. 1-3 (1998), pp. 143–152.
- [86] Skylaris, C.-K. et al. "On the resolution of identity Coulomb energy approximation in density functional theory". In: *Journal of Molecular Structure: THEOCHEM*. vol. 501 (2000), pp. 229–239.
- [87] Weigend, F., Köhn, A., and Hättig, C. "Efficient use of the correlation consistent basis sets in resolution of the identity MP2 calculations". In: *The Journal of Chemical Physics*. vol. 116, no. 8 (2002), pp. 3175–3183.
- [88] Löwdin, P.-O. "Quantum theory of many-particle systems. III. Extension of the Hartree-Fock scheme to include degenerate systems and correlation effects". In: *Physical Review*. vol. 97, no. 6 (1955), p. 1509.
- [89] Hetzer, G., Pulay, P., and Werner, H.-J. "Multipole approximation of distant pair energies in local MP2 calculations". In: *Chemical Physics Letters*. vol. 290, no. 1-3 (1998), pp. 143–149.
- [90] Werner, H.-J. "Communication: Multipole approximations of distant pair energies in local correlation methods with pair natural orbitals". In: *The Journal of Chemical Physics*. vol. 145, no. 20 (2016), p. 201101.
- [91] Kristensen, K. et al. "The divide–expand–consolidate MP2 scheme goes massively parallel". In: *Molecular Physics*. vol. 111, no. 9-11 (2013), pp. 1196–1210.
- [92] Kristensen, K. et al. "Molecular gradient for second-order Møller-Plesset perturbation theory using the divide-expand-consolidate (DEC) scheme". In: *The Journal of Chemical Physics*. vol. 137 (2012), p. 114102.
- [93] Mulliken, R. S. "Electronic population analysis on LCAO–MO molecular wave functions. I". In: *The Journal of Chemical Physics*. vol. 23, no. 10 (1955), pp. 1833–1840.
- [94] Kristensen, K. et al. "A locality analysis of the divide–expand–consolidate coupled cluster amplitude equations". In: *Journal of Chemical Theory and Computation*. vol. 7, no. 6 (2011), pp. 1677–1694.

- [95] Manby, F. *Accurate Condensed-Phase Quantum Chemistry*. CRC press, 2010.
- [96] Maschio, L. et al. “Fast local-MP2 method with density-fitting for crystals. I. Theory and algorithms”. In: *Physical Review B*. vol. 76, no. 7 (2007), p. 075101.
- [97] Jung, Y. et al. “Auxiliary basis expansions for large-scale electronic structure calculations”. In: *Proceedings of the National Academy of Sciences*. vol. 102, no. 19 (2005), pp. 6692–6697.
- [98] Milko, M., Noga, J., and Varga, Š. “Accuracy of density fitting in calculation of two-electron repulsion integrals in periodic systems”. In: *International Journal of Quantum Chemistry*. vol. 107, no. 11 (2007), pp. 2158–2168.
- [99] Reine, S., Helgaker, T., and Lindh, R. “Multi-electron integrals”. In: *Wiley Interdisciplinary Reviews: Computational Molecular Science* vol. 2, no. 2 (2012), pp. 290–303.
- [100] Varga, Š. “On robust density fitting in molecules and extended systems”. In: *Journal of Mathematical Chemistry*. vol. 49, no. 1 (2011), pp. 1–5.
- [101] Dombroski, J. P., Taylor, S. W., and Gill, P. M. “KWIK: Coulomb energies in O (N) work”. In: *The Journal of Physical Chemistry*. vol. 100, no. 15 (1996), pp. 6272–6276.
- [102] Dunlap, B. “Robust and variational fitting: Removing the four-center integrals from center stage in quantum chemistry”. In: *Journal of Molecular Structure: THEOCHEM*. vol. 529, no. 1-3 (2000), pp. 37–40.
- [103] Pisani, C. et al. “Local-MP2 electron correlation method for nonconducting crystals”. In: *The Journal of Chemical Physics*. vol. 122, no. 9 (2005), p. 094113.
- [104] Pisani, C. et al. “Periodic local MP2 method for the study of electronic correlation in crystals: Theory and preliminary applications”. In: *Journal of Computational Chemistry*. vol. 29, no. 13 (2008), pp. 2113–2124.
- [105] Halo, M. et al. “Periodic local-MP2 computational study of crystalline neon”. In: *Physical Chemistry Chemical Physics*. vol. 11, no. 3 (2009), pp. 586–592.
- [106] Pisani, C. et al. “C ryscor: a program for the post-Hartree–Fock treatment of periodic systems”. In: *Physical Chemistry Chemical Physics*. vol. 14 (2012), pp. 7615–7628.
- [107] Valeev, E. F. and Fermann, J. “Libint: A library for the evaluation of molecular integrals of many-body operators over Gaussian functions”. In: *For the current version, see <https://github.com/evaleev/libint> (accessed January 2020). For the originating project, see <http://libint.valeev.net> (2017).*

- [108] Aidas, K. et al. “The Dalton quantum chemistry program system”. In: *Wiley Interdisciplinary Reviews: Computational Molecular Science*. vol. 4, no. 3 (2014), pp. 269–284.
- [109] Olsen, J. M. H. et al. “Dalton Project: A Python platform for molecular- and electronic-structure simulations of complex systems”. In: *The Journal of Chemical Physics*. vol. 152, no. 21 (2020), p. 214115.
- [110] Dalcin, L. D. et al. “Parallel distributed computing using Python”. In: *Advances in Water Resources*. vol. 34, no. 9 (2011), pp. 1124–1139.
- [111] Meurer, A. et al. “SymPy: symbolic computing in Python”. In: *PeerJ Computer Science* vol. 3 (Jan. 2017), e103.
- [112] Buth, C. “A priori Wannier functions from modified Hartree-Fock and Kohn-Sham equations”. In: *Physical Review B*. vol. 75 (12 2007), p. 125121.
- [113] Shukla, A. et al. “An ab initio embedded-cluster approach to electronic structure calculations on perfect solids: a Hartree-Fock study of lithium hydride”. In: *Chemical Physics Letters*. vol. 262, no. 3 (1996), pp. 213–218.
- [114] Peintinger, M. F., Oliveira, D. V., and Bredow, T. “Consistent Gaussian basis sets of triple-zeta valence with polarization quality for solid-state calculations”. In: *Journal of Computational Chemistry*. vol. 34, no. 6 (2013), pp. 451–459.
- [115] Jensen, F. “Analysis of energy-optimized Gaussian basis sets for condensed phase density functional calculations”. In: *Theoretical Chemistry Accounts*. vol. 132, no. 8 (2013), p. 1380.
- [116] Towler, M. *An introductory guide to Gaussian basis sets in solid-state electronic structure calculations*. 2000. URL: https://vallico.net/mike_towler/basis_sets/basis_sets_2000.ps.
- [117] Grüneich, A. and Heß, B. A. “Choosing GTO basis sets for periodic HF calculations”. In: *Theoretical Chemistry Accounts*. vol. 100, no. 1-4 (1998), pp. 253–263.
- [118] Daga, L. E., Civalleri, B., and Maschio, L. “Gaussian Basis Sets for Crystalline Solids: All-Purpose Basis Set Libraries vs System-Specific Optimizations”. In: *Journal of Chemical Theory and Computation*. vol. 16, no. 4 (2020), pp. 2192–2201.
- [119] VandeVondele, J. and Hutter, J. “Gaussian basis sets for accurate calculations on molecular systems in gas and condensed phases”. In: *The Journal of Chemical Physics*. vol. 127, no. 11 (2007), p. 114105.
- [120] Kállay, M. “A systematic way for the cost reduction of density fitting methods”. In: *The Journal of Chemical Physics* vol. 141, no. 24 (2014), p. 244113.

- [121] Bozkaya, U. and Sherrill, C. D. “Analytic energy gradients for the coupled-cluster singles and doubles method with the density-fitting approximation”. In: *The Journal of Chemical Physics* vol. 144, no. 17 (2016), p. 174103.
- [122] Bozkaya, U. “Derivation of general analytic gradient expressions for density-fitted post-Hartree-Fock methods: An efficient implementation for the density-fitted second-order Møller–Plesset perturbation theory”. In: *The Journal of chemical physics* vol. 141, no. 12 (2014), p. 124108.

Papers

Paper I

Divide–Expand–Consolidate Second–Order Møller–Plesset Theory with Periodic Boundary Conditions

**Elisa Rebolini, Gustav Baardsen, Audun Skau Hansen, Karl
Roald Leikanger, Thomas Bondo Pedersen**

Journal of Chemical Theory and Computation. vol. 14, no. 5, (2018),
pp. 2427—2438

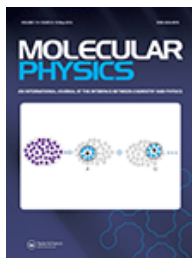
Paper II

Representation of the virtual space in extended systems – a correlation energy convergence study

Audun Skau Hansen, Gustav Baardsen, Elisa Rebolini, Lorenzo Maschio, Thomas Bondo Pedersen

Molecular Physics. vol. 118, no. 19-20, (2020), e1733118.





Molecular Physics

An International Journal at the Interface Between Chemistry and Physics

ISSN: 0026-8976 (Print) 1362-3028 (Online) Journal homepage: <https://www.tandfonline.com/loi/tmph20>

Representation of the virtual space in extended systems – a correlation energy convergence study

A. S. Hansen, G. Baardsen, E. Rebolini, L. Maschio & T. B. Pedersen

To cite this article: A. S. Hansen, G. Baardsen, E. Rebolini, L. Maschio & T. B. Pedersen (2020): Representation of the virtual space in extended systems – a correlation energy convergence study, Molecular Physics, DOI: [10.1080/00268976.2020.1733118](https://doi.org/10.1080/00268976.2020.1733118)

To link to this article: <https://doi.org/10.1080/00268976.2020.1733118>



© 2020 The Author(s). Published by Informa UK Limited, trading as Taylor & Francis Group



Published online: 02 Mar 2020.



Submit your article to this journal [↗](#)



Article views: 341



View related articles [↗](#)



View Crossmark data [↗](#)



Citing articles: 1 View citing articles [↗](#)

Representation of the virtual space in extended systems – a correlation energy convergence study

A. S. Hansen , G. Baardsen^a, E. Rebolini , L. Maschio  and T. B. Pedersen 

^aHylleraas Centre for Quantum Molecular Sciences, Department of Chemistry, University of Oslo, Oslo, Norway; ^bInstitut Laue Langevin, Grenoble, France; ^cDipartimento di Chimica, Università di Torino, Torino, Italy

ABSTRACT

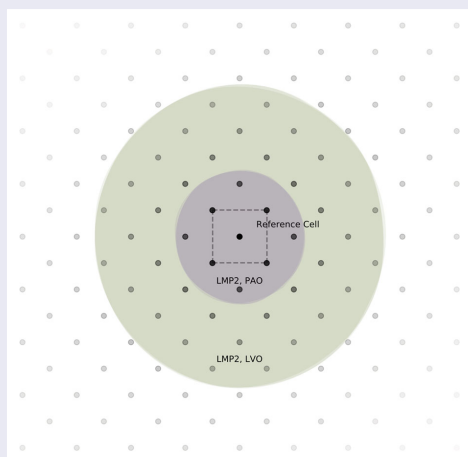
We present an investigation of the convergence behaviour of the local second-order Møller-Plesset perturbation theory (MP2) correlation energy toward the canonical result for three insulating crystals with either projected atomic orbitals (PAOs) or various orthonormal representations of the virtual orbital space. Echoing recent results for finite molecular systems, we find that significantly fewer PAOs than localised orthonormal virtual orbitals are required to reproduce the canonical correlation energy. We find no clear-cut correlation between conventional measures of orbital locality and the ability of the representation to span the excitation space of local domains. We show that the PAOs of the reference unit cell span parts of the excitation space that can only be reached with distant local orthonormal virtual orbitals.

ARTICLE HISTORY

Received 11 December 2019
Accepted 12 February 2020

KEYWORDS



Local correlation; periodic systems; pao; localisation



1. Introduction

Orbital localisation is a powerful tool in molecular and solid-state quantum chemistry, providing both intuitively appealing interpretations and visualisations of electronic structure [1–3], and opportunities for efficient implementations of correlated theories. Spatially localised orbitals can be obtained either by a suitably

chosen unitary transformation of the inherently delocalised canonical Hartree-Fock (HF) or Kohn-Sham orbitals [4] or directly through a restrained noncanonical self-consistent optimisation [5]. From an algorithmic perspective, localised orbitals pave the way for the implementation of orbital-based embedding/fragment schemes [6, 7] and for exploiting the short-range character of electron correlation effects to greatly reduce the

CONTACT A. S. Hansen  a.s.hansen@kjemi.uio.no  Hylleraas Centre for Quantum Molecular Sciences, Department of Chemistry, University of Oslo, P.O. Box 1033 Blindern, Oslo N-0315, Norway

© 2020 The Author(s). Published by Informa UK Limited, trading as Taylor & Francis Group
This is an Open Access article distributed under the terms of the Creative Commons Attribution-NonCommercial-NoDerivatives License (<http://creativecommons.org/licenses/by-nc-nd/4.0/>), which permits non-commercial re-use, distribution, and reproduction in any medium, provided the original work is properly cited, and is not altered, transformed, or built upon in any way.

computational complexity of post-HF methods [8–10]. In this work, we will be concerned with the latter aspect.

The concept of ‘localized orbitals’ is not uniquely defined, however, and different localisation functionals have been proposed. Among the oldest and most widely used proposals are the Foster-Boys [11, 12], Pipek-Mezey [13], and Edmiston-Ruedenberg [14, 15] functionals, which produce localised orbitals that minimise the orbital spread, maximise the orbital partial Mulliken charges over as few atoms as possible, and maximise the Coulomb self-repulsion of the orbitals, respectively. Neither of these locality measures is directly related to the electron-correlation problem, i.e. they are not defined through a quantity that directly enters an expression for the correlation energy. Consequently, it is far from obvious which localisation functional leads to the most efficient general-purpose local-correlation algorithm.

Local electron-correlation methods rely on at least two features:

- (1) The occupied and virtual orbitals should be confined within a small volume in space [16], such that the differential overlap between them decay as rapidly as possible with distance.
- (2) At the same time, the virtual orbitals should be constructed in such a way that a very small number of them is sufficient to accurately represent the excitation space of each pair of occupied orbitals.

The latter has been tackled mainly through the introduction of orbital-specific [17] or pair-specific [18] virtual orbitals. These sets are constructed from an initial set of localised virtual orbitals by means of first-order estimates of the correlation amplitudes – that is, they are constructed directly from features of the electron correlation effects of the system at hand.

Much effort has been devoted to point (1), albeit using measures not directly related to electron correlation effects. It is an open question whether nonorthonormal local orbitals are preferable to orthonormal ones [19–21]. Relaxing the orthogonality constraint leads to simpler nodal structures, which, in particular, may lead to smoother and more rapid decay of the tails of the functions. At the same time, however, the resulting set will be linearly dependent, which one might fear can lead to a larger number of orbitals required to span a given subspace. The most widely-used approach in local correlation theories is to choose an orthonormal set for the occupied space, obtained through localisation of the occupied HF orbitals, while nonorthogonal, linearly dependent projected atomic orbitals (PAOs) are used to represent the virtual manifold. The PAOs are easily computed from the converged HF density matrix and, historically, the choice

of PAOs as virtual orbital basis has more to do with the lack of robust algorithms for the localisation of orthonormal virtual orbitals than superior performance in local correlation treatments. With the robust localisation algorithms developed in recent years by Høyvik, Jørgensen, and coworkers [4, 22–24], orthonormal virtual-orbital localisation can be performed reliably and efficiently, warranting a comparison of the performance of PAOs versus localised orthonormal virtual orbitals (LVOs) in local correlation treatments.

Recently, Werner and coworkers [25–27] reported that PAOs outperform LVOs in molecular calculations. While the LVOs are more local than PAOs in terms of orbital spread, significantly fewer PAOs than LVOs are required in the excitation domains to recover the same fraction of the exact correlation energy. The authors did not present a definitive reason for this somewhat counterintuitive result, however.

The central role of locality in electron correlation treatments is even more pertinent in 3D periodic systems, where the canonical orbitals are forced by translation symmetry to be delocalised over the entire infinite solid. The dense packing of 3D periodic systems enhances the effectiveness of locality-based screening procedures, leading to even more pronounced computational savings than for finite molecular systems.

In this work, we compare the performance of PAOs and different sets of LVOs for local second-order Møller-Plesset (MP2) theory of representative insulators: the covalent diamond crystal, the ionic lithium hydride crystal, and the molecular prussic acid crystal.

2. Theoretical background

The electronic correlation energy of a weakly correlated system can be written in the coupled-cluster (CC) formalism as [28]

$$E_c = \sum_{ij} \sum_{ab} (t_{ij}^{ab} - t_i^a t_j^b) (2(ia | jb) - (ib | ja)), \quad (1)$$

where we have assumed a closed-shell system for simplicity. We use latin letters i, j, k to denote occupied spatial orbitals and a, b, c to denote virtual spatial orbitals obtained from a preceding HF calculation. With real orbitals, the electron repulsion integrals (ERIs) are defined as

$$(ia | jb) = \iint \frac{\varphi_i(\mathbf{r})\varphi_a(\mathbf{r})\varphi_j(\mathbf{r}')\varphi_b(\mathbf{r}')}{|\mathbf{r} - \mathbf{r}'|} d\mathbf{r}' d\mathbf{r}. \quad (2)$$

The single- and double-excitation amplitudes, t_i^a and t_{ij}^{ab} , respectively, are determined from a nonlinear equation system that, for an n -electron system, may involve up

to n -tuple excitations, depending on the chosen CC model. The simplest model is second-order Møller-Plesset (MP2) theory [28] where the single-excitation amplitudes vanish due to the Brillouin condition. The double-excitation amplitudes are obtained from the set of equations [23]

$$t_{ij}^{ab} = \sum_c (f_{ac} t_{ij}^{cb} + t_{ij}^{ac} f_{cb}) - \sum_k (f_{ik} t_{kj}^{ab} + t_{ij}^{ab} f_{ik}) + (ia | jb) = 0, \quad (3)$$

where f is the Fock matrix and all orbitals are assumed to be orthonormal. Solving the MP2 equations scales as $O(N^5)$ with N a measure of system size such as the number of atom-centred basis functions used to expand the occupied and virtual orbitals. The MP2 energy, Equation (1), and amplitude equations, Equation (3), are invariant to rotations among occupied and among virtual orbitals separately. For insulators, this can be exploited to bring forth significant sparsity in the Fock matrix and ERIs which, in turn, imply sparsity in the amplitudes. This observation dates back to Pulay [8] and forms the basis for linear-scaling implementations that today approach a near-black-box level of sophistication [23, 27, 29–33].

Linear scaling can be achieved as the following simple argument shows. Given suitably localised occupied and virtual orbitals, the integral $(ia | jb)$ will be negligible unless a is centred in the vicinity of i in the sense that the product $\varphi_i(\mathbf{r})\varphi_a(\mathbf{r})$ must be non-vanishing in some region of space for the integral to be nonzero. A similar argument applies to j and b , of course. This alone leads to quadratic scaling of the number of significant ERIs. Furthermore, multipole expansion of $(ia | jb)$ reveals an asymptotic decay rate proportional to R^{-3} , where R is a measure of the distance between i and j , leading to linear scaling of the number of significant integrals [34, 35]. The amplitudes and the residuals in Equation (3) inherit the decay property of the integrals, paving the way for a linear-scaling algorithm. By the same token, it follows that the correlation-energy contribution from pairs of occupied orbitals decays asymptotically as R^{-6} , consistent with the decay of London dispersion forces. This argument can be extended to cover also higher-order CC models.

The arguments underpinning linear-scaling correlation treatments thus rely heavily on the concept of orbital locality. As mentioned in the Introduction, this concept is not uniquely defined and a number of localisation functionals have been proposed. In this work, we will consider the central-moment functionals of Høyvik and Jørgensen along with their statistics-based measures of orbital locality [4]. The m th power of the second central

moment (PSM- m) functionals are defined in terms of the second moment orbital spread of each orbital p ,

$$\sigma_2(p) = \langle p | (\mathbf{r} - \langle p | \mathbf{r} | p \rangle)^2 | p \rangle^{1/2}, \quad (4)$$

as

$$\xi^{\text{PSM-}m} = \sum_p \sigma_2(p)^{2m}, \quad (5)$$

where the summation over orbitals should be restricted to either occupied or virtual orbitals to maintain the Brillouin condition. The PSM-1 functional is identical to the Foster-Boys functional [36, 37]. Minimising the PSM-1 functional with respect to unitary rotations of the (orthonormal) orbitals leads to the set of orbitals with the smallest possible sum of orbital spreads. In the context of periodic systems, such orbitals are commonly referred to as maximally localised Wannier functions [38].

Similarly, the PSM-2 orbitals are computed by minimising the objective function in Equation (5) with $m = 2$. The PSM-2 objective function reduces the spread of the least local orbitals at the expense of the most local ones. The motivation behind the PSM-2 functional is the conjecture that the least local orbitals in the PSM-1 set lead to excessive computational effort in a local correlation treatment [22]. Increasing the value of m does not bring any further advantages with respect to the least local orbital(s).

The PSM- m objective functions do not address the problem of long-range tails of the orbitals. The tail of orbital p can be measured by the fourth moment orbital spread σ_4 :

$$\sigma_4(p) = \langle p | (\mathbf{r} - \langle p | \mathbf{r} | p \rangle)^4 | p \rangle^{1/4}, \quad (6)$$

and letting this quantity take the role of $\sigma_2(p)$ leads to the m th power of the fourth central moment (PFM- m) class of localisation functionals [4, 16]

$$\xi^{\text{PFM-}m} = \sum_p \sigma_4(p)^{4m}. \quad (7)$$

Minimising the PFM-1 objective function leads to ‘minimally tailed’ orthonormal orbitals and, in analogy with the PSM-2 case above, heavy-tailed outliers may be removed by putting $m = 2$. Following Høyvik and Jørgensen [4], we use the tail spread $\beta(p)$, defined as the fourth root of the kurtosis,

$$\beta(p) = \frac{\sigma_4(p)}{\sigma_2(p)}, \quad (8)$$

to measure tail thickness. The more heavy-tailed an orbital is, the greater the value of its tail spread.

In this work, we will focus on orthonormal orbitals obtained by minimising the PSM-1, PSM-2, and PFM-2 objective functions.

The by far most commonly used virtual basis is composed of PAOs [8], which are straightforwardly constructed by projecting out the occupied orbitals from the atomic orbital (AO) basis, so that a normalised PAO $|\tilde{\mu}\rangle$ is given by

$$|\tilde{\mu}\rangle = N_{\mu} \left(1 - \sum_i |i\rangle\langle i| \right) |\mu\rangle, \quad (9)$$

where $|\mu\rangle$ are the AOs and $N_{\mu} = \langle \mu | (1 - \sum_i |i\rangle\langle i|) | \mu \rangle^{-1/2}$. In this way, a redundant set of orbitals is obtained, having in principle the same size as the AO basis. The PAOs inherit a certain degree of locality from the HF density matrix used for the projection and are free from the delocalisation (tail) effects resulting from the orthogonality constraint [24].

We are in this work mainly interested in the impact of the choice of virtual orbitals on the efficiency and accuracy of periodic local MP2 calculations. Although the choice of virtual orbitals can not be entirely decoupled from the choice of localised occupied orbitals, we will use the PSM-1 localised occupied orbitals in conjunction with different sets of either LVOs or PAOs. As proposed by Pinski et al. [30], we may then characterise the so-called multiplicative sparsity between the occupied and virtual sets of orbitals through differential overlap integrals (DOIs). The DOI for an occupied orbital φ_i and a virtual orbital φ_a is defined as

$$\Omega_{ia} = \sqrt{\int \varphi_i(\mathbf{r})^2 \varphi_a(\mathbf{r})^2 d\mathbf{r}}. \quad (10)$$

The DOIs measure the extent to which the occupied and virtual orbitals have a non-vanishing intersection in \mathbb{R}^3 and thus can be used to map the sparsity of the ERIs, Equation (2), with the chosen virtual orbital basis.

While the focus of the localising objective functions and construction procedures is on the spatial distribution of the orbitals, they are each implicitly assumed to bring forth a condition where the significant part of the correlation can be attributed to a subset of the full amplitude space, determined from locality considerations. Although most modern implementations of local correlation theories reduce the impact of the initial choice of virtual basis through further refinements like orbital-specific virtuals [39] or pair-natural orbitals [30, 32, 33], it is of fundamental importance to compare the behaviour of PAOs and orthonormal virtual orbitals in the context of computing the ground-state correlation

energy. It is, however, not trivial to devise a fair comparison between different types of orbitals (orthonormal or non-orthonormal, atom-centred or not), where the correlation energy is closely related to the number of virtual orbitals used in the calculation. In this work, we have chosen to treat the excitation space in the following manner:

- (1) For each occupied orbital a list of atomic centres in its vicinity is compiled, and PAOs centred on such atoms constitute the initial excitation domain. This list is built by taking the n atoms closest to the occupied-orbital centroid, and then rounding up such that all atoms within the same distance are included (within a numerical threshold).
- (2) Through the orbital-specific virtuals (OSV) methodology [39], a set of virtuals is built as a linear combination of the initial set by diagonalising the MP2 pair density matrices \mathbf{D}^{ii} corresponding to diagonal pairs ii in the reference unit cell:

$$D_{ab}^{ii} = \sum_c t_{ii}^{ac} t_{ii}^{cb} \quad (11)$$

- (3) The resulting set of orbitals is trimmed to keep the error in the total correlation energy within a threshold.
- (4) The number of OSVs retained for each domain is then a function of (i) the size of the original PAO domain, and (ii) the number of orbitals significantly contributing to the correlation energy.
- (5) Finally, the virtual space of a local pair domain (which, for diagonal pairs, coincides with the orbital domain) is transformed into a local orthonormal (LON) space for the pair-domain amplitudes, in which redundant orbitals are discarded according to a threshold of 10^{-4} on the overlap eigenvalue.

While thresholds on the LON redundancy check in point (5) above are generally tighter in molecular applications, the closer packing of bulk solids makes the algorithm more sensitive to linear dependencies and, by experience, the chosen value is reasonable. Sets of LON orbitals are constructed in the same manner starting from each initial set of LVOs (PSM-1, PSM-2, or PFM-2 LVOs). In this procedure, each LVO is associated with the atom nearest to its orbital centroid. The convergence of the local MP2 correlation energy toward the exact (canonical) result as a function of the average number of LON orbitals retained in the diagonal domains provides a measure of the ability of the initial virtual-orbital (PAO or LVO) set to capture the main correlation effects.

3. Computational details

We shall consider MP2 energy calculations for three simple bulk insulators: diamond, LiH, and HCN. These are chosen as representatives of the different chemical situations that can be found in a nonmetallic (and non-magnetic) solid: a purely covalently bonded, a purely ionic, and a molecular crystal. The systems are also chosen to keep the complexity low enough to facilitate analysis of the orbitals and their effect on correlation energies.

The localised occupied orbitals are obtained from the Wannierization algorithm [40] implemented in the CRYSTAL program [41]. This procedure includes a Foster-Boys localisation [11, 12] that minimises the PSM-1 objective function given in Equation (5). The PAOs are constructed as in Equation (9) and those with norm below 10^{-3} are discarded.

As opposed to many other codes developed for ab initio studies of solid-state materials, CRYSTAL adopts atom-centred Gaussian basis sets, making it comparable

with molecular programs – and, in fact, fully equivalent when zero-dimensional periodicity is invoked. A 6-31G** basis was used for HCN [42, 43], 6-21G* for diamond [44], while a simpler basis set was adopted for LiH (3-11G** on H [45], 6-1G** on Li [46]). Detailed structures (nuclear coordinates, unit cell parameters) and technical details regarding the initial HF calculations are provided in the Appendix. In all cases the experimental lattice parameters have been adopted. The lattice constants of the cubic diamond and LiH crystal structures are 3.56679 Å [47] and 4.0834 Å [48], respectively, while those of the tetragonal HCN crystal structure are $a = 4.13$ Å, $b = 4.85$ Å, and $c = 4.34$ Å [49]. Note that we use primitive unit cells in all calculations.

The LVO orbitals are generated by the same Wannierization algorithm in CRYSTAL, yielding the PSM-1 LVOs (see the Appendix for more technical details). The PSM-2 and PFM-2 LVOs are obtained by further optimisation of the PSM-1 LVOs in a stochastic procedure where only

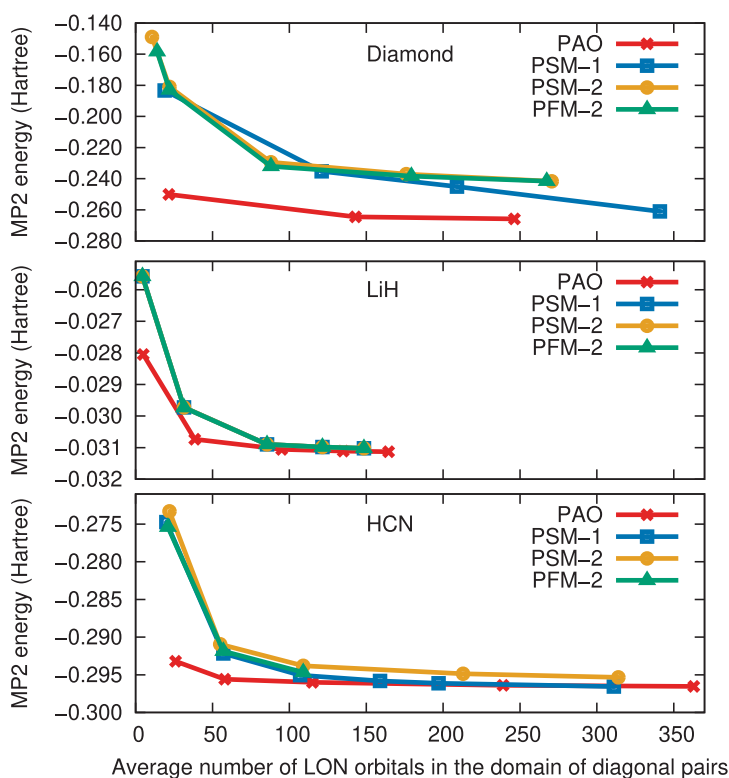


Figure 1. Convergence of the MP2 correlation energy with respect to the average number of LON orbitals in the diagonal pairs. The panels from top to bottom show results for bulk diamond, LiH and HCN, respectively, for the PAO and various LVO sets.

unitary transformations amongst the virtual orbitals in the reference unit cell are permitted. The LVOs associated with all other unit cells of the crystal are then obtained by simple translations.

For each representation of the virtual space, we quantify locality by computing second- and fourth moment orbital spreads, Equations (4) and (6), as well as the tail spread, Equation (8). Further analysis of sparsity in the orbital sets is performed by estimating the DOIs, Equation (10), using the Monte Carlo integration scheme outlined in appendix II.

Periodic local MP2 calculations are performed with the CRYSCOR suite [50–54]. Within the present CRYSCOR implementation [54], the initial excitation domains are constructed by means of the OSV method as outlined in the previous section with the default number of neighbouring atoms $n = 30$. This number is incrementally increased for each of the systems under consideration, recording the local MP2 correlation energy as a function of the average number of LON orbitals in the domains of diagonal pairs. As in Refs. [17, 54], symmetric OSV pair domains are used in the evaluation of the MP2 correlation energy.

4. Results and discussion

Figure 1 shows the convergence behaviour of the local MP2 correlation energy with respect to the average size of the LON space for each set of initial virtual orbitals. The convergence is strikingly better with PAOs than with LVOs for all three systems. Across a range of chemically distinct systems – covalent diamond, ionic LiH and molecular HCN – we thus observe that the PAOs capture more of the correlation energy within smaller domains than the PSM-1, PSM-2, and PFM-2 LVOs. Overall, the performance of the three LVO sets is equally poor. For LiH, the PAO set yields an essentially converged correlation energy with an average LON dimension of about 40, whereas roughly twice as many LON orbitals are required with the LVO sets. For HCN, the LON dimension required for convergence with the LVO sets is roughly thrice that of the PAO set. The diamond crystal is more challenging, also with PAOs, which yield convergence at a LON dimension just below 150, whereas LVOs require at least about 350 LON orbitals.

As apparent from the locality measures compiled in Figure 2, the superior convergence of the PAOs can not be unambiguously attributed to their being more local or light-tailed than the LVOs. The σ_2 data show that the PAOs are on average the least local choice and, consequently, orbital spreads can not explain the very different convergence behaviours. This agrees with the observations for molecules by Krause and Werner [25]. Nor

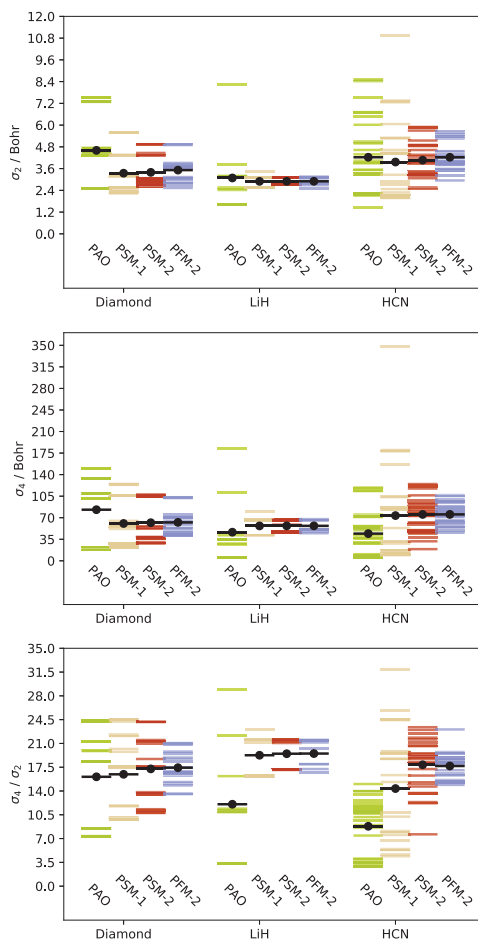


Figure 2. Second- and fourth moment orbital spreads and tail spreads for the various sets of virtual orbitals for diamond, LiH, and HCN. Horizontal lines give the value for each orbital in each set, while average values are indicated by the horizontal black lines.

can a clear distinction of the PAOs be made from the σ_4 data. While the PAOs do have the smallest average σ_4 for LiH and HCN, they also show the greatest maximum value for LiH and diamond. In all cases, the smallest maximum σ_4 is observed for the PFM-2 set. The average β values, on the other hand, are smaller for the PAOs than for the LVO sets across all three systems. While this is fully consistent with the observed correlation-energy convergence behaviour in Figure 1, we note that the maximum β value is greater for the PAOs than for the PFM-2 sets for both diamond and LiH. Judging from the β values alone, one would expect the

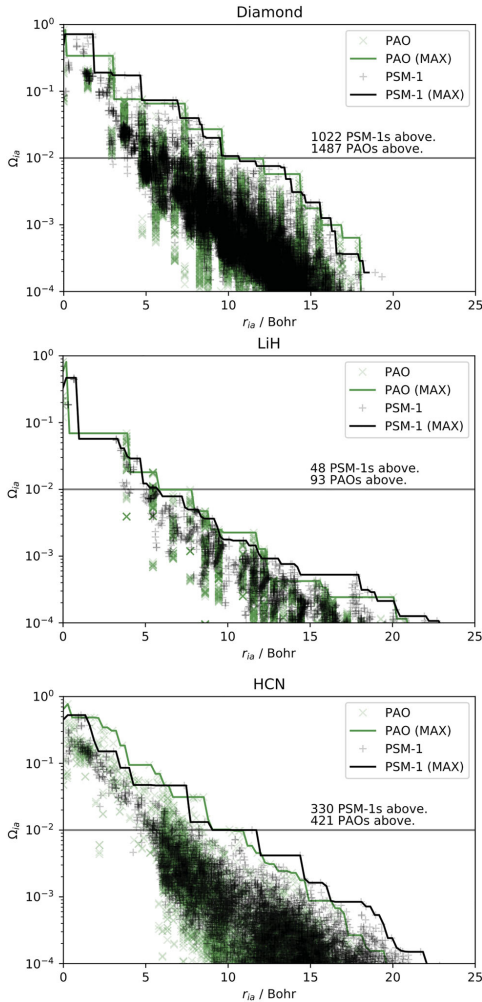


Figure 3. Differential overlap integrals between the occupied orbitals of the reference unit cell and the PAO and PSM-1 virtual orbital spaces for diamond (top), LiH (center), and HCN (bottom), as a function of the inter-orbital distance r_{ia} between occupied orbitals in the reference cell and PAOs or PSM-1 virtual orbitals throughout the crystal. The graphs show the maximum DOI for each orbital set above a given distance.

correlation-energy convergence behaviour to be similar for PAOs and either of the LVO sets in the case of diamond, while the PAOs should be vastly superior to the LVOs in the case of HCN. As seen from Figure 1, however, the LVO sets struggle even more for diamond than for HCN and LiH. We thus conclude that neither second moment spread, fourth moment spread, nor tail spread

can unambiguously explain the observed convergence behaviour.

An alternative explanation might be that the PAOs provide greater multiplicative sparsity, translating into smaller diagonal excitation domains by allowing for a smaller cutoff distance from each occupied orbital. According to this hypothesis, the PAOs should show few important DOIs at short range followed by rapid decay at longer distances, whereas the LVOs should decay more slowly with distance. The estimated DOIs for PAOs and PSM-1 virtual orbitals are plotted in Figure 3. For each crystal, the overall DOI decay rates are comparable for both sets of virtual orbitals, although the DOIs of the PAOs are more scattered with values at each distance both above and below those of the PSM-1 orbitals. A DOI cutoff threshold of 10^{-2} , as recommended by Pinski et al. [30], would suggest that about the same or even *more* PAOs than PSM-1 orbitals must be included in the correlation treatment.

Evidently, neither the statistics-based locality measures nor the DOIs provide a clear-cut explanation of the more rapid correlation-energy convergence with the PAOs. Although the LVOs span the same space as the PAOs when the entire crystal is considered, a distance-based truncation of the PAOs clearly captures more of the correlation energy. From the viewpoint of the LVOs, this implies that the PAOs of a given cell must contain components that are only present in more distant orbitals in the orthonormal representation. To investigate this effect, we expand the PAOs of the reference unit cell, denoted $|0\tilde{\mu}\rangle$ where 0 indicates that the parent AO $|\mu\rangle$ is located in the reference unit cell, in a basis defined by a given set of LVOs,

$$|0\tilde{\mu}\rangle = \sum_L \sum_a |La\rangle \langle La | 0\tilde{\mu}\rangle \equiv \sum_L \sum_a |La\rangle C_{a\tilde{\mu}}^L, \quad (12)$$

where L is a lattice index (including 0, the reference unit cell). The expansion coefficients can be computed directly from their definition. In order to measure the extent to which distant LVOs are represented in the PAO set of the reference unit cell, we introduce the ‘weight’ of each virtual orbital $|La\rangle$ as the square of the corresponding expansion coefficient,

$$W_{a\tilde{\mu}}^L = \left(C_{a\tilde{\mu}}^L\right)^2. \quad (13)$$

These weights are plotted in Figure 4 as a function of the inter-orbital distance $r_{\tilde{\mu}a}$ between the PAOs in the reference cell and PSM-1 LVOs throughout the crystal.

Only plots for the PSM-1 set are shown. Essentially identical plots are obtained for the PSM-2 and PFM-2 sets. While the weights decay quite rapidly, significant contributions ($W_{a\tilde{\mu}}^L \gtrsim 10^{-3}$) may indeed be

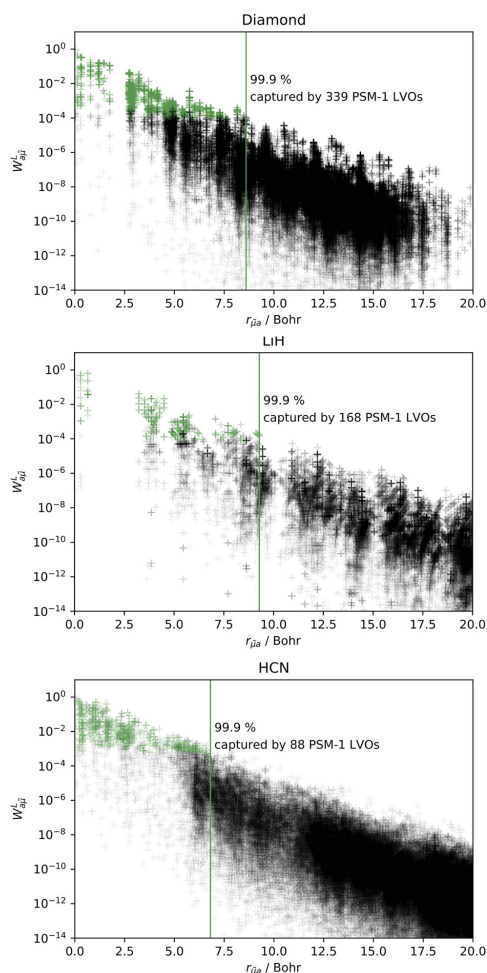


Figure 4. Expansion coefficients squared, Equation (13), of the PSM-1 virtual orbitals for the reference-cell PAOs as a function of the distance between the reference cell PAOs and each virtual orbital for diamond (top panel), LiH (middle panel), and HCN (bottom panel). Green points indicate expansion coefficients that are required to recover 99.9% of the norm of every single PAO. There are 26, 11 and 32 such PAOs for diamond, LiH, and HCN, respectively. The most distant orbital that has to be included to capture the same span is indicated with a vertical green line.

observed between 5 and 10 bohr from the origin of the reference cell. This is consistent with the observed correlation-energy convergence behaviour. Furthermore, it is evident from the vertical lines of Figure 4 that a distance-based truncation of the LVOs leads to the inclusion of a large number of redundant components, ultimately resulting in inefficient (but still linear-scaling)

calculations of the MP2 correlation energy. Interestingly, the distribution of the green points suggests that a more sparse subspace of LVOs may be chosen based on their importance in spanning the same space as the reference-cell PAOs.

5. Concluding remarks

We have studied the impact of the initial choice of virtual-orbital basis, PAOs and three different sets of LVOs, on the convergence of the local MP2 correlation energy toward the canonical result for three insulating crystals with qualitatively different chemical bonding situations, diamond (covalent crystal), LiH (ionic crystal), and HCN (molecular crystal). Our results confirm recent findings by Werner and coworkers [25–27] for molecules: the performance of PAOs is significantly better than LVOs.

This result is somewhat counterintuitive since the LVOs are generally more local according to second moment orbital spread data, have thinner tails according to fourth moment orbital spread data, and provide comparable or even greater multiplicative sparsity in conjunction with localised orthonormal occupied orbitals than the PAOs. Although we do observe a certain agreement with tail spread data for the PAOs and LVOs, correctly indicating superiority of the former, there is no one-to-one mapping between β values and the observed convergence behaviour. Inspecting the expansion of the reference-cell PAOs in the LVO basis, we find that the PAOs contain surprisingly large components of distant LVOs. It seems, therefore, that the efficiency of the PAOs can be traced to their being sufficiently local *and* linearly dependent such that by choosing a subset of them based on the location of the atomic centres of the parent AOs, we get a greater fraction of the excitation space than we would have obtained with the LVOs centred in the same spatial region.

Disclosure statement

No potential conflict of interest was reported by the author(s).

Funding

This work was supported by the Research Council of Norway (RCN)–Norges Forskningsråd through its Centres of Excellence scheme, project number 262695, by the RCN Research Grant No. 240698, and by the Norwegian Supercomputing Program NOTUR Grant No. NN4654K.

ORCID

A. S. Hansen  <http://orcid.org/0000-0003-0962-3143>

E. Rebolini  <http://orcid.org/0000-0001-5709-5547>

L. Maschio  <http://orcid.org/0000-0002-4657-9439>

T. B. Pedersen  <http://orcid.org/0000-0001-8967-6055>

References

- [1] A.E. Reed, R.B. Weinstock and F. Weinhold, *J. Chem. Phys.* **83**, 735–746 (1985).
- [2] A.E. Reed, L.A. Curtiss and F. Weinhold, *Chem. Rev.* **88**, 899–926 (1988).
- [3] G. Knizia, *J. Chem. Theory Comput.* **9**, 4834–4843 (2013).
- [4] I.M. Høyvik and P. Jørgensen, *Chem. Rev.* **116**, 3306–3327 (2016).
- [5] M. Ziolkowski, B. Jansik, P. Jørgensen and J. Olsen, *J. Chem. Phys.* **131**, 124112 (2009).
- [6] J.M. Herbert, *J. Chem. Phys.* **151**, 170901 (2019).
- [7] D. Usvyat, L. Maschio and M. Schütz, *WIREs: Comp. Mol. Sci.* **8**, e1357 (2018).
- [8] P. Pulay, *Chem. Phys. Lett.* **100**, 151–154 (1983).
- [9] M. Schütz, G. Hetzer and H.J. Werner, *J. Chem. Phys.* **111**, 5691–5705 (1999).
- [10] F. Neese, A. Hansen and D.G. Liakos, *J. Chem. Phys.* **131**, 064103 (2009).
- [11] J.M. Foster and S.F. Boys, *Rev. Mod. Phys.* **32**, 300–302 (1960).
- [12] S.F. Boys, *Rev. Mod. Phys.* **32**, 296–299 (1960).
- [13] J. Pipek and P.G. Mezey, *J. Chem. Phys.* **90**, 4916 (1989).
- [14] C. Edmiston and K. Ruedenberg, *Rev. Mod. Phys.* **35**, 457 (1963).
- [15] C. Edmiston and K. Ruedenberg, *J. Chem. Phys.* **43**, S97 (1965).
- [16] I.M. Høyvik, B. Jansik and P. Jørgensen, *J. Chem. Phys.* **137**, 224114 (2012).
- [17] J. Yang, G.K.L. Chan, F.R. Manby, M. Schütz and H.J. Werner, *J. Chem. Phys.* **136**, 144105 (2012).
- [18] R. Ahlrichs and W. Kutzelnigg, *J. Chem. Phys.* **48**, 1819–1832 (1968).
- [19] S. Liu, J.M. Pérez-Jordá and W. Yang, *J. Chem. Phys.* **112**, 1634–1644 (2000).
- [20] B. Paulus, K. Rościszewski, H. Stoll and U. Birkenheuer, *Phys. Chem. Chem. Phys.* **5**, 5523–5529 (2003).
- [21] D. Usvyat and M. Schütz, *Theor. Chem. Acc.* **114**, 276–282 (2005).
- [22] B. Jansik, S. Høst, K. Kristensen and P. Jørgensen, *J. Chem. Phys.* **134**, 194104 (2011).
- [23] I.M. Høyvik, K. Kristensen, B. Jansik and P. Jørgensen, *J. Chem. Phys.* **136**, 014105 (2012).
- [24] I.M. Høyvik, K. Kristensen, T. Kjærgaard and P. Jørgensen, *Theor. Chem. Acc.* **133**, 1–10 (2014).
- [25] C. Krause and H.J. Werner, *Phys. Chem. Chem. Phys.* **14**, 7591–7604 (2012).
- [26] H.J. Werner, C. Köppl, Q. Ma and M. Schwilk, in *Fragmentation: Toward Accurate Calculations on Complex Molecular Systems*, edited by Mark S. Gordon (John Wiley & Sons, Ltd, Chichester, UK, 2017), Chap. 1, pp. 1–79.
- [27] Q. Ma and H.J. Werner, *WIREs: Comp. Mol. Sci.* **8**, e1371 (2018).
- [28] T. Helgaker, P. Jørgensen and J. Olsen, *Molecular Electronic-Structure Theory* (John Wiley and Sons, Ltd, Chichester, 2000).
- [29] Z. Rolik, L. Szegedy, I. Ladjánszki, B. Ladóczki and M. Kállay, *J. Chem. Phys.* **139**, 094105 (2013).
- [30] P. Pinski, C. Riplinger, E.F. Valeev and F. Neese, *J. Chem. Phys.* **143**, 034108 (2015).
- [31] J.J. Eriksen, P. Baudin, P. Ettenhuber, K. Kristensen, T. Kjærgaard and P. Jørgensen, *J. Chem. Theory Comput.* **11**, 2984–2993 (2015).
- [32] C. Riplinger, P. Pinski, U. Becker, E.F. Valeev and F. Neese, *J. Chem. Phys.* **144**, 024109 (2016).
- [33] H.J. Werner, G. Knizia, C. Krause, M. Schwilk and M. Dornbach, *J. Chem. Theory Comput.* **11**, 484–507 (2015).
- [34] G. Hetzer, P. Pulay and H.J. Werner, *Chem. Phys. Lett.* **290**, 143–149 (1998).
- [35] H.J. Werner, *J. Chem. Phys.* **145**, 201101 (2016).
- [36] S.F. Boys, *Rev. Mod. Phys.* **32**, 296 (1960).
- [37] J.M. Foster and S.F. Boys, *Rev. Mod. Phys.* **32**, 300 (1960).
- [38] N. Marzari, A.A. Mostofi, J.R. Yates, I. Souza and D. Vanderbilt, *Rev. Mod. Phys.* **84**, 1419–1475 (2012).
- [39] J. Yang, Y. Kurashige, F.R. Manby and G.K.L. Chan, *J. Chem. Phys.* **134**, 044123 (2011).
- [40] C.M. Zicovich-Wilson, R. Dovesi and V.R. Saunders, *J. Chem. Phys.* **115**, 9708–9719 (2001).
- [41] R. Dovesi, A. Erba, R. Orlando, C.M. Zicovich-Wilson, B. Civalieri, L. Maschio, M. Rérat, S. Casassa, J. Baima, S. Salustro and B. Kirtman, *WIREs: Comp. Mol. Sci.* **8**, e1360 (2018).
- [42] R. Dovesi, C. Ermondi, E. Ferrero, C. Pisani and C. Roetti, *Phys. Rev. B* **29**, 3591–3600 (1984).
- [43] C. Gatti, V.R. Saunders and C. Roetti, *J. Chem. Phys.* **101**, 10686–10696 (1994).
- [44] M. Catti, A. Pavese, R. Dovesi and V.R. Saunders, *Phys. Rev. B* **47**, 9189–9198 (1993).
- [45] M.F. Peintinger, D.V. Oliveira and T. Bredow, *J. Comput. Chem.* **34**, 451–459 (2013).
- [46] B. Civalieri, A.M. Ferrari, M. Llunell, R. Orlando, M. Mérawa and P. Ugliengo, *Chem. Mat.* **15**, 3996–4004 (2003).
- [47] R.W.G. Wyckoff, *Crystal Structures*, Vol. 1, 2nd ed. (Interscience Publishers, New York, 1963).
- [48] E. Staritzky and D. Walker, *J. Annal. Chem.* **28**, 1055 (1956).
- [49] W.J. Dulmage and W.N. Lipscomb, *Acta Cryst.* **4**, 330 (1951).
- [50] C. Pisani, M. Busso, G. Capocchi, S. Casassa, R. Dovesi, L. Maschio, C. Zicovich-Wilson and M. Schütz, *J. Chem. Phys.* **122**, 094113 (2005).
- [51] L. Maschio, D. Usvyat, F. Manby, S. Casassa, C. Pisani and M. Schütz, *Phys. Rev. B* **76**, 075101 (2007).
- [52] C. Pisani, L. Maschio, S. Casassa, M. Halo, M. Schütz and D. Usvyat, *J. Comput. Chem.* **29**, 2113–2124 (2008).
- [53] C. Pisani, M. Schütz, S. Casassa, D. Usvyat, L. Maschio, M. Lorenz, A. Erba, M. Schutz, S. Casassa, D. Usvyat, L. Maschio, M. Lorenz and A. Erba, *Phys. Chem. Chem. Phys.* **14**, 7615–7628 (2012).
- [54] D. Usvyat, L. Maschio and M. Schütz, *J. Chem. Phys.* **143**, 102805 (2015).
- [55] Crystal manual <http://www.crystal.unito.it/documentation.php> 2019 (Accessed: 2019-12-03).
- [56] S.T. Tokdar and R.E. Kass, *WIREs Comp. Stat.* **2**, 54–60 (2010).

Appendices

Appendix 1. Geometries

The reader is referred to the Crystal manual [55] for details regarding the keywords given in the following discussion. All calculations were performed for 3D periodicity. In all cases the two-electron integrals were treated exactly (invoked with keyword NOBIPOLA) when setting up the Fock-matrix.

Diamond was computed with space group 227 and lattice parameter 3.56679 Å. With a standard shift of the origin (IFSO set to 1), a carbon was placed in $\mathbf{r}_C = (0, 0, 0)$. The Hartree-Fock optimisation was performed with SHRINK set to 8 and an energy tolerance of 10^{-10} . The integral tolerances were 8 8 8 10 20. For the Wannierization, we used a NEWK of 9.

For LiH we used space group 225 with lattice parameter 4.0834 Å. Lithium was placed at $\mathbf{r}_{Li} = (0, 0, 0)$ and hydrogen at $\mathbf{r}_H = (\frac{1}{2}, \frac{1}{2}, \frac{1}{2})$, both in units given as fractions of the lattice vectors. For the Hartree-Fock optimisation we used a SHRINK factor of 7 with a convergence tolerance on the energy (TOLDEE) 10^{-12} . Integral tolerances (ITOL) was set to 8 8 8 25 50. For the Wannierization we used a NEWK of 11.

For HCN we used space group 44 and lattice parameters 4.13 Å, 4.85 Å, 4.34 Å, 90° , 90° , and 90° . The fractional coordinates of hydrogen, carbon and nitrogen were $\mathbf{r}_H = (0, 0, -0.2459793977425)$, $\mathbf{r}_C = (0, 0, 0.003572703972826)$, and $\mathbf{r}_N = (0, 0, 0.2701066937697)$, respectively. For the Hartree-Fock optimisation we used a SHRINK factor of 7 and integral tolerances of 7 7 7 20 40. The energy tolerance (TOLDEE) was set to 10^{-10} . The subsequent Wannierization was performed with NEWK 11.

Appendix 2. DOI estimates

The differential overlap integrals (DOIs) [30] were estimated using Monte Carlo (MC) integration [56] within finite volumes of the full integration domain (\mathbb{R}^3).

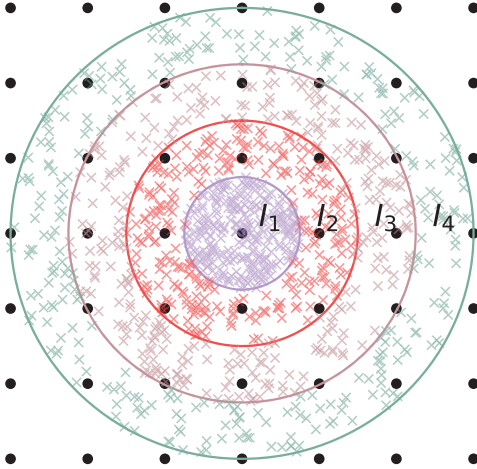


Figure A1. Illustration of Monte Carlo integration within concentric shells. The density of samples is higher in the centre. The final integral is estimated by $I = \sum_{n=1}^{N_{shells}} I_n$.

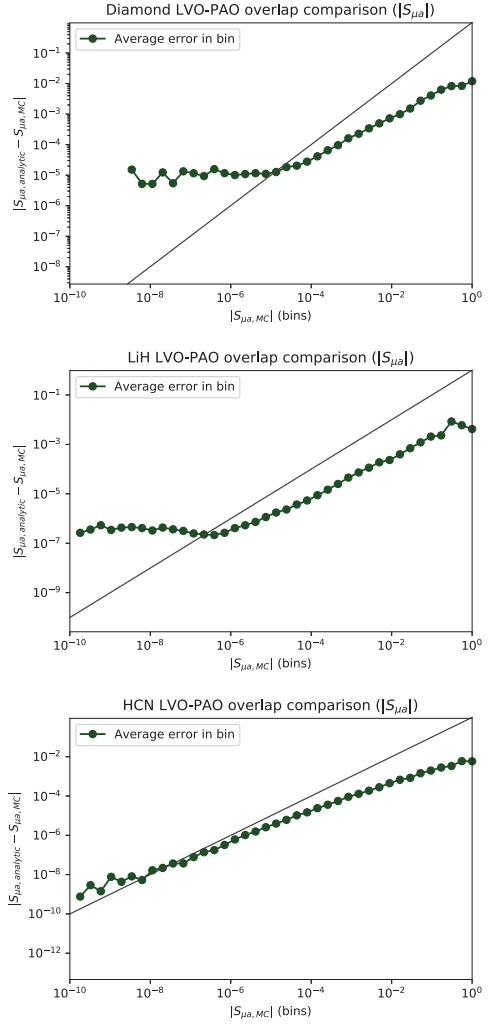


Figure A2. Absolute difference of analytical and MC estimates for the PAO-LVO ($S_{\mu\alpha}$) overlap matrix elements. The elements are sorted into bins depending on the absolute value of the MC-estimates, whereby the average error within each bin is calculated and plotted. The diagonal line shows where the absolute deviation equals the MC-estimate. The intersection between the diagonal and the average can be used to identify a lower bound at which the loss of precision in the MC estimates becomes too severe to draw any conclusions. This intersection appears well below 10^{-4} in all three cases.

For each pair of unit cells, the full integration domain is divided into concentric spherical shells as illustrated in Figure A1, with their origin situated halfway between the lattice vectors associated with the relevant cells. The outermost layer

is placed at 50 Bohr, with its interior divided into 121 shells uniformly spaced in the radial direction.

The overlap and differential overlap integrals are computed 20 times for all orbitals associated with the two cells using MC integration with 2000 random samples uniformly distributed inside every finite volume. The integrals over every volume are then summed, and the final integrals are estimated as the average of the 20 separate estimates.

In total, each integrand is sampled in 4.84×10^6 coordinates. The discretisation of the integration domain can be considered a discrete importance sampling [56], with the consequence of more dense sampling in regions where higher variance in the integrand is expected. The assumption of the concentric spherical shells being a reasonable sample distribution thus relies on the orbitals being localised to their associated cells, so that the products of orbitals have most of their significant distribution between the cells.

Confidence in the estimates can be established by (1) assessment of the error in the PAO-LVO overlap matrix, and (2) assuming that the same error applies to the DOIs due to the similarities in the integrand with respect to variance. While we can not directly infer the error in the DOIs from the error in the PAO-LVO overlaps, it is clear that the regions with most variance in the integrands coincide in these cases. Hence, if the sampled coordinates has the ability to reproduce the overlaps they should be an equally reasonable choice for the DOIs.

The absolute deviation of the MC estimates of the PAO-LVO overlap matrix elements is compared to their magnitude in Figure A2, where we observe a significant loss of relative accuracy below 10^{-4} for diamond, and below 10^{-6} for LiH and HCN. We thus conclude that the DOI estimates presented in Figure 3 are reliable.

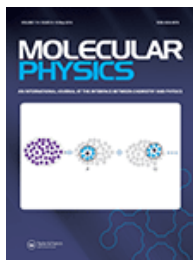
Paper III

Smooth potential-energy surfaces in fragmentation-based local correlation methods for periodic systems

Audun Skau Hansen, Einar Aurbakken, Thomas Bondo Pedersen

Molecular Physics. (2021), e1896046.





Molecular Physics

An International Journal at the Interface Between Chemistry and Physics

ISSN: (Print) (Online) Journal homepage: <https://www.tandfonline.com/loi/tmph20>

Smooth potential-energy surfaces in fragmentation-based local correlation methods for periodic systems

A. S. Hansen, E. Aurbakken & T. B. Pedersen

To cite this article: A. S. Hansen, E. Aurbakken & T. B. Pedersen (2021): Smooth potential-energy surfaces in fragmentation-based local correlation methods for periodic systems, Molecular Physics, DOI: [10.1080/00268976.2021.1896046](https://doi.org/10.1080/00268976.2021.1896046)

To link to this article: <https://doi.org/10.1080/00268976.2021.1896046>



© 2021 The Author(s). Published by Informa UK Limited, trading as Taylor & Francis Group



[View supplementary material](#)



Published online: 04 Mar 2021.



[Submit your article to this journal](#)



Article views: 25



[View related articles](#)



[View Crossmark data](#)

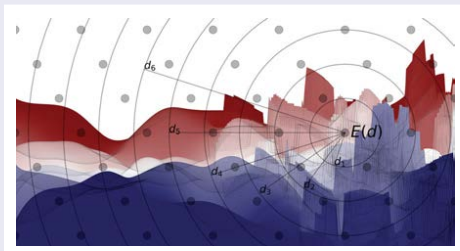
Smooth potential-energy surfaces in fragmentation-based local correlation methods for periodic systems

A. S. Hansen , E. Aurbakken and T. B. Pedersen 

Department of Chemistry, Hylleraas Centre for Quantum Molecular Sciences, University of Oslo, Oslo, Norway

ABSTRACT

Local approximations facilitate the application of post-Hartree–Fock methods in the condensed phase, but simultaneously introduce errors leading to discontinuous potential-energy surfaces. In this work, we explore how these discontinuities arise in periodic systems, their implications, and possible ways of controlling them. In addition, we present a fully periodic Divide-Expand-Consolidate second-order Møller–Plesset approach using an attenuated resolution-of-the-identity approximation for the electron repulsion integrals and a convenient class to handle translation-symmetric tensors in block-Toeplitz format.



ARTICLE HISTORY

Received 16 December 2020
Accepted 19 February 2021

KEYWORDS

Periodic systems; MP2; attenuated fitting; local correlation; fragmentation



1. Introduction

The theoretical description of electronic interactions at the quantum level is fundamentally the same for periodic systems as for molecules. Challenges posed by the computational scaling of correlated wavefunction methods have, however, proven much more limiting in the periodic case, and condensed-phase wavefunction-based results beyond Kohn–Sham density-functional theory (KS-DFT) [1] or Hartree–Fock (HF) [2] theory remain fairly uncommon in the literature relative to the molecular case.

With today's line-up of efficient and publicly available coupled-cluster (CC) implementations, it is possible to perform highly accurate electronic structure calculations for moderately sized molecules at an affordable computational cost [3]. While valuable in their own right, such

results are often used to ensure the quality of other less reliable but more efficient methods, such as KS-DFT or semi-empirical methods. The results provided by these implementations would have been unattainable, if not for several important developments made in the past 2–3 decades, where the computational scaling with respect to the number of electrons has been reduced towards linearity by means of various approximations. Distance-based approximations dating back to Pulay and others [4–10] commonly referred to as *local correlation methods* have been essential in this regard.

Notably, we have seen the revival of Meyer's pair natural orbitals (PNO) [11] in the work from Neese [12–16], followed by Werner [17], where the most significant part of the virtual orbital space is represented in a compact manner for each pair of occupied orbitals.

CONTACT A. S. Hansen  a.s.hansen@kjemi.uio.no  Department of Chemistry, Hylleraas Centre for Quantum Molecular Sciences, University of Oslo, P.O. Box 1033 Blindern, Oslo N-0315, Norway.

 Supplemental data for this article can be accessed here. <https://doi.org/10.1080/00268976.2021.1896046>

© 2021 The Author(s). Published by Informa UK Limited, trading as Taylor & Francis Group
This is an Open Access article distributed under the terms of the Creative Commons Attribution-NonCommercial-NoDerivatives License (<http://creativecommons.org/licenses/by-nc-nd/4.0/>), which permits non-commercial re-use, distribution, and reproduction in any medium, provided the original work is properly cited, and is not altered, transformed, or built upon in any way.

Simultaneously, extensive research into the decoupling of the orbital spaces has been made. Various approaches for decoupling the CC equations have been presented in the literature, including the divide-expand-consolidate (DEC) approach by Jørgensen and coworkers [18–22] and the closely related cluster-in-molecule (CIM) approach by Li et al. [23,24], and the generalisation of the Pulay–Sæbø scheme by Werner and coworkers [25], to name a few.

While these methods have greatly reduced the computational cost of molecular CC calculations, their adaptation to the periodic case has not been without complications. The natural way of dealing with the electronic wavefunction in bulk materials is to assume an infinite periodic extent, which subsequently allows mapping the infinite problem onto the finite unit cell by means of a Fourier transform [26,27]. The solution of these equations, the Bloch orbitals, are expressed as linear combinations of delocalised plane waves [28]. As a consequence, periodic systems are not just simply huge molecules – they are truly infinite, yet subject to symmetries which reduce the computational expense of the correlation treatment. One approach to correlation methods in solids thus is to deal with the problem in its canonical form, expanded in either plane waves [29–31] or localised atomic orbitals such as Gaussian basis functions [32–36]. The connection to the more familiar local quantum chemical treatment of correlation is, however, conditioned on the availability of a Wannier representation of the orbital spaces [37], which is restricted to non-conducting systems [38–41]. In this representation, each orbital is no longer uniquely associated with a wave vector and the decoupling conditions are thus different than in the Bloch case. Still, the prospect of achieving similar results as for molecules has motivated a line of research into the application of these methods on periodic systems, as documented by the work of Usvyat et al. [42], Li et al. [43], and ourselves [44,45]. Beyond alleviating the notable computational challenges of obtaining the ground-state solution, local correlation methods may provide novel pathways towards the calculation of band gaps, thus providing promising venues for application and a closer connection to experiment [46,47].

As we gain experience with these methods in the periodic realm, it becomes increasingly clear that an efficient implementation requires many layers of approximations, rather than one single principle. This includes approximate schemes for the electron repulsion integrals (ERIs) [48–50] and screening, as well as the local approximation itself. While the resolution of the identity (RI) approximation has been demonstrated to greatly accelerate ERI generation and transformation in local second-order Møller-Plesset (MP2) theory calculations [51,52],

there are open questions regarding fitting basis sets and methodology which warrants further studies [50,53]. From new layers of approximations, new input parameters follow, each affecting the final result of the calculation in various ways. Careful consideration should thus be taken in order to retain the best possible control of the error in the result, so it can be suppressed or extrapolated away in a systematic manner. In this work, we focus on the error due to truncated orbital spaces, with special focus on how it impacts potential-energy surfaces (PESs) at the MP2 level of theory for periodic systems. This is likely the most significant error present in these calculations [54–57] and should be treated accordingly.

2. Theory

Within the adiabatic Born–Oppenheimer approximation, the electronic ground-state energy of a periodic many-electron system defines the PES as a function of the parameters describing the lattice and the coordinates of the atoms associated with one unit cell, the reference cell, in the lattice. The accuracy of the PES depends on the level of theory used to calculate the energy, and can in principle be treated systematically within convergent hierarchies of wavefunction methods, such as the CC methods [3]. However, the steep computational scaling of post-HF methods combined with the infinite nature of periodic systems impose severe limitations already at the level of MP2 theory, which has resulted in a considerable effort being put into the adaptation of local correlation methods [4–10] to the periodic case. While these methods greatly reduce the computational cost of post-HF calculations, they are known to simultaneously introduce discontinuities in PESs which can potentially be difficult to control [54,58].

In order to understand how these discontinuities emerge in periodic systems, we shall look closer into how the local energies are computed in the first place. The periodic Hartree–Fock equations are conventionally solved in reciprocal space using either a plane-wave basis or a translational symmetry-adapted local atomic orbital (AO) basis such as Gaussian AOs. In both cases [59], the resulting canonical representation of the orbital space is the completely delocalised and complex-valued Bloch orbitals [28].

For insulators, it is possible to obtain a non-canonical, local representation of the orbital space by means of an inverse Fourier transform and localisation in direct space [41]. In this picture, the space is spanned by Wannier orbitals $\varphi_{\mathbf{L}p}$, where the uppercase, boldfont index refers to the cell in the periodic structure in which the orbital p belongs.

In addition to being local in the sense of having a finite spatial extent, the Wannier orbitals are translationally orthogonal to each other [41]:

$$\int_{\mathbb{R}^3} \varphi_{Lp} \varphi_{Mq} d\mathbf{r} = \delta_{LM} \delta_{pq}, \quad (1)$$

and can be real-valued by constraining the localisation procedure [41].

Post-HF calculations from a non-canonical reference determinant must account for non-diagonal terms in the Fock matrix, meaning that, for instance, computing the MP2 correlation energy is no longer a one-step procedure. Pulay and Sæbø [9], therefore, derived an MP2 formulation from the Hylleraas functional that is independent of unitary rotations within the occupied and virtual spaces. In the periodic case, for Wannier functions, these equations are

$$0 = (\mathbf{IiAa|JjBb}) + \sum_{Cc} t_{ij}^{CcBb} f_{AaCc} + \sum_{Cc} t_{ij}^{AaCc} f_{BbCc} - \sum_{Kk} t_{kij}^{AaBb} f_{KkLi} - \sum_{Kk} t_{ikj}^{AaBb} f_{KkLj}. \quad (2)$$

where f is the Fock matrix, t are the MP2 amplitudes and the periodic ERIs for real Wannier functions are

$$(\mathbf{0iAa|JjBb}) := \iint_{\mathbb{R}^3} \frac{\varphi_{0i}(\mathbf{r}) \varphi_{Aa}(\mathbf{r}) \varphi_{Jj}(\mathbf{r}') \varphi_{Bb}(\mathbf{r}')}{|\mathbf{r} - \mathbf{r}'|} d\mathbf{r}' d\mathbf{r}. \quad (3)$$

The cell summations in Equation (2) run over the full, infinite lattice. Due to the translational symmetry in the amplitudes and ERIs, given by

$$t_{ij}^{AaBb} = t_{0i(j-I)j}^{(A-I)a(B-I)b}, \quad (4)$$

we may choose to keep the first occupied index fixed in the reference cell $\mathbf{0}$ without any loss of information. Upon solving Equation (2) for the amplitudes, the correlation energy per unit cell can be computed as

$$\Delta E_{MP2} = \sum_{\mathbf{J}} \sum_{\mathbf{AB}} \sum_{ij} \sum_{ab} t_{0ij}^{AaBb} (2(\mathbf{0iAa|JjBb}) - (\mathbf{0iBb|JjAa})). \quad (5)$$

It is well known that for localised orbitals, the ERIs tend exponentially to zero with the *inter-orbital* distances $R_{\mathbf{0iAa}}$ and $R_{\mathbf{JjBb}}$, and proportional to $R_{\mathbf{0ij}}^{-3}$ with the *inter-pair* distance $R_{\mathbf{0ij}}$ [60,61], where

$$R_{\mathbf{p}p\mathbf{Q}q} = \sqrt{((\varphi_{\mathbf{p}p}|\hat{\mathbf{r}}|\varphi_{\mathbf{p}p}) - (\varphi_{\mathbf{Q}q}|\hat{\mathbf{r}}|\varphi_{\mathbf{Q}q}))^2}. \quad (6)$$

These decay properties reveal a certain decoupling in the amplitude equations and form the basis for various local

correlation methods. Linear scaling can be achieved by partitioning the summations in Equations (2) and (5) into weakly coupled subspaces Ω_k , where only the subsets of occupied and virtual orbitals that significantly affect the energy of these subspaces are included. After solving the equations on these fragmented subspaces, the total correlation energy can finally be approximately expressed as a sum over the contribution from each:

$$\Delta E_{MP2} \approx \sum_k \Delta E_{MP2}(\Omega_k). \quad (7)$$

The equations are typically solved on slightly larger domains by inclusion of so-called buffer spaces [18] to ensure that the energy inside each subspace is properly converged.

The correlation energy is distributed across the excitation space, and will smoothly flow between configurations following smooth changes in geometry and representations of the orbital spaces. Changes in the weakly coupled local subspaces following the inclusion or exclusion of orbitals depending on distance measures will, however, inevitably introduce discontinuous changes in the energy. Consequently, local correlation methods are prone to yield non-smooth – or *fractured* – PESs and careful consideration should thus be put into the algorithms by which these local subspaces are constructed in order to minimise such effects.

We shall distinguish the fragmentation schemes, i.e. the principles used to construct the subspaces, from the various other approximations involved. In terms of fragmentation, the challenges associated with fractured PESs have been addressed in various ways, with the most common being that of choosing the subspaces sufficiently large to suppress discontinuities [57]. Other approaches include freezing the domains close to the equilibrium geometry [55] or bumping the amplitudes [56]. The orbital specific virtual (OSV) representation of the virtual space has been of particular interest, as it has been shown to yield smoother surfaces both for molecules and periodic systems [57,62–64].

The divide-expand-consolidate (DEC) family of methods takes a different approach and aims at controlling the magnitude of the discontinuities by converging the energy with respect to changes in the orbital subspaces. The various fragmentation schemes are themselves in principle agnostic with respect to the representations of the orbital spaces, which for the virtual space include local virtual orbitals (LVOs), projected atomic orbitals (PAOs), OSVs and pair natural orbitals (PNOs) [11–17]. While it is well known that the choice of virtual representation makes a significant impact on the energy and thus the PES, it currently remains unclear

how to determine the suitability of such a representation without performing the actual energy calculation [45,65].

Positions and locality can be ascribed to a set of orbitals in a number of ways [45], and the exact definition of the local subspaces on which the amplitude equations are solved may therefore differ between various implementations. Following an “ERI-centric” approach, we shall infer sparsity in the ERIs directly from distance considerations, meaning that we assume $\langle 0iAa|JjBb \rangle = 0$ for distances R_{0iAa} , R_{JjBb} and R_{0ij} above some pre-determined thresholds. This approach is convenient from a periodic perspective, since it incorporates the translational symmetry of the product orbitals that appear in the bra and ket of the ERIs,

$$\hat{T}_M \varphi_{0i}(\mathbf{r}) \varphi_{Aa}(\mathbf{r}) = \varphi_{Mi}(\mathbf{r}) \varphi_{(A+M)a}(\mathbf{r}), \quad (8)$$

where \hat{T}_M is the lattice translation operator that offsets the product orbitals in cellwise increments, such that any excitation included in the reference cell is also included in the translated copies.

By defining the elements

$$E_{ij}^{AaBb} := {}_i AaBb_{ij} (2 \langle iAa|JjBb \rangle - \langle iBb|JjAa \rangle), \quad (9)$$

we may express the full MP2 energy per cell more compactly as

$$\Delta E_{\text{MP2}} = \sum_{i \in \mathcal{O}_0} \sum_{Jj \in \mathcal{O}} \sum_{Aa \in \mathcal{V}} \sum_{Bb \in \mathcal{V}} E_{0ij}^{AaBb}, \quad (10)$$

where the summations are now partitioned in such a way that the individual orbitals are emphasised rather than the lattice structure. The summation is still infinite, but we explicitly denote the full orbital spaces as \mathcal{V} and \mathcal{O} (\mathcal{O}_0 for the reference cell) for the virtual and occupied spaces, respectively.

In this setting, a *fragmentation* may be regarded as a partitioning within the various terms, while the local approximation may be regarded as a distance-based truncation of the orbital spaces. Taken together, this forms a *fragmentation scheme*, and with the addition of approximative techniques such as various representations of the orbital spaces, it can be seen as a *local correlation method*, as found in a number of implementations.

The DEC family of methods [18–20] was originally devised for molecules and has been extended to the periodic case recently [44]. In the DEC approach, the amplitude equations are solved within subspaces called amplitude orbital spaces (AOSs) and the resulting energies are computed on a smaller subspace of each AOS called the energy orbital space (EOS). In order to gain control over the error in these calculations, these spaces are constructed such that the error in the energy is below a predefined threshold.

In terms of fragmentation, the DEC approach first divides the occupied space into fragments, which are non-overlapping sets \underline{P} of occupied orbitals in each others vicinity. The AOS for a fragment is

$$\Omega_{k(0P)} = \mathcal{O}_{\underline{P}} \cup \mathcal{V}_{0P}, \quad (11)$$

where the notation $\mathcal{O}_{\underline{P}}$ and \mathcal{V}_{0P} signifies sets of occupied and virtual orbitals in the vicinity of \underline{P} (explicit definition will follow later). The energy associated with a fragment is in terms of Equation (7):

$$\Delta E_{\text{frag,MP2}}(\Omega_{k(0P)}) = \sum_{ij \in \underline{P}} \sum_{AaBb \in \mathcal{V}_{0P}} E_{0ij}^{AaBb}, \quad (12)$$

where the summation domain constitutes the EOS of the fragment. The AOS of a fragment can be determined by expanding $\mathcal{O}_{\underline{P}}$ and \mathcal{V}_{0P} successively until the change in energy is below a certain threshold referred to as the fragment optimisation threshold (FOT). The converged fragment spaces obtained in the expansive step may then be used to set up the so-called pair-fragment spaces with AOSs

$$\Omega_{k(0P,LQ)} = \mathcal{O}_{\underline{P}} \cup \mathcal{V}_{0P} \cup \mathcal{O}_{LQ} \cup \mathcal{V}_{LQ}, \quad (13)$$

on which the pair-fragment amplitude equations are then solved. Finally, the fragment energies can be consolidated with the pair-fragment energies of successively increasing inter-pair distance until the energy is converged, where the pair-fragment energy is

$$\Delta E_{\text{pair,MP2}}(\Omega_{k(0PLQ)}) = \sum_{i \in \underline{P}} \sum_{j \in \underline{Q}} \sum_{AaBb \in \mathcal{V}_{0P} \cup \mathcal{V}_{LQ}} E_{0ij}^{AaBb}, \quad (14)$$

where again the summation domain is the EOS of the pair-fragment. In contrast to molecular DEC we have in the above made no distinction between the virtual spaces used in the AOS and EOS. The AOS does, however, contain buffer orbitals in the form of occupied orbitals used merely to converge the energy inside the EOS.

The partitioning used to arrive at the sets \underline{P} can of course be varied, all the way from no partitioning ($\underline{P} = \mathcal{O}_0$) to full partitioning ($\underline{P}_i = \varphi_i$). In the latter case, this closely resembles what is known as the Pulay–Sæbø approach [7,66], where every unique combination of occupied orbitals are referred to as *pairs*. The fragmentation, which has later been generalised by Werner and coworkers [25,67], has been extended to periodic systems in the CRYSCOR program [42,51,57,68–71]. In this approach, the DEC fragment is referred to as a *strong pair*, while the pair fragments are classified into *close*, *weak* or *distant* pairs depending on the inter-orbital distance

between the constituent occupied orbitals. In the context of Equation (7), these subspaces can be expressed as

$$\Omega_{k(0i\mathbf{l}_j)} = \varphi_{0i} \cup \mathcal{V}_{0i} \cup \varphi_{\mathbf{l}_j} \cup \mathcal{V}_{\mathbf{l}_j}, \forall \mathbf{l} \in \mathbb{Z}^3, \quad (15)$$

and the energy of such a subspace is

$$\Delta E_{\text{MP2}}(\Omega_{k(0i\mathbf{l}_j)}) = \sum_{AaBb \in \mathcal{V}_{0i} \cup \mathcal{V}_{\mathbf{l}_j}} E_{0i\mathbf{l}_j}^{AaBb}. \quad (16)$$

The pair-classification scheme is well suited for a multi-level approach, where the pairs can be treated within various approximations, ranging from exact MP2 for strong and close pairs, to multipole expansion for weak pairs and Lennard–Jones extrapolation for distant pairs. Its implementation in `CRYSCOR` is currently capable of running MP2-calculations on systems with more than 100 atoms per cell. [49]

With the inclusion of the occupied buffer space in the vicinity of a given fragment (or strong pair), it is tempting to include the corresponding amplitudes in the energy calculation since they are likely already close to convergence. This can be done by extending each fragment (or strong pair) space $P_i = \varphi_i$ with all pair-fragment spaces where one of the occupied orbitals pertain to the given fragment, forming the subspace

$$\Omega_{k(0i)} = \varphi_{0i} \cup \mathcal{O}_{0i} \cup \mathcal{V}_{0i}, \quad (17)$$

and computing the energy

$$\Delta E_{\text{MP2}}(\Omega_{k(0i)}) = \sum_{\mathbf{J} \in \mathcal{O}_{0i}} \sum_{AaBb \in \mathcal{V}_{0i}} E_{0i\mathbf{J}}^{AaBb}. \quad (18)$$

This fragmentation corresponds to the periodic cluster-in-molecule (CIM) method [43], where the constituent subspaces are referred to as *clusters*. In CIM, the spaces are determined by including all orbitals up to a given distance, typically fixed at 5.5 Å [43].

To summarise, the DEC and Pulay–Sæbø fragmentation schemes become identical in the case where each DEC-fragment is comprised of one single occupied orbital, while the CIM fragmentation differs from the two others in the sense that the pair-contributions are always included in each cluster. An illustrative comparison of the three fragmentation schemes is presented in Figure 1. While the smoothness of the PES in the DEC approach can in principle be controlled by the FOT, discontinuities in the Pulay–Sæbø or CIM scheme are conditioned on the default or user-defined domains being sufficiently large. As with the incremental scheme DEC offers a systematic path towards the exact correlation energy for solids, yet in smaller increments and applicable only to insulators [72,73]. All three fragmentation

schemes may serve as suitable starting points for embedding approaches, where higher-level correlation methods designed for molecules can be used to improve upon the results [74–76].

It thus turns out that by not fully contracting the energy, but rather solving for the amplitudes within the local subspace and thereafter storing the elements $E_{0i\mathbf{l}_j}^{AaBb}$ in addition to the positions of the orbitals, the energy can be retrospectively recast as a Pulay–Sæbø-like, CIM-like or DEC-like result. Furthermore, by computing a range of such energies for various local truncations of the occupied and virtual subspaces, it becomes possible to gain insight into how and where discontinuities emerge in the PES depending on the cutoff parameters. We have implemented this functionality in the current XDEC-code, but stress that this procedure does not equate to `CRYSCOR` or CIM, since it lacks the many other approximative techniques and orbital space representations that are used in these implementations.

3. Implementation

The implementation of XDEC presented in this paper shall be referred to as XDEC-RI (extended DEC with a resolution of the identity approximation for the ERIs) in order to distinguish it from our previous implementation, XDEC, since there are fundamental differences between the two.

As with our XDEC implementation [44], the Wannier functions in XDEC-RI are obtained from `CRYSTAL` [41,71] and the AO integrals from `LIBINT` [77]. A notable change is the fact that the ERIs are now fitted to a periodic basis using an attenuated Coulomb metric [50]. A global fitting at the onset of the calculation saves computational time, since the ERIs can be easily computed on demand and reused in the expansive steps of the fragment optimisation. Furthermore, all integrals and orbital spaces now fully incorporate translational symmetry.

The size of the local subspace is controlled as follows. Each WF is assigned a position according to its centre. The occupied orbitals may thereafter be subdivided into fragments depending on their positions or they may be kept in separate fragments depending on the user’s preference. A fragment centre is typically chosen to be the centre of the first orbital in each fragment. The local subspace pertaining to the fragment is then chosen to consist of all occupied and virtual orbitals inside given radii d_{occ} and d_{virt} .

In our previous implementation of the XDEC algorithm [44], we treated fragments and pair-fragments as finite clusters. Although this, in principle, would allow for the exploitation of highly optimised molecular algorithms, we here report an implementation that maintains

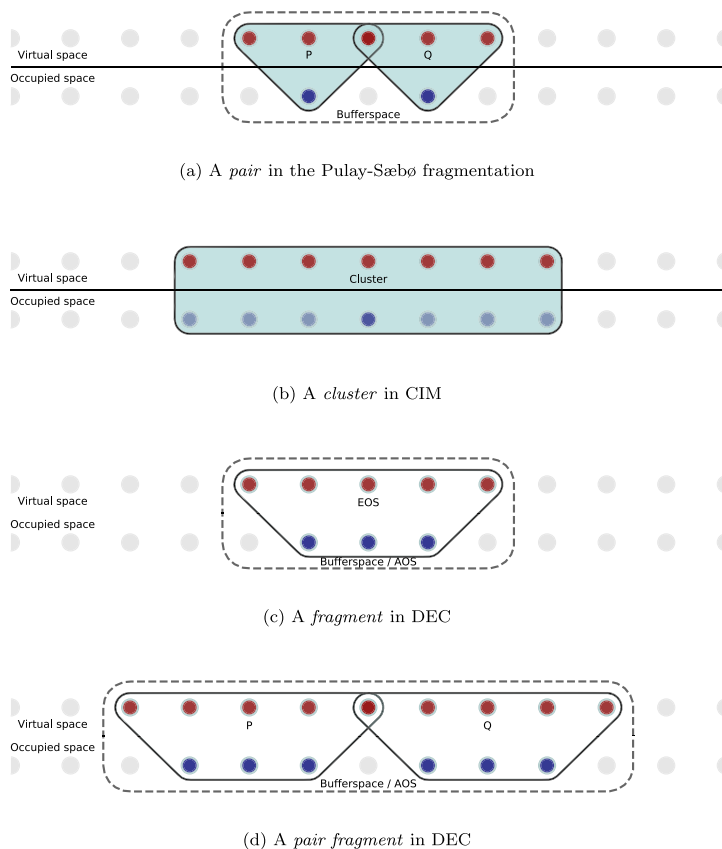


Figure 1. Illustration of the various periodic fragmentation schemes under consideration. Virtual and occupied orbitals inside the local subspaces are coloured red and blue, respectively. CIM differs from the other two in the sense that the energy contributions from amplitudes where i and j are not the same is included in the central cluster of i , here indicated by varying opacity in the occupied orbitals. (a) A *pair* in the Pulay-Sæbø fragmentation. (b) A *cluster* in CIM. (c) A *fragment* in DEC. (d) A *pair fragment* in DEC.

full translational symmetry throughout the calculation. This allows us to circumvent the main bottleneck of the XDEC algorithm, namely the repeated evaluation of ERIs, by reusing integrals in the fragment and pair-fragment calculations. The main disadvantage of this approach is that the resulting algorithm is no longer embarrassingly parallel due to the increased amount of communication between computer nodes.

To support full translational symmetry we have implemented a Python class named *TMAT* (Toeplitz Matrix), which is specifically designed to facilitate linear-algebra operations on bi-infinite block-Toeplitz and block-Circulant matrices [78] (definitions are given below).

Using local Gaussian basis sets from quantum chemistry, translational symmetry manifests itself in

equivalence among blocks of matrix elements of translationally invariant operators. A typical example is the infinite overlap matrix, whose elements obey

$$S_{\mu\nu}^{M,N} = \langle \mathbf{M}\mu | \mathbf{N}\nu \rangle = S_{\mu\nu}^{M+L, N+L}. \quad (19)$$

Matrices with this block structure are called bi-infinite block Toeplitz (IBT) matrices. Using $i, j \in \mathbb{Z}$ to denote row and column block indices, an IBT matrix is defined by

$$\mathbf{A}^{ij} = A^{j-i} := A^m. \quad (20)$$

The matrix product of two IBT matrices \mathbf{A} and \mathbf{B} is itself an IBT matrix, since

$$(\mathbf{AB})^{(i+n),(j+n)} = \sum_{k=-\infty}^{\infty} A^{(k-n)-i} B^{j-(k-n)} = (\mathbf{AB})^{ij}, \quad (21)$$

and can thus be compactly expressed as

$$(\mathbf{AB})_{IBT}^m = \sum_{k=-\infty}^{\infty} A^k \cdot B^{m-k}. \quad (22)$$

If we assign to \mathbf{A} a bandwidth N such that

$$A^m = 0 \text{ for } |m| > N \quad (23)$$

we can define a discrete Fourier transformation

$$\mathcal{F}\{\mathbf{A}\}^m = \sum_{n=-N}^N e^{-i(\frac{2\pi}{M})mn} A^n := \tilde{A}^m, \quad (24)$$

and its inverse

$$\mathcal{F}^{-1}\{\tilde{\mathbf{A}}\}^n = \frac{1}{M} \sum_{m=-N}^N e^{-i(\frac{2\pi}{M})mn} \tilde{A}^m = A^n, \quad (25)$$

where $M = 2N + 1$. The discrete Fourier transformation followed by its inverse introduces a type of periodicity in the matrices that satisfy the Born–von Karman boundary condition [28], as apparent when considering blocks outside the bandwidth:

$$A^{M+n} = \sum_{n'=-N}^N A^{n'} \left(\frac{1}{M} \sum_{m=-N}^N e^{i2\pi \frac{m}{M}(M+n-n')} \right) = A^n. \quad (26)$$

In order to account for this behaviour, it makes sense to define a non-standard *circulant* operator

$$i \circlearrowleft N := (i + N) \bmod (2N + 1) - N, \quad (27)$$

where *mod* implies the remainder of integer division, producing the following infinite series (in positive increments of 1):

$$\dots, N, -N, \dots, 0, \dots, N, -N, \dots, \quad (28)$$

such that the transformation to and from reciprocal space can be expressed

$$A^n = \sum_{n'=-N}^N A^{n'} \underbrace{\left(\frac{1}{M} \sum_{m=-N}^N e^{i2\pi \frac{m}{M}(n-n')} \right)}_{\delta_{n \circlearrowleft N, n'}}, \quad (29)$$

where we explicitly have pointed out the circulant nature of the series expansion of the Kronecker delta by including the circulant operator. A matrix subject to these conditions can be referred to as an *infinite block-circulant*

(IBC) matrix, defined by

$$\mathbf{A}^{ij} = A^{(j-i) \circlearrowleft N} := A^{n \circlearrowleft N}. \quad (30)$$

We now consider for given n the inverse Fourier transform of an element-wise multiplication of two IBT matrices $\tilde{\mathbf{A}}$ and $\tilde{\mathbf{B}}$ in reciprocal space:

$$\mathcal{F}^{-1}(\mathcal{F}\{\mathbf{A}\} * \mathcal{F}\{\mathbf{B}\})^n = \frac{1}{M} \sum_{m=-N}^N e^{i\frac{2\pi}{M}mn} \tilde{A}^m \tilde{B}^m. \quad (31)$$

Expanding $\tilde{\mathbf{A}}$ and $\tilde{\mathbf{B}}$ in terms of their blocks in direct space,

$$\begin{aligned} & \mathcal{F}^{-1}(\mathcal{F}\{\mathbf{A}\} * \mathcal{F}\{\mathbf{B}\})^n \\ &= \sum_{n_1=-N}^N \sum_{n_2=-N}^N \\ & \times \left(\frac{1}{M} \sum_{m=-N}^N e^{i\frac{2\pi}{M}m(n-n_1-n_2)} \right) A^{n_1} B^{n_2}, \quad (32) \end{aligned}$$

which by the circulant Kronecker delta can be reduced to the IBC product

$$\begin{aligned} \mathcal{F}^{-1}(\mathcal{F}\{\mathbf{A}\} * \mathcal{F}\{\mathbf{B}\})^n &= \sum_{n_1=-N}^N A^{n_1} B^{n-n_1 \circlearrowleft N} \\ &= (\mathbf{AB})_{IBC}^n. \quad (33) \end{aligned}$$

A comparison of Equations (33) and (22) reveals the relation

$$\begin{aligned} (\mathbf{AB})_{IBT}^n &= (\mathbf{AB})_{IBC}^n \\ &- \sum_{k=1}^{k \leq |n|} A^{-\text{sgn}(n)(N-k+1)} B^{n-\text{sgn}(n)(N+k)}, \quad (34) \end{aligned}$$

where the superscript IBT indicates the result from Equation ((22)), thus showing that these products can be made equivalent in any given bandwidth by padding the outer layers in the matrices with zeros so that the last term in the above is zero.

Equation (33) is basically the familiar convolution theorem. It provides key insight into the reciprocal space treatment of infinite systems. In conjunction with Equation ((34)), it shows that any factorisation in reciprocal space carries over to direct space in a well-defined manner, paving the way for a straightforward implementation via reciprocal space of widely used linear-algebra techniques such as singular value decomposition, Cholesky factorisation, or diagonalisation.

Furthermore, with a periodic definition of the matrix product there is no need for explicit inclusion of the

lattice-summations in the notation, as they simply follow from the definition. Most of the familiar tensor notation in quantum chemistry thus smoothly carries over to the periodic domain, making the process of extending methods from finite to extended systems conceptually simpler. By implementing the IBT and IBC matrix structures as a class in Python, the process of writing a periodic code much more closely resembles what is typically done for the molecular case, and the cumbersome process of dealing with summations over lattice vectors is conveniently dealt with automatically in the background. Efficiency is ensured by using the Fast Fourier Transform (FFT) algorithm [79] and level 3 BLAS routines [80], exploiting multi-threaded and architecture-optimised libraries. This computational efficiency, in conjunction with the conditions provided by Equation ((33)), is extensively used in our code.

The calculation of ERIs constitutes the main bottleneck in the XDEC implementation, which requires re-calculation of integrals for each fragment and pair-fragment optimisation, including re-calculation in each optimisation cycle. While embarrassingly parallel [22], this approach is too costly to be applicable on small and medium-sized commodity computer clusters. As mentioned above, we here exploit full translational symmetry to enable the reuse of ERIs across fragments and pair-fragments. Still, the calculation of the ERIs for the MP2 approximation formally scales as N^5 with N being the number of atomic orbitals in the supercell. To accelerate the ERI generation and to reduce the memory footprint of the algorithm, we use a periodic adaptation of the resolution of the identity (RI) approximation [81–91].

In a suitable auxiliary basis $\{\varphi_{\mathbf{NK}}\}$, the product of two Wannier orbitals $\varphi_{\mathbf{0iAa}}$ can be approximated as a linear combination [42]:

$$|\mathbf{0iAa}\rangle \approx \sum_{\mathbf{NK}} |\mathbf{NK}\rangle d_{\mathbf{K},\mathbf{0iAa}}^{\mathbf{N}} := |\widetilde{\mathbf{0iAa}}\rangle. \quad (35)$$

The optimal fitting coefficients d are obtained by minimising the residual norm in any positive, semidefinite metric [86],

$$\langle \mathbf{0iAa} - \widetilde{\mathbf{0iAa}} | \mathbf{0iAa} - \widetilde{\mathbf{0iAa}} \rangle := \langle \Delta \mathbf{0iAa} | \Delta \mathbf{0iAa} \rangle, \quad (36)$$

upon which the residual is orthogonal to the fitting basis, so that

$$\langle \mathbf{NK} | \Delta \mathbf{0iAa} \rangle = 0. \quad (37)$$

The latter expression yields a set of fitting equations for d :

$$\langle \mathbf{NK} | \mathbf{0iAa} \rangle = \sum_{\mathbf{MJ}} \langle \mathbf{NK} | \mathbf{MJ} \rangle d_{\mathbf{J},\mathbf{0iAa}}^{\mathbf{M}}. \quad (38)$$

If we define the infinite block-Toeplitz matrices \mathbf{O} and \mathbf{V} with elements $O_{\mathbf{K},\mathbf{0iAa}}^{\mathbf{N}} = \langle \mathbf{NK} | \mathbf{0iAa} \rangle$ and $V_{\mathbf{KJ}}^{\mathbf{M}-\mathbf{N}} :=$

$\langle \mathbf{NK} | \mathbf{MJ} \rangle$, the above relation may be cast into matrix form with a straightforward solution for the coefficients

$$\mathbf{d} = \mathbf{V}^{-1} \mathbf{O}, \quad (39)$$

provided the matrix \mathbf{V} is nonsingular – i.e. – provided the auxiliary basis functions constitute a linearly independent set in the chosen metric.

A natural choice for metric in Equation (37) is the Coulomb operator, as this is the metric of the ERIs themselves. The Coulomb operator, however, decays slowly with distance (R^{-1}), making it computationally expensive for infinite periodic systems. Noting that the Coulomb operator is obtained from an *attenuated* Coulomb operator expressed in terms of the complementary error function [92],

$$\frac{1}{r} = \lim_{\omega \rightarrow 0} \frac{\text{erfc}(\omega r)}{r}, \quad (40)$$

we may enforce more rapid decay by selecting a small positive value for the attenuation parameter ω . The attenuated Coulomb operator maintains characteristics similar to the true Coulomb operator for small ω , while for increasingly large values it approaches the overlap metric. As noted by several authors in the past [48,50,51], this makes it an interesting candidate for fitting metric in periodic systems. We shall indicate the usage of this operator with a tilde in the affected matrices. The fitting equations in the attenuated Coulomb metric thus become

$$\widetilde{\mathbf{V}} \mathbf{d} = \widetilde{\mathbf{O}}. \quad (41)$$

Although the matrices involved are in principle infinite, they exhibit to a certain degree a regular blockwise decay in the elements with respect to the distance to the reference cell which can be tuned by ω . The matrices can therefore be computed up to a given truncation threshold by incrementally including chunks of blocks in spherical shells extending outwards from the reference cell (see Algorithms 1 and 2). We shall use this approach in the construction of the matrices required. The expression for the three-index tensor elements can be reorganised as

$$\begin{aligned} \langle \mathbf{LJ} | \widetilde{\mathbf{0iAa}} \rangle &= \sum_{M\mu N\nu} \langle \mathbf{LJ} | \widetilde{\mathbf{M}\mu} (\mathbf{M} + \mathbf{N}) \nu \rangle c_{\mu i}^{-\mathbf{M}} c_{\nu a}^{-(\mathbf{M}+\mathbf{N})+\mathbf{A}} \\ &:= \sum_{N\nu} \widetilde{O}_{\mathbf{J}N\nu}^{-\mathbf{L}} c_{\nu a}^{-\mathbf{N}+\mathbf{A}}, \end{aligned} \quad (42)$$

where c denotes the expansion coefficients of the Wannier orbitals in the AO basis, and

$$\widetilde{O}_{\mathbf{J}N\nu}^{-\mathbf{L}} := \sum_{M\mu} \langle \mathbf{LJ} | \widetilde{\mathbf{M}\mu} N \nu \rangle c_{\mu i}^{-\mathbf{M}}, \quad (43)$$

is an intermediate contraction tensor for the occupied orbitals.

There are two attractive features of this fitting scheme that makes it especially well suited for XDEC. First, by organising the elements in the intermediate tensor $\tilde{\mathbf{O}}$ in the appropriate way, the contraction of any subset of the virtual orbitals may be done efficiently by means of a matrix product. This is useful for incrementally including larger virtual spaces. Second, the circulant product makes it possible to simultaneously compute for all \mathbf{J}

$$\begin{aligned} (\mathbf{0}i\mathbf{A}a|Jj(\mathbf{J} + \mathbf{B})b) &\approx (\tilde{\mathbf{0}}i\tilde{\mathbf{A}}a|Jj(\tilde{\mathbf{J}} + \tilde{\mathbf{B}})b) \\ &= (\tilde{\mathbf{d}}_{0,A}^T \mathbf{V} \tilde{\mathbf{d}}_{0,B})_{iajb}^J, \end{aligned} \quad (44)$$

by means of the IBC matrix product in Equation (33). The final contractions are with the full Coulomb matrix, but since the attenuated fitting coefficients are only non-zero on a finite extent of the infinite lattice, we only have to compute the blocks in \mathbf{V} that are required to make the circulant product consistent with the Toeplitz product inside the supercell. For simultaneous excitations inside and outside the supercell (\mathbf{J} outside) we can compute the required extra layers in \mathbf{V} on demand.

While the periodic auxiliary basis is infinite, two additional screening parameters ξ_0 and ξ_1 ensure a finite bandwidth of the RI tensors, as outlined in Algorithms 1 and 2. The screening parameters are in effect a truncation threshold on the level of blocks for the three-index AO integrals and the contracted three-index tensor $\tilde{\mathbf{O}}$. Assuming monotonic decay, the screening has been implemented such that the maximum element of all blocks outside a spherical volume centred on the reference cell is below the threshold. This allows the matrices to be incrementally constructed outwards from the reference cell until the requested precision is reached. We finally remark that this fitting approach is not *robust* [93]. In order to make it robust, one would have to compute the corresponding \mathbf{O} tensors in Coulomb-metric, defeating the purpose of using attenuation in the first place. Our procedure is specifically designed with flexible orbitals spaces in mind and will likely benefit from incorporating aspects from other similar approaches in the future [53,94].

4. Computational details

The systems studied in this work are chosen to be sufficiently complex for a meaningful analysis, while small enough to make calculations relatively inexpensive and keeping the analysis simple. Similarly, focusing on sources of PES discontinuities rather than on highly accurate results, we use basis sets relatively far from the basis set limit.

Algorithm 1 AO screening procedure implemented in the XDEC-RI-LMP2 code

- 1: Compile a list Ω containing chunks of coordinate vectors $\{\mathbf{M}\}_R$ grouped together into concentric spherical shells in order of increasing radial distance $\|\mathbf{R}_M\|$ to the reference cell.
 - 2: **for** $\{\mathbf{M}\}_R$ in Ω **do**
 - 3: Compute all $(\mathbf{0}J|\mathbf{0}\mu\mathbf{M}\nu)$'s for the shell
 - 4: **if** all $|\mathbf{0}J|\mathbf{0}\mu\mathbf{M}\nu|_{\max} \leq \xi_0$ **then**
 - 5: Break
 - 6: **end if**
 - 7: Append all \mathbf{M} s to the screened domain Ξ
 - 8: **end for**
 - 9: Set an initial reasonably large cutoff R_{cut}
 - 10: **for** \mathbf{M} in Ξ **do**
 - 11: Compute all cells $(N|J|\mathbf{0}\mu\mathbf{M}\nu)$ within $R_N \leq R_{\text{cut}}$
 - 12: **if** any $(\mathbf{K}_{\text{boundary}}|J|\mathbf{0}\mu\mathbf{M}\nu) \geq \xi_0$, where $0.95R_{\text{cut}} < R_{\mathbf{K}_{\text{boundary}}} \leq R_{\text{cut}}$ **then**
 - 13: Halt execution, warn/advise user to increase domains.
 - 14: **else**
 - 15: Append all blocks where $(N|J|\mathbf{0}\mu\mathbf{M}\nu) \geq \xi_0$ to screening domain Ξ_M
 - 16: Let $R_{\text{cut}} = 1.1R_{N_{\text{outer}}}$ where $R_{N_{\text{outer}}}$ corresponds to the outermost cell in the appended blocks.
 - 17: **end if**
 - 18: **end for**
-

Algorithm 2 MO fitting screening procedure implemented in the XDEC-RI-LMP2 code

- 1: Set $R_{\text{tolerance}} = 10^{-12}$
 - 2: Construct a list Ω of cell-indices \mathbf{L} in order of increasing distance $\|\mathbf{R}_L\|$ to the reference cell.
 - 3: **for** \mathbf{L} in Ω **do**
 - 4: Compute all $\tilde{\mathbf{O}}_{J\nu p}^{L,N}$
 - 5: **if** $R_L - R_{L_{\text{prev}}} \geq R_{\text{tolerance}}$ and $|\tilde{\mathbf{O}}_{J\nu p}^{L,N}| \leq \xi_1$ **then**
 - 6: Break
 - 7: **end if**
 - 8: Store columns ($N\nu$) and column indices of $\tilde{\mathbf{O}}_{LJp,N\nu}$ with max absolute value above ξ_1 for the subsequent contraction of virtual coefficients.
 - 9: **end for**
-

Validation of the implementation, including selection of the Coulomb attenuation parameter for the RI approximation, is performed using the same three-dimensional (3D) and one-dimensional (1D) systems of neon atoms, and the 1D system of ethylene molecules as in Ref. [44]. In addition, we use a 1D system with a unit cell containing two water molecules arranged as shown in Figure 2.

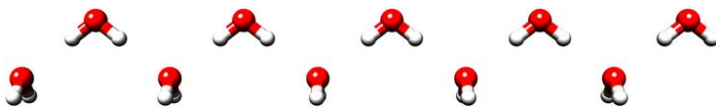


Figure 2. The $2\text{H}_2\text{O}$ system, where two water molecules per cell are repeated in a 1D lattice.

We use an experimentally determined internal geometry of water [95]. For the fixed geometry calculations, we use a lattice parameter of approximately 4.8035 Å (see supplementary information for details). In the PES calculations, we vary the lattice parameter while the O–O–O angles remain fixed. The water system contains more significant inter-molecular correlation effects than ethylene, and is thus more interesting with regard to the exploration of PESs.

Convergence of the MP2 correlation energy with respect to truncation of the local subspaces is investigated for the water and ethylene systems along with water molecules adsorbed on a LiH (001) surface in the slab approximation. The geometry of the water adsorption system is taken from Tsatsoulis et al. [96], with the unit cell containing eight LiH and one water molecule, as shown in Figure 3. This system will be referred to as LiH- H_2O .

Finally, the water and LiH- H_2O systems are used to investigate the continuity of PESs. For the LiH- H_2O system, we start from the equilibrium geometry reported by Tsatsoulis et al. [96] and vary the distance between Li and O to generate a one-dimensional cut through the PES. This system has a lattice parameter of approximately 5.78 Å, thus increasing the interaction between neighbouring water molecules at the surface as compared to systems with lower density. Detailed geometric data for all systems can be found in the supplementary information.

We use the CRYSTAL program [71] to compute the HF reference determinant and to perform the Wannierization and Foster-Boys localisation [41] of the occupied and virtual orbitals separately. In order to converge the HF reference determinant of LiH- H_2O , we use a Fock matrix mixing of 35 % in place of the default value (30% [97]) used for the other systems. The Brillouin zone shrinking factor determining the density in reciprocal space is set to 3 for the LiH- H_2O system. This is not as close to the thermodynamic limit as in Tsatsoulis et al. [96], but sufficient for our purpose. The remaining shrinking factors were 9 for neon and 8 for $2\text{H}_2\text{O}$ and ethylene.

The 6-31G basis set [98] obtained from the basis set exchange database [99,100] is used for the 1D ethylene system. For the hydrogen atoms in the $2\text{H}_2\text{O}$ and LiH- H_2O systems, we use a valence triple-zeta basis set with

polarisation functions [101], and for Li we use a 6-1G [102] basis set. The 6-31G basis set for oxygen [103] is used both in $2\text{H}_2\text{O}$ and LiH- H_2O .

The cc-pVDZ RI fitting basis by Weigend et al. [91] is used for ethylene and LiH- H_2O , while the cc-pVTZ RI fitting basis [91] is used for neon and $2\text{H}_2\text{O}$, both for XDEC and CRYSCOR calculations. In order to avoid linear dependence, exponents less than 0.4 are removed for LiH- H_2O and less than 0.1 for the remaining systems.

We use the frozen-core approximation in the correlation treatment for all cases except 3D neon. The MP2 equations are solved iteratively using fixed point iterations until the residual norm is below a numerical threshold set to 10^{-10} , except for the $2\text{H}_2\text{O}$ system where it is determined dynamically from the FOT as $10^{-3} \times \text{FOT}$. In the expansive step of the fragment optimisation, we include by default a minimum of 6 new orbitals in the local subspace in each iteration. For 3D neon, however, we include a minimum of 10 new orbitals in order to be consistent with Ref. [44].

5. Results and discussion

The XDEC-RI implementation differs fundamentally from our previous work [44], so we first validate the implementation by comparing fragment and pair-fragment MP2 energies for 3D neon, ethylene, and $2\text{H}_2\text{O}$ with results obtained with CRYSCOR [42,51,57,68–71] and the original XDEC implementation [44]. In all cases, the occupied space is completely fragmented, i.e. each occupied orbital defines a fragment. The XDEC-RI truncation parameters are set to $\xi_0 = 10^{-14}$ and $\xi_1 = 10^{-14}$, and the attenuation is $\omega = 0.1 \text{ Bohr}^{-1}$. For 3D neon, we use the XDEC-RI approach for the virtual space, converging each fragment energy to $\text{FOT} = 10^{-4}$ Hartree, while a CIM-like fragmentation is used for ethylene and $2\text{H}_2\text{O}$, where for each occupied orbital the amplitudes are solved within $d_{\text{occ}} = d_{\text{virt}} = 20 \text{ Bohr}$ and thereafter cast into pairwise energy contributions. The results, depicted as functions of the pair separation up to 20 Bohr in Figure 4, show excellent agreement across the implementations.

To gain more insight into the impact of the attenuated RI approximation, we present total MP2 energies for 1D neon in Table 1 for various values of the attenuation parameter ω , using the CIM result from

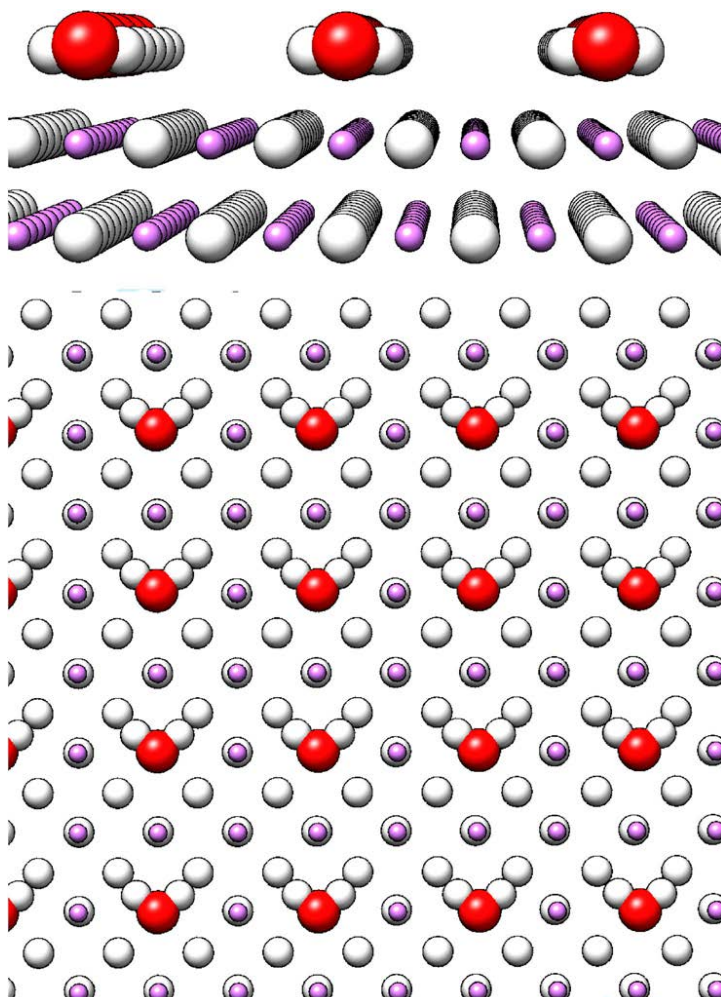


Figure 3. Geometrical setup of the LiH-H₂O adsorption system. A sideview is shown on top, while a top-down view is shown below. The equilibrium geometry was taken from the work of Tsatsoulis et al. [96]

Ref. [43] as reference. With a cc-pVDZ fitting basis [91], XDEC-parameters of $\xi_0 = 10^{-12}$, $\xi_1 = 10^{-12}$, FOT = 10^{-6} Hartree and orbital increment 10 [44], we find fairly good results already at $\omega = 100.0 \text{ Bohr}^{-1}$. This is likely due to the fact that most of the significant correlation effects in this system occur internally on the atoms. The results are numerically the same as CIM for $\omega = 0.5 \text{ Bohr}^{-1}$, and we observe no significant change below this value for this system.

Ideally, we would like the effect of the attenuation to be minimal in comparison to the ones caused by the

distance cutoffs, so a closer scrutiny of the attenuation dependence in the energy is warranted. We therefore compute the CIM-like MP2 energies for ethylene and 3D neon for a range of ω -values, as shown in Figure 5. Again, we obtain validating results from CRYSOR using the same auxiliary basis with a Coulomb-metric fit, PAOs for the virtual orbital space and a local excitation domain for all strong pairs which includes all virtual orbitals associated with the 25 nearest neighbouring atoms for ethylene, and 10 nearest neighbours for neon.

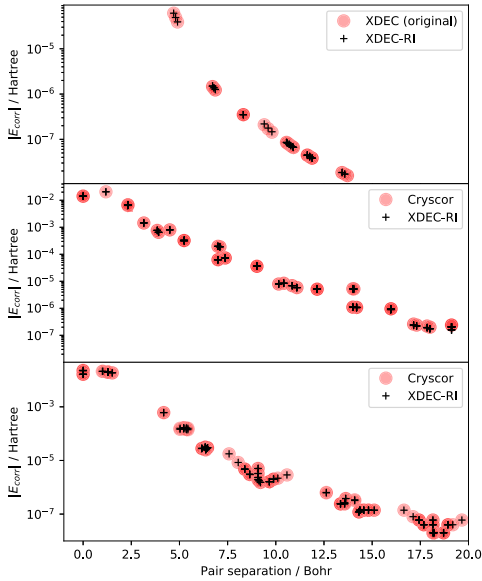


Figure 4. Validation of pair-fragment energies for (top to bottom) 3D neon, ethylene and $2\text{H}_2\text{O}$ by comparison to *Cryscor* and the original XDEC implementation. The fragment energy for 3D neon is not included.

With a cutoff for the local subspace $d_{\text{virt}} = 15.0$ Bohr for ethylene and $d_{\text{virt}} = 6.0$ Bohr for 3D neon, and a range of d_{occ} -values, we find that both cases show the energy approaching in a smooth fashion the Coulomb-metric fit as indicated by the *Cryscor* results when ω is decreased. The dependence on the attenuation parameter is similar to that reported for molecules in the past [50,104], with a stable region for $\omega \leq 0.3$ Bohr $^{-1}$. In the region from 0.3 Bohr $^{-1}$ to 10.0 Bohr $^{-1}$, the energy changes smoothly before it stabilises not too far from the values obtained close to the Coulomb-metric fit.

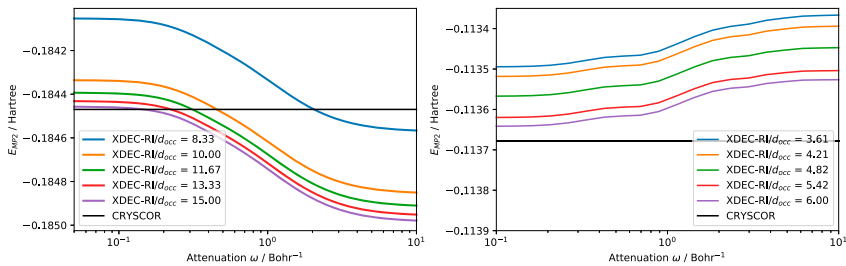


Figure 5. Dependence of the LMP2 energy on the attenuation parameter ω for ethylene (left) and 3D neon (right). For ethylene, we had $d_{\text{virt}} = 15.0$ Bohr, while for 3D neon we had $d_{\text{virt}} = 6.0$ Bohr.

Table 1. Total MP2 energy for 1D neon compared to CIM results from Wang et al. [43].

	Attenuation	$E_{\text{MP2}} / \text{Hartree}$
XDEC-RI	100.0	-0.114314
	10.0	-0.114319
	1.0	-0.114351
	0.5	-0.114363
	0.1	-0.114363
	0.07	-0.114363
	0.05	-0.114363
CIM	-	-0.114363

Variations in the cohesion energy for ethylene following changes in attenuation in the region below $\omega = 0.3$ Bohr $^{-1}$ is found to be less than 1% relative to $796.5 \mu\text{Ha}$, obtained at $\omega = 0.05$ Bohr $^{-1}$. In general, the changes in energy due to attenuation below 0.3 Bohr $^{-1}$ are fairly small in comparison to the changes in the cutoff parameter d_{occ} , so we conclude that we may safely choose $\omega \leq 0.3$ Bohr $^{-1}$ in our further examination.

The features of the curves in Figure 5 corresponding to the various distance cutoffs appear more or less internally unchanged, while they are simply shifted in energy as the distance cutoff changes. This indicates that the correlation energy distributes similarly across the pairs independent of the attenuation parameter, but it does not decisively tell us whether or not the attenuation could cause artefacts in the PES beyond the ones we expect from the fragmentation. Since the position of each orbital remains fixed after the localisation, we expect abrupt changes in energy to occur at the same distance cutoffs regardless of the various other parameters used in the approximation. Thus, in order to rule out such attenuation-related effects in the energy, we compute for $\omega = 0.1$ Bohr $^{-1}$ and $\omega = 0.2$ Bohr $^{-1}$, both safely within the limit of $\omega = 0.3$ Bohr $^{-1}$, the CIM-like energies for $2\text{H}_2\text{O}$ for a range of cutoffs. This is a slightly more correlated system, since it features hydrogen bonds both within and between the cells. In the results, presented in Figure 6, we find our first indications of abrupt

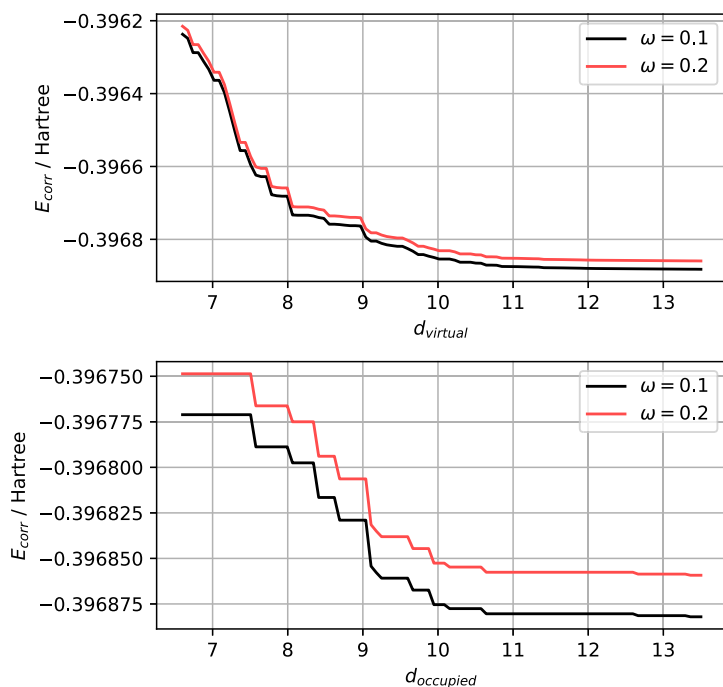


Figure 6. The XDEC-RI MP2 energy of $2\text{H}_2\text{O}$ for various distance cutoffs. In the upper panel, $d_{\text{occ}} = 13$ Bohr and in the lower panel $d_{\text{virt}} = 13$ Bohr.

energetic changes, represented by an irregular convergence pattern featuring cliffs and plateaus as the cutoff parameters are increased in both the virtual and occupied direction. The cliffs in this system are an order of magnitude larger in the virtual direction, on the order of 10^{-4} Hartree, as compared to 10^{-5} Hartree in the occupied direction. Comparing the curves for each ω , we find that discontinuities along both d_{occ} and d_{virt} remain stationary when the attenuation parameter is changed. This suggests that any discontinuities we see here are independent of the attenuation parameter for $\omega \leq 0.3 \text{ Bohr}^{-1}$, and are primarily caused by discrete changes in the local subspace.

A more complete picture of the convergence pattern can be revealed by varying d_{occ} and d_{virt} simultaneously. In order to illustrate the theoretical considerations we have made in regards to discontinuities, we therefore use our code to compute energies for a range of distance cutoff parameters for ethylene and $2\text{H}_2\text{O}$, shown in Figure 7. In this way, the local MP2 energy can be shown as a surface, approaching the exact result as d_{occ} and d_{virt} becomes large. Both systems again show the expected non-smooth yet monotonically decreasing energy with

respect to the domain sizes in the form of cliffs and plateaus across the surface. The abrupt changes occur at the same distances for one of the cutoff parameters seemingly independently of the other. This feature suggests that it is possible to converge the energy first with regards to one cutoff, thereafter the other, in contrast to repeated successive convergence of these two parameters conventionally used in DEC methods [19,44].

We have indicated the *mean* number of occupied or virtual orbitals per local subspace that are included in the calculation for some chosen cutoffs, in order to highlight that the sharp cliffs do not necessarily correspond to distances at which a large number of orbitals enter the calculation. Rather, it shows there are certain orbitals that yield more significant contributions to the local correlation energy, whether it be through direct contributions or indirect buffer effects. These are scattered throughout the neighbourhood of the reference cell, not necessarily ordered by distance.

Large contributions to the energy from close pairs are clearly present in both cases, while the contributions in the virtual direction tend to be more evenly spread out over larger intervals. This latter effect can likely be

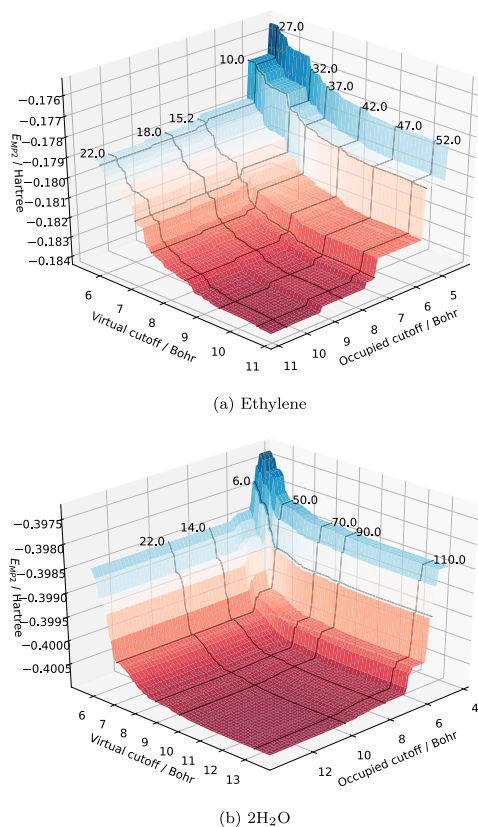


Figure 7. Convergence of the CIM-like energy of the ethylene system (top) and a 2H₂O system with respect to occupied and virtual cutoff distances. The numbered lines on the surface indicate the mean number of virtual and occupied orbitals per occupied that are included per local subspace at a given truncation. Note that there are energies from several local subspaces superimposed in these figures, thus the number of orbitals may be fractional. (a) Ethylene. (b) 2H₂O.

explained by the centres of the virtual orbitals being more arbitrarily dispersed in comparison to the occupied orbitals who will likely be positioned close to atoms or bonding sites in the lattice. Within the DEC formalism, it is customary to assign orbitals to atomic sites by means of for instance Mulliken or Löwdin charges [18,21,44]. If we instead assign the virtual orbitals to their closest atomic centres and include all virtual orbitals for all atoms inside d_{virt} in the local subspace, we obtain for ethylene the results shown in Figure 8 in support of this explanation. Here, we see clearly that the energy for the atomic association features more distinct plateaus and cliffs in

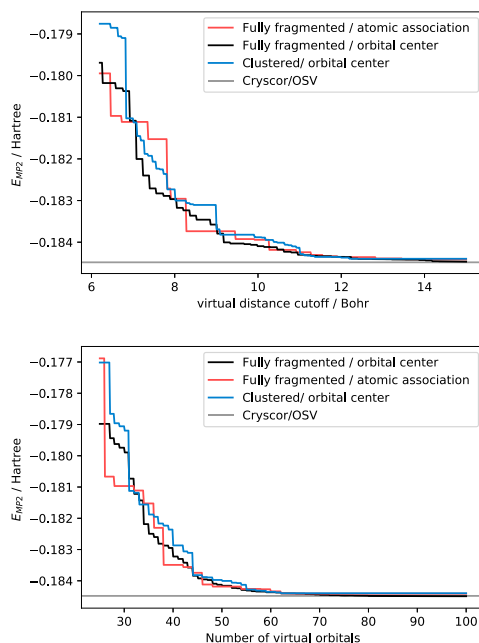


Figure 8. The convergence of the virtual space for ethylene; a comparison of a setup where orbitals are associated with atoms and the default orbital-centred approach. We have also included results where the occupied space was partitioned into two groups based on their nearest neighbour rather than into individual orbitals. The occupied cutoff is fixed at $d_{\text{occ}} = 15.0$ Bohr. As a reference, Cryscor results for OSV tolerance 10^{-5} are shown. The average size of the OSV orbital domains is 26.

the virtual direction as compared to the one where the orbital centres are used directly. This effect persists independently of whether we count distance or number of virtual orbitals along the x -axis, which further reinforces the point that the significance of each orbital with respect to the correlation energy is not simply a function of the distance.

We see similar irregularities emerge if we allow for more than one orbital per fragment or cluster, as shown for ethylene and 2H₂O in Figures 8 and 9, respectively. For ethylene, we here compare the outcome of a CIM-like MP2 calculation where the occupied space has been subdivided into two clusters based on distance as outlined in the implementational details, to the completely fragmented calculation. Similarly, for water, we compare two clusters to the complete fragmentation. In both cases, we find slightly sharper cliffs and flatter plateaus for the clustered approach. The effect is independent of whether

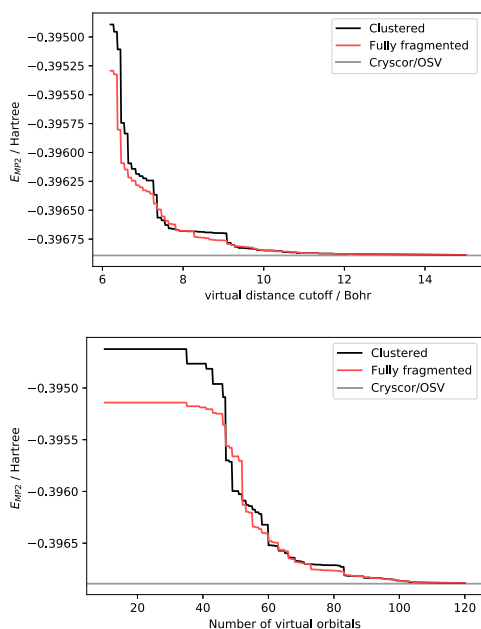


Figure 9. The convergence of the virtual space for $2\text{H}_2\text{O}$; a comparison between a setup where the occupied space is fully fragmented into individual orbitals and another setup where they are partitioned into 4 groups based on their nearest neighbours. The occupied cutoff is fixed at $d_{\text{occ}} = 15.0$ Bohr. As a reference, Cryscor results for OSV tolerance 10^{-5} are shown.

distance or number of virtual orbitals is used for the x -axis. When spatially non-coincident occupied orbitals are grouped into the same fragment or cluster, a purely distance-based ordering of the virtual space can result in a more irregular convergence pattern than that of a totally fragmented occupied space, likely due to the fact that being close does not necessarily guarantee strong coupling to the same virtual subspace.

These results show that the discontinuities are clearly dependent on the fragmentation, where both the clustering of occupied orbitals and the common practice of associating the virtual orbitals to atoms may increase the likelihood of false convergence of the MP2 energy with respect to d_{virt} .

We then focus on geometry dependence in the PES by considering the adsorption of a water molecule on a surface of LiH, as shown in Figure 3. We keep the internal geometry of H_2O fixed, while its distance perpendicular to the surface is varied between -1 to 2 Bohr relative to its equilibrium. The equilibrium geometry is taken from Ref. [96], where the water molecule has been relaxed at the LiH surface at the KS-DFT level with the

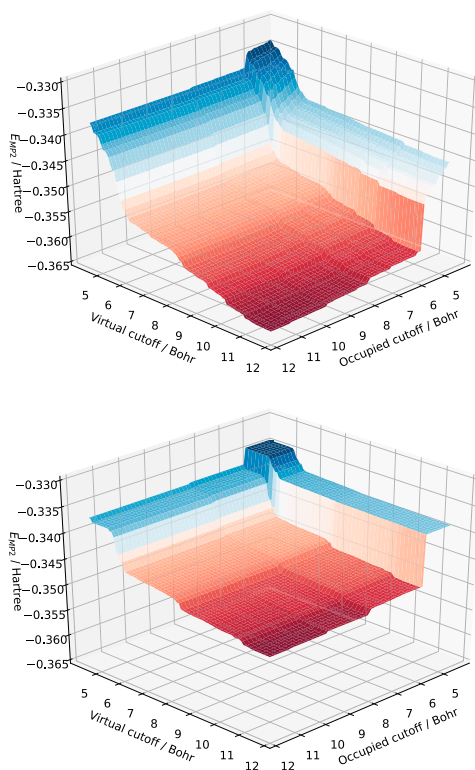


Figure 10. The MP2 energy as a function of the local subspace definition for a displacement of H_2O from equilibrium perpendicular to the surface of $\Delta z_{\text{H}_2\text{O}} = -1.115$ Bohr (above) and $\Delta z_{\text{H}_2\text{O}} = 1.871$ Bohr (below). As the water molecule approach the surface, the energy decreases and the sharp discontinuities becomes smeared out – or eroded – resulting in a more smooth convergence pattern.

Perdew–Burke–Ernzerhof (PBE) XC functional [105]. We let $\omega = 0.15$ Bohr $^{-1}$.

As expected, varying the geometry results in significant changes in the convergence pattern, as shown in Figure 10. The position of the orbitals in the LiH surface moves as the water molecule approaches the surface, resulting in a type of erosion of the sharp cliffs and plateaus. Also, the MP2 energy is generally decreased when water comes close as the interactions with the surface intensifies. In Figure 11, we show the effect of various choices for distance truncations of the local subspace.

Discontinuities are visible even for the largest subspace, and upon inspection, they are found to be on the order of 10^{-4} Hartree. More discontinuities emerge for

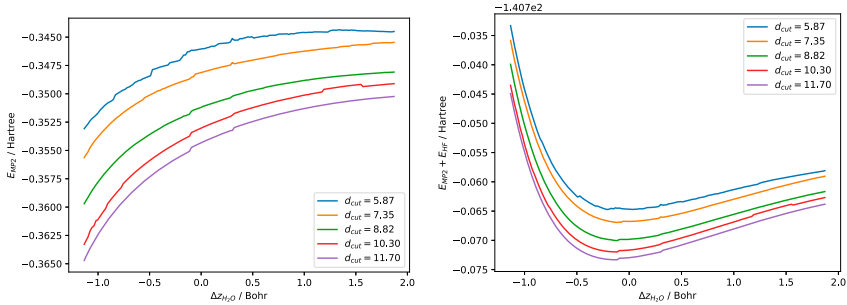


Figure 11. MP2 energy (left) and MP2 + reference energy (right) for the LiH-H₂O surface. The x-axis shows the displacement of the water molecule relative to the relaxed geometry perpendicular to the surface. The distance truncation of the local subspace is in this case $d_{\text{cut}} = d_{\text{occ}} = d_{\text{virt}}$.

the smaller domains. We can observe at least two discontinuities at approximately -0.1 and 0.3 Bohr which persists across the various cutoffs. The one at -0.1 Bohr is positioned awkwardly close to the minimum of the total energy, highlighting exactly how these kinds of effects can influence the results. In this case, the minimum of the potential curve is shifted slightly towards negative $\Delta z_{\text{H}_2\text{O}}$ due to the presence of a discontinuity.

The MP2 adsorption energy is computed using a similar definition as in Refs [96], where only inter H₂O-surface pairs up to our maximum cutoff threshold are included in the energy. In terms of the energy expression in Equation (9), this corresponds to

$$E_{\text{ads,MP2}} = 2 \sum_{i \in \Omega_0} \sum_{j \in \mathcal{O} \setminus \Omega_0} \sum_{ab \in \mathcal{V}} E_{ij}^{ab}, \quad (45)$$

where Ω_0 signifies the set of occupied orbitals situated at the H₂O molecule in the reference cell.

From the convergence pattern of the MP2 adsorption energy at equilibrium ($\Delta z_{\text{H}_2\text{O}} = 0$ Bohr), shown in Figure 12, we can clearly see a step-like pattern for pairs at distances below 8 Bohr where significant contributions to the energy are present. These significant contributions can be attributed to surface-molecule pairs close to the water molecule, as to be expected with localised orbitals. An unexpected effect is, however, present in the virtual cutoff, where sharp cliffs are present beyond distances $d_{\text{virt}} \geq 8$ Bohr.

The effect on the convergence pattern from the moving water molecule is shown in Figure 13. Also here we can identify the step-like pattern for close pairs, and the more distant contributions from the virtual space. The movement of the water molecule reveals a distinction between these effects; while the discontinuities in the occupied direction move along with the geometry, the virtual discontinuities appear to remain stationary. The

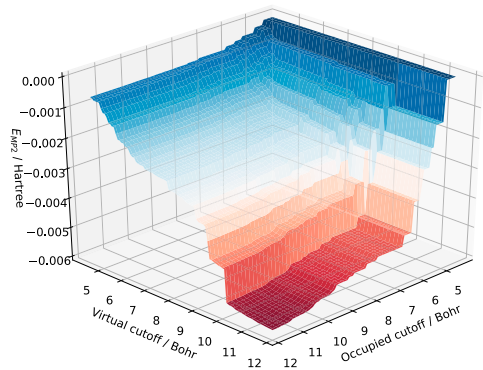


Figure 12. MP2 adsorption energy in Hartrees (LiH-H₂O surface-molecule pairs within cutoff distances specified) as a function of the distance truncation parameters at equilibrium ($\Delta z_{\text{H}_2\text{O}} = 0$ Bohr).

distance at which they occur is just below the lattice parameter (10.91 Bohr) and suggests that these contributions may be attributed to virtual orbitals at neighbouring water molecules, or similarly virtual orbitals at the corresponding Li- or H-atoms in neighbouring cells.

When compared to Figure 12, we find that these distant contributions from the virtual space persist also for small occupied cutoffs, meaning that the distant virtual orbitals are significant even when both occupied orbitals are close to the origin. This could be an effect pertaining to the LVO representation of the virtual space, but further studies are required in order to determine whether or not it would be resolved by replacing them with PAOs or OSVs.

The DEC approach of converging the domains can in principle be applied to any of the fragmentation schemes under consideration. In order to demonstrate this, we

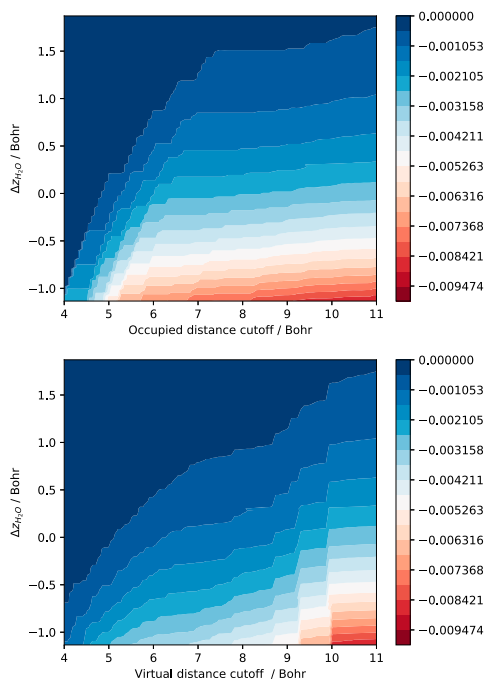


Figure 13. MP2 adsorption energy in Hartrees (LiH-H₂O surface – molecule pairs within cutoff distances specified) as a function of the distance truncation parameters in the occupied direction when d_{virt} is at its maximum value (top) and similarly as a function of d_{virt} when d_{occ} is at its maximum value (bottom). The y axis shows the vertical offset from equilibrium of the water molecule.

finally investigate the relationship between the magnitude of the discontinuities and the FOT in the 2H₂O-system by converging the CIM-like MP2 energy successively in the virtual and occupied directions as described in Ref. [44]. We increase the spaces by a minimum of 6 orbitals per expansive step. As the lattice parameter is altered, one H₂O molecule is moved such that the bond angles are preserved. The results are shown in Figure 14. We finally find that the magnitude of the discontinuities appears to be proportional to the FOT, which confirms that the discontinuities indeed can be systematically suppressed in this manner.

6. Concluding remarks

Discontinuities are inherently present in periodic PESs produced with local correlation methods. The overall source of these discontinuities is discrete changes in the orbital spaces, and as long as the spaces are chosen sufficiently large these problems may be insignificant. Exactly

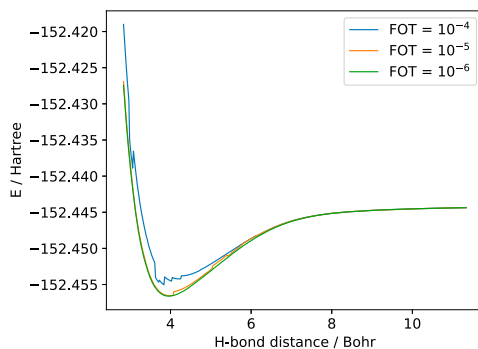


Figure 14. Adaptive CIM approach for a chain of H₂O (two molecules per cell). The figure demonstrates that discontinuities can be systematically suppressed for a CIM-based fragmentation scheme by converging the energy of each cluster analogous to what is done in XDEC.

what constitutes sufficiently large is, however, system dependent and difficult to determine in a black box manner. The DEC approach of converging the energies of each subspace can in principle provide control of the magnitude of the discontinuities for most fragmentation schemes, but the practical complications due to the irregular convergence behaviour represent a challenge. Ideally, one would like every new set of orbitals that enters the subspace to yield an energy contribution smaller than the preceding ones. Our results confirm as expected that this is not the situation for the purely distance-based selection of the WFs, but that in large enough increments the overall behaviour is convergent.

The convergence behaviour is dependent on several fragmentation-specific choices that are easy to control. Notably, the risk of false convergence can be reduced by choosing more fine-grained fragmentation and avoid coincidental position definitions. Furthermore, the balanced treatment of the virtual space of the Pulay-Sæbø pairs and DEC pair fragments is natural to include in periodic systems, for example by means of OSVs [57] or a global fitting scheme, and may further reduce the risk of discontinuities from the virtual cutoff.

In order to converge the local subspace, efficient handling of the integrals is crucial. Such efficiency can be achieved with a global fitting scheme as demonstrated in this work. While the initial partial contraction of the occupied space is computationally demanding, the subsequent contraction of virtual spaces and calculation of integrals is relatively cheap, and the intermediate contraction tensor contains all the required information to obtain all ERIs for the crystal.

Disclosure statement

No potential conflict of interest was reported by the author(s).

ORCID

A. S. Hansen  <http://orcid.org/0000-0003-0962-3143>

T. B. Pedersen  <http://orcid.org/0000-0001-8967-6055>

References

- [1] W. Kohn and L.J. Sham, *Phys. Rev.* 140, A1133–A1138 (1965). doi:10.1103/PhysRev.140.A1133
- [2] C.C.J. Roothaan, *Rev. Mod. Phys.* 23, 69–89 (1951). doi:10.1103/RevModPhys.23.69
- [3] R.J. Bartlett and M. Musiał, *Rev. Mod. Phys.* 79, 291–352 (2007). doi:10.1103/RevModPhys.79.291
- [4] O. Sinanoğlu, *Adv. Chem. Phys.* 6, 315–412 (1964). doi:10.1002/9780470143520.ch7
- [5] R.K. Nesbet, *Adv. Chem. Phys.* 9, 321–363 (1965). doi:10.1002/9780470143551.ch4
- [6] J.M. Cullen and M.C. Zerner, *J. Chem. Phys.* 77, 4088–4109 (1982). doi:10.1063/1.444319
- [7] P. Pulay, *Chem. Phys. Lett.* 100, 151–154 (1983). doi:10.1016/0009-2614(83)80703-9
- [8] S. Sæbø and P. Pulay, *Chem. Phys. Lett.* 113, 13–18 (1985). doi:10.1016/0009-2614(85)85003-X
- [9] P. Pulay and S. Sæbø, *Theor. Chim. Acta* 69, 357–368 (1986). doi:10.1007/BF00526697
- [10] P. Pulay and S. Sæbø, *J. Chem. Phys.* 914, 914–922 (1987). doi:10.1063/1.452293
- [11] W. Meyer, *J. Chem. Phys.* 58, 1017–1035 (1973). doi:10.1063/1.1679283
- [12] F. Neese, F. Wennmohs and A. Hansen, *J. Chem. Phys.* 130, 114108 (2009). doi:10.1063/1.3086717
- [13] F. Neese, A. Hansen and D.G. Liakos, *J. Chem. Phys.* 131, 064103 (2009). doi:10.1063/1.3173827
- [14] C. Riplinger and F. Neese, *J. Chem. Phys.* 138, 034106 (2013). doi:10.1063/1.4773581
- [15] P. Pinski, C. Riplinger, E.F. Valeev and F. Neese, *J. Chem. Phys.* 143, 034108 (2015). doi:10.1063/1.4926879
- [16] C. Riplinger, P. Pinski, U. Becker, E.F. Valeev and F. Neese, *J. Chem. Phys.* 144, 024109 (2016). doi:10.1063/1.4939030
- [17] H.-J. Werner, G. Knizia, C. Krause, M. Schwikl and M. Dornbach, *J. Chem. Theory Comput.* 11, 484–507 (2015). doi:10.1021/ct500725e
- [18] M. Ziolkowski, B. Jansik, T. Kjærgaard and P. Jørgensen, *J. Chem. Phys.* 133, 014107 (2010). doi:10.1063/1.3456535
- [19] K. Kristensen, M. Ziolkowski, B. Jansik, T. Kjærgaard and P. Jørgensen, *J. Chem. Theory Comput.* 7, 1677–1694 (2011). doi:10.1021/ct200114k
- [20] I.-M. Høyvik, K. Kristensen, B. Jansik and P. Jørgensen, *J. Chem. Phys.* 136, 014105 (2012). doi:10.1063/1.3667266
- [21] K. Kristensen, P. Jørgensen, B. Jansik, T. Kjærgaard and S. Reine, *J. Chem. Phys.* 137, 114102 (2012). doi:10.1063/1.4752432
- [22] K. Kristensen, T. Kjærgaard, I.-M. Høyvik, P. Etenhuber, P. Jørgensen, B. Jansik, S. Reine and J. Jakowski, *Mol. Phys.* 111, 1196–1210 (2013). doi:10.1080/00268976.2013.783941
- [23] S. Li, J. Ma and Y. Jiang, *J. Comput. Chem.* 23 (2), 237–244 (2002). doi:10.1002/(ISSN)1096-987X
- [24] S. Li, J. Shen, W. Li and Y. Jiang, *J. Chem. Phys.* 125 (7), 074109 (2006). doi:10.1063/1.2244566
- [25] H.-J. Werner and K. Pflüger, *Annu. Rep. Comput. Chem.* 2, 53–80 (2006). doi:10.1016/15174-1400(06)02004-4
- [26] F. Bloch, *Z. Phys.* 52, 555–600 (July 1929). doi:10.1007/BF01339455
- [27] R.D.L. Kronig, W.G. Penney and R.H. Fowler, *Proc. Math. Phys. Eng. Sci.* 130, 499–513 (1931). doi:10.1098/rspa.1931.0019
- [28] N.W. Ashcroft and N.D. Mermin, *Solid State Physics* (Saunders, Holt-Saunders, 1976).
- [29] A. Grüneis, M. Marsman, J. Harl, L. Schimka and G. Kresse, *J. Chem. Phys.* 131, 154115 (2009). doi:10.1063/1.3250347
- [30] G.H. Booth, A. Grüneis, G. Kresse and A. Alavi, *Nature* 493, 365–370 (2013). doi:10.1038/nature11770
- [31] T.D. Kühne, M. Iannuzzi, M. Del Ben, V.V. Rybkin, P. Seewald, F. Stein, T. Laino, R.Z. Khaliullin, O. Schütt and F. Schifmann, *J. Chem. Phys.* 152, 194103 (2020). doi:10.1063/5.0007045
- [32] J.-Q. Sun and R.J. Bartlett, *J. Chem. Phys.* 104, 8553–8565 (1996). doi:10.1063/1.471545
- [33] S. Hirata and S. Iwata, *J. Chem. Phys.* 109, 4147–4155 (1998). doi:10.1063/1.477020
- [34] S. Hirata and R.J. Bartlett, *J. Chem. Phys.* 112, 7339–7344 (2000). doi:10.1063/1.481372
- [35] P.Y. Ayala, K.N. Kudin and G.E. Scuseria, *J. Chem. Phys.* 115, 9698–9707 (2001). doi:10.1063/1.1414369
- [36] J. McClain, Q. Sun, G.K.-L. Chan and T.C. Berkelbach, *J. Chem. Theory Comput.* 13, 1209–1218 (2017). doi:10.1021/acs.jctc.7b00049
- [37] G.H. Wannier, *Phys. Rev.* 52, 191 (1937). doi:10.1103/PhysRev.52.191
- [38] W. Kohn, *Phys. Rev.* 115, 809–821 (1959). doi:10.1103/PhysRev.115.809
- [39] D. Fiorenza, D. Monaco and G. Panati, *Ann. Henri Poincaré* 17, 63–97 (2016). doi:10.1007/s00023-015-0400-6
- [40] N. Marzari, A.A. Mostofi, J.R. Yates, I. Souza and D. Vanderbilt, *Rev. Mod. Phys.* 84, 1419–1475 (2012). doi:10.1103/RevModPhys.84.1419
- [41] C.M. Zicovich-Wilson, R. Dovesi and V.R. Saunders, *J. Chem. Phys.* 115, 9708–9719 (2001). doi:10.1063/1.141-5745
- [42] C. Pisani, L. Maschio, S. Casassa, M. Halo, M. Schütz and D. Usvyat, *J. Comput. Chem.* 29, 2113–2124 (2008). doi:10.1002/jcc.v29:13
- [43] Y. Wang, Z. Ni, W. Li and S. Li, *J. Chem. Theory Comput.* 15, 2933–2943 (2019). doi:10.1021/acs.jctc.8b01200
- [44] E. Rebolini, G. Baardsen, A.S. Hansen, K.R. Leikanger and T.B. Pedersen, *J. Chem. Theory Comput.* 14, 2427–2438 (2018). doi:10.1021/acs.jctc.8b00021
- [45] A.S. Hansen, G. Baardsen, E. Rebolini, L. Maschio and T.B. Pedersen, *Mol. Phys.* 1–11 (2020). doi:10.1080/00268976.2020.1733118
- [46] M. Lorenz, D. Usvyat and M. Schütz, *J. Chem. Phys.* 134, 094101 (2011). doi:10.1063/1.3554209

- [47] M. Lorenz, L. Maschio, M. Schütz and D. Usvyat, *J. Chem. Phys.* 137, 204119 (2012). doi:10.1063/1.4767775
- [48] M. Milko, J. Noga and Š. Varga, *Int. J. Quantum Chem.* 107, 2158–2168 (2007). doi:10.1002/(ISSN)1097-461X
- [49] L. Maschio, *J. Chem. Theory Comput.* 7, 2818–2830 (2011). doi:10.1021/ct200352g
- [50] Y. Jung, A. Sodt, P.M. Gill and M. Head-Gordon, *Proc. Natl. Acad. Sci. U.S.A.* 102, 6692–6697 (2005). doi:10.1073/pnas.0408475102
- [51] L. Maschio, D. Usvyat, F.R. Manby, S. Casassa, C. Pisani and M. Schütz, *Phys. Rev. B* 76, 075101 (2007). doi:10.1103/PhysRevB.76.075101
- [52] D. Usvyat, L. Maschio, F.R. Manby, S. Casassa, M. Schütz and C. Pisani, *Phys. Rev. B* 76, 075102 (2007). doi:10.1103/PhysRevB.76.075102
- [53] F.R. Manby, editors, *Accurate Condensed-Phase Quantum Chemistry* (Boca Raton, CRC Press, 2010).
- [54] N.J. Russ and T.D. Crawford, *J. Chem. Phys.* 121, 691–696 (2004). doi:10.1063/1.1759322
- [55] R.A. Mata and H.-J. Werner, *J. Chem. Phys.* 125, 184110 (2006). doi:10.1063/1.2364487
- [56] J.E. Subotnik, A. Sodt and M. Head-Gordon, *J. Chem. Phys.* 112, 034103 (2008). doi:10.1063/1.2821124
- [57] D. Usvyat, L. Maschio and M. Schütz, *J. Chem. Phys.* 143, 102805 (2015). doi:10.1063/1.4921301
- [58] M.S. Lee, P.E. Maslen and M. Head-Gordon, *J. Chem. Phys.* 112, 3592–3601 (2000). doi:10.1063/1.480512
- [59] P. Löwdin, *J. Chem. Phys.* 18, 365–375 (1950). doi:10.1063/1.1747632
- [60] G. Hetzer, P. Pulay and H.-J. Werner, *Chem. Phys. Lett.* 290, 143–149 (1998). doi:10.1016/S0009-2614(98)00491-6
- [61] H.-J. Werner, *J. Chem. Phys.* 145, 201101 (2016). doi:10.1063/1.4968595
- [62] J. Yang, Y. Kurashige, F.R. Manby and G.K. Chan, *J. Chem. Phys.* 134, 044123 (2011). doi:10.1063/1.3528935
- [63] Y. Kurashige, J. Yang, G.K.-L. Chan and F.R. Manby, *J. Chem. Phys.* 136, 124106 (2012). doi:10.1063/1.3696962
- [64] D. Kats and F.R. Manby, *J. Chem. Phys.* 138, 144101 (2013). doi:10.1063/1.4798940
- [65] C. Krause and H.-J. Werner, *Phys. Chem. Chem. Phys.* 14, 7591–7604 (2012). doi:10.1039/c2cp40231a
- [66] S. Saebø and P. Pulay, *Annu. Rev. Phys. Chem.* 44, 213 (1993). doi:10.1146/annurev.pc.44.100193.001241
- [67] H.-J. Werner, P.J. Knowles, G. Knizia, F.R. Manby and M. Schütz, *Wiley Interdiscip. Rev. Comput. Mol. Sci.* 2, 242–253 (2012). doi:10.1002/wcms.82
- [68] C. Pisani, M. Busso, G. Capecchi, S. Casassa, R. Dovesi, L. Maschio, C. Zicovich-Wilson and M. Schütz, *J. Chem. Phys.* 122, 094113 (2005). doi:10.1063/1.1857479
- [69] M. Halo, S. Casassa, L. Maschio and C. Pisani, *Phys. Chem. Chem. Phys.* 11, 586–592 (2009). doi:10.1039/B812870G
- [70] C. Pisani, M. Schütz, S. Casassa, D. Usvyat, L. Maschio, M. Lorenz and A. Erba, *Phys. Chem. Chem. Phys.* 14, 7615–7628 (2012). doi:10.1039/c2cp23927b
- [71] R. Dovesi, A. Erba, R. Orlando, C.M. Zicovich-Wilson, B. Civalleri, L. Maschio, M. Rérat, S. Casassa, J. Baima and S. Salustro, *Wiley Interdiscip. Rev. Comput. Mol. Sci.* 8, e1360 (2018). doi:10.1002/wcms.2018.8.isue-4
- [72] H. Stoll, *Phys. Rev. B* 46, 6700 (1992). doi:10.1103/PhysRevB.46.6700
- [73] B. Paulus, *Phys. Rep.* 428, 1–52 (2006). doi:10.1016/j.physrep.2006.01.003
- [74] M. Alessio, D. Usvyat and J. Sauer, *J. Chem. Theory Comput.* 15, 1329–1344 (2018). doi:10.1021/acs.jctc.8b01122
- [75] O. Masur, M. Schütz, L. Maschio and D. Usvyat, *J. Chem. Theory Comput.* 12, 5145–5156 (2016). doi:10.1021/acs.jctc.6b00651
- [76] H.-H. Lin, L. Maschio, D. Kats, D. Usvyat and T. Heine, *J. Chem. Theory Comput.* 16, 7100–7108 (2020). doi:10.1021/acs.jctc.0c00576
- [77] E.F. Valeev and J.T. Fermann, *Libint: A library for the evaluation of molecular integrals of many-body operators over Gaussian functions* (2017). <https://github.com/evaleev/libint/>, Accessed: 2020-01-15.
- [78] C.V. van der Mee, S. Seatzu and G. Rodriguez, *Linear Algebra Appl.* 343, 355–380 (2002). doi:10.1016/S0024-3795(01)00441-4
- [79] H.J. Nussbaumer, *Fast Fourier Transform and Convolution Algorithms* (Springer, 1981)
- [80] C.L. Lawson, R.J. Hanson, D.R. Kincaid and F.T. Krogh, *ACM Trans. Math. Softw.* 5, 308–323 (1979). doi:10.1145/355841.355847
- [81] J.L. Whitten, *J. Chem. Phys.* 58, 4496–4501 (1973). doi:10.1063/1.1679012
- [82] E.J. Baerends, D. Ellis and P. Ros, *Chem. Phys.* 2, 41–51 (1973). doi:10.1016/0301-0104(73)80059-X
- [83] B.I. Dunlap, J. Connolly and J. Sabin, *J. Chem. Phys.* 71, 3396–3402 (1979). doi:10.1063/1.438728
- [84] B. Dunlap, *J. Chem. Phys.* 78, 3140–3142 (1983). doi:10.1063/1.445228
- [85] M. Feyereisen, G. Fitzgerald and A. Komornicki, *Chem. Phys. Lett.* 208, 359–363 (1993). doi:10.1016/0009-2614(93)87156-W
- [86] O. Vahtras, J. Almlöf and M. Feyereisen, *Chem. Phys. Lett.* 213, 514–518 (1993). doi:10.1016/0009-2614(93)89151-7
- [87] K. Eichkorn, O. Treutler, H. Öhm, M. Häser and R. Ahlrichs, *Chem. Phys. Lett.* 240, 283–290 (1995). doi:10.1016/0009-2614(95)00621-A
- [88] K. Eichkorn, F. Weigend, O. Treutler and R. Ahlrichs, *Theor. Chem. Acc.* 97, 119–124 (1997). doi:10.1007/s002140050244
- [89] F. Weigend, M. Häser, H. Patzelt and R. Ahlrichs, *Chem. Phys. Lett.* 294, 143–152 (1998). doi:10.1016/S0009-2614(98)00862-8
- [90] C.-K. Skylaris, L. Gagliardi, N.C. Handy, A.G. Ioannou, S. Spencer and A. Willetts, *J. Mol. Struct. THEOCHEM* 501, 229–239 (2000). doi:10.1016/S0166-1280(99)00434-0
- [91] F. Weigend, A. Köhn and C. Hättig, *J. Chem. Phys.* 116, 3175–3183 (2002). doi:10.1063/1.1445115
- [92] J.P. Dombroski, S.W. Taylor and P.M. Gill, *J. Phys. Chem.* 100, 6272–6276 (1996). doi:10.1021/jp952841b
- [93] B. Dunlap, *J. Mol. Struct. THEOCHEM* 529, 37–40 (2000). doi:10.1016/S0166-1280(00)00528-5
- [94] A.M. Burow, M. Sierka and F. Mohamed, *J. Chem. Phys.* 131, 214101 (2009). doi:10.1063/1.3267858
- [95] A. Hoy and P.R. Bunker, *J. Mol. Spectrosc.* 74, 1–8 (1979). doi:10.1016/0022-2852(79)90019-5

- [96] T. Tsatsoulis, F. Hummel, D. Usvyat, M. Schütz, G.H. Booth, S.S. Binnie, M.J. Gillan, D. Alfè, A. Michaelides and A. Grüneis, *J. Chem. Phys.* 146, 204108 (2017). doi:10.1063/1.4984048
- [97] R. Dovesi, V.R. Saunders, C. Roetti, R. Orlando, C.M. Zicovich-Wilson, F. Pascale, B. Civalleri, K. Doll, N.M. Harrison, I.J. Bush, P. D'Arco, M. Llunell, M. Causà, Y. Noël, L. Maschio, A. Erba, M. Rerat and S. Casassa, *Crystal 17 user's manual* (2018). <https://www.crystal.unito.it/documentation.php>, Accessed: 2020-12-04.
- [98] W.J. Hehre, R. Ditchfield and J.A. Pople, *J. Chem. Phys.* 56, 2257–2261 (1972). doi:10.1063/1.1677527
- [99] D. Feller, *J. Comput. Chem.* 17, 1571–1586 (1996). doi:10.1002/(ISSN)1096-987X
- [100] K.L. Schuchardt, B.T. Didier, T. Elsethagen, L. Sun, V. Gurumoorthi, J. Chase, J. Li and T.L. Windus, *J. Chem. Inf. Mod.* 47, 1045–1052 (2007). doi:10.1021/ci600510j
- [101] M.F. Peintinger, D.V. Oliveira and T. Bredow, *J. Comput. Chem.* 34, 451–459 (2013). doi:10.1002/jcc.23153
- [102] B. Civalleri, A.M. Ferrari, M. Llunell, R. Orlando, M. Mérawa and P. Ugliengo, *Chem. Mater.* 15, 3996–4004 (2003). doi:10.1021/cm0342804
- [103] C. Gatti, V.R. Saunders and C. Roetti, *J. Chem. Phys.* 101, 10686–10696 (1994). doi:10.1063/1.467882
- [104] S. Reine, E. Tellgren, A. Krapp, T. Kjærgaard, T. Helgaker, B. Jansik, S. Høst and P. Salek, *J. Chem. Phys.* 129, 104101 (2008). doi:10.1063/1.2956507
- [105] J.P. Perdew, K. Burke and M. Ernzerhof, *Phys. Rev. Lett.* 77, 3865–3868 (1996). doi:10.1103/PhysRevLett.77.3865